REGOLITH BASED POLYMER MATRIX COMPOSITES FOR IN-SITU ADDITIVE MANUFACTURING FOR LONG TERM EXTRATERRESTRIAL MISSIONS

A Thesis
Submitted to the Graduate Faculty
of the
North Dakota State University
of Agriculture and Applied Science

By

Christopher Mark Matetich

In Partial Fulfillment of the Requirements
for the Degree of
MASTER OF SCIENCE

Major Department:
Mechanical Engineering

June 2022

Fargo, North Dakota

North Dakota State University
Graduate School

Title

Regolith Based Polymer Matrix Composites for In-Situ Additive Manufacturing for Long Term Extraterrestrial Missions

By

Christopher Mark Matetich

The Supervisory Committee certifies that this ***disquisition*** complies with North Dakota State University's regulations and meets the accepted standards for the degree of

MASTER OF SCIENCE

SUPERVISORY COMMITTEE:

Dr. Jessica Vold
Chair

Dr. Adam Gladen

Dr. Chad Ulven

Dr. Dean Webster

Approved:

07/02/2022
Date

Dr. Alan Kallmeyer
Department Chair

ABSTRACT

The completed study investigated Martian regolith simulant composites' material properties when there was variation in the type of used Martian regolith simulant. Four types of Martian regolith simulant were mixed at varying weight percent loadings with polypropylene using twin screw extrusion. Test parts were made via injection molding with all the polymeric composites, and additive manufacturing with select polymeric composites. ASTM standard based tests and ANOVA tests were completed to investigate material characteristics. Depending on the creation process, the results suggested that Martian regolith simulant type impacted several material characteristics. During material processing, a foaming behavior was observed with all the materials, especially material that used MGS-1S. Additive manufactured parts were found to be impacted by the foaming behavior. A literature based thermal breakdown study suggested that thermal releases from the Martian regolith simulants were the likely candidates for the foaming behavior.

ACKNOWLEDGEMENTS

I would like to thank my advising professor, Dr. Vold, for the opportunity to learn and the support to succeed.

I would like to thank my family for supporting me throughout the work completed in this research and degree.

I would like to acknowledge the staff, faculty, and students of NDSU for use/support of laboratory equipment as a part of this research.

I would also like to thank Bamberger Polymers, Phillips 66, and Exolith Labs for their generosity in supplying material for this research.

I would finally like to acknowledge financial support from the ND EPSCoR STEM grants program for this research.

TABLE OF CONTENTS

LIST OF TABLES

LIST OF FIGURES

LIST OF ABREVIATIONS

MSC .....Martian Regolith Simulant Composite

MRS .....Martian Regolith Simulant

NDSU .....North Dakota State University

Wt. % .....Weight Percent

PP .....Polypropylene

FGF .....Fused Granulate Fabrication

TGA .....Thermogravimetric Analysis / Analyzer

IM.....Injection Molded / Molding

AM .....Additive Manufactured / Manufacturing

DMA .....Dynamic Mechanical Analysis

HDT .....Heat Deflection Temperature

CLTE.....Coefficient of Linear Thermal Expansion

IPA .....Isopropyl Alcohol

ANOVA .....Analysis of Variance

Df1 .....Degree of Freedom 1

Df2 .....Degree of Freedom 2

LIST OF SYMBOLS

T_g.....Glass transition temperature

ρ_{solid} .....Density of solid object

A .....Mass of solid object dry

B .....Mass of solid object immersed in test liquid

ρ_{liquid} .....Test liquid density at measured testing temperature

LIST OF APPENDIX TABLES

LIST OF APPENDIX FIGURES

CHAPTER 1. INTRODUCTION

The current progress in space exploration is at a point where long-term space missions on extraterrestrial bodies is being considered [1], [2]. A major component of making such missions possible is the ability for parts, tools, and/or structural elements to be created on the extraterrestrial body. Given the material and time expense of transporting materials from Earth, the potential of part, tool, and/or structural element construction using in-situ resources is being researched for such long-term space missions [3]. One such material available on-site of some extraterrestrial bodies is regolith. Regolith can be generally defined as loose, unconsolidated rock/dust material that overlays solid rock (bedrock) on a planetary-like body. This includes bodies such as the Earth, Moon, and Mars [4], [5].

To investigate the potential for the creation of regolith-based polymeric materials and in-situ additive manufacturing, this review studied the material properties of polymer matrix composites created using various Martian regolith simulants and a thermoplastic polymer. This included the characterization of polymer/regolith simulant composite material properties created using Earth based injection molding vs. on-site additive manufacturing, and the performance of the polymer/regolith simulant composite materials compared to neat polymer. The potential short-term benefit of this information was the creation of a Martian regolith simulant material property database, as created with the considerations of in-situ manufacturing, for use in future studies involving the study of material creation utilizing regolith simulant. The potential long-term benefit of this information was to outline a way in which the in-situ additive manufacturing of mission critical parts on extraterrestrial bodies might be achieved for future space missions.

1.1. Space Material Challenges

Understanding why the construction of space-based materials using in-situ manufacturing is needed for future long-term space missions provided context and reason to perform this research. For this paper, the extraterrestrial body that was focused on was Mars.

1.1.1. Radiation

The primary item to discuss when planning for a long-term mission on the surface of an extraterrestrial body is a way to shield against radiation. Outside the Earth's influence, the main types of radiation that pose a large threat to astronaut health on the extraterrestrial body's surfaces within the solar system of interest for surface missions are galactic cosmic radiation and solar flare radiation [6]. Any consideration of landing a crew of astronauts on the surface of one of these extraterrestrial bodies must provide an appropriate method of shielding the astronauts from these types of radiation due to long term, and in some cases short term, exposure to this radiation having adverse effects on the crew's health.

Galactic cosmic and solar flare radiation are both present on the surface of Mars [6], [7]. Thus, shielding against both types of radiation on the surface of this extraterrestrial body would be vital to the successes of a planned crewed surface mission. A practical solution to this would be to have walls constructed that can protect against the radiation. One method of accomplishing this is to use an extraterrestrial body's regolith to create the outer walls of a surface habitat via additive manufacturing [3], [8]. Both wall thickness and material type play a role in how effective the created walls would be against the radiation. This would depend on the specific extraterrestrial body which the mission is designed for (in this case Mars). The use of in-situ materials is preferable to the use of Earth based materials as using Earth based materials to create the walls would require a large amount of materials to be transported to the extraterrestrial body.

1.1.2. Materials

A major component to any space mission is the utilization of physical resources. Physical resources from Earth, such as a potential replacement part for a habitat, are a challenge to get to extraterrestrial bodies as transporting them into space requires vehicles capable of reaching orbit and traveling to the desired body. Such equipment has a baseline cost that is expensive on its own. SpaceX currently lists the cost of transporting a payload of 16,800 kg to Mars using their Falcon Heavy rocket at approximately $90 Million [9]. This expense is increased with every gram of added mass to the initial payload of the vehicle regardless of the destination.

In the case of Mars, the substantial amount of materials that would be required for a "basic" Martian habitat are expected to be have a high expense associated with them (both in a monetary value, and physical resource context) [8]. Some estimates, as displayed in Table 1, project a three-person module, with appropriate crew support items, designed for long term Martian mission being approximately 22,000 kg just for the necessary equipment to get onto the surface of Mars [10].

Table 1. Theoretical Mars Habitat Decent Payload Total, Reproduced from Reference [10]

Mass Estimates for the Descent Payload	
System	**Mass (kg)**
MAV stage 1	4483
MAV stage 2 (including 2675 kg for capsule)	7089
ISRU and surface power systems	6000
Consumables for the crew	4500
Total payload mass	**22,072**

These numbers suggest that the equivalent of two Falcon Heavy launches would be required to transport the required mass of materials for a pre-constructed three person Martian habitat to the surface of Mars. It is important to point out that this mass value only considers the necessary mass for habitat, crew, and other mission critical items to make it to the surface of Mars. The number does not include the mass consideration for the additional equipment and fuel required

to transport the crew from and to Earth. It is possible that such considerations would add additional mass to the original 22,000 kg payload. The conclusion of this is that more rocket launches would be required to send all the necessary materials to Mars for a fully crewed mission beyond the initial number required to just bring the habitat itself.

1.1.3. Time

In the previous section, the large amount of material resources required to bring Earth made materials into space was discussed. The cost of this process is also that of time. Creating the necessary components to launch a single, small-scale item into space takes time. Larger payloads only increase the amount of time required to launch into space given, at the very least, that it may require multiple launches to accomplish.

This also brings up the fact that fuel efficient rockets destined for different extraterrestrial bodies cannot be launched at any time of the year. There are certain windows of time in which rockets should launch to reach a particular celestial body. In the case of getting an object to Mars, the ideal launch window for a rocket occurs approximately every 26 months. At this point, Earth and Mars are at the ideal positions for a rocket to travel from one body to the other with the least amount of time and fuel costs [11]. This makes the time cost of launching items into space even more of a factor when considering long term space missions, especially how much time it would take just to launch the multiple payloads of necessary habit construction materials into orbit around the Earth before sending them to any extraterrestrial body.

Time is also a large consideration when it is factored in that any long-term surface habitats would need to be constructed before any humans arrived for a long-term space mission. This is so the astronauts have a safe, secure location to live while on a celestial body’s surface. The construction of the habitat would add even more time requirements to any long-term space

missions in addition to the time requirements of transporting astronauts to an extraterrestrial body. Thus, the cost of building a habitat on the body's surface is one that cannot be overlooked in planning future space missions.

In addition, any new/replacement parts that an astronaut crew may require while on planet would also have a time cost associated with them. Given that certain aspects of a mission (such as a new case for a sensor) may not be possible due to a part failure, any time delays from waiting for a part shipped from Earth would impact the mission's overall progression. If the delay was long enough, the mission's goals may not be able to be completed at all as by the time the new part arrives the crew may have had to begin their return trip to Earth. This gives even more reason to develop ways in which to utilize resources on an extraterrestrial body to create new/replacement parts necessary for a mission.

1.1.4. Martian Atmosphere/Environment

It is important to note details about the atmosphere and environment of Mars as its makeup may impact any material creation done in situ. A record of this would also be beneficial to any future standards created for material creation on the extraterrestrial body. In general, the Martian atmosphere is composed of three primary elements; Carbon Dioxide (~95%), Nitrogen (~2.5%), and Argon (~1.9%). The rest of the atmosphere is made up of small amounts of other various elements. These include oxygen, carbon monoxide, water, nitrogen oxide, neon, hydrogen-deuterium-oxygen, krypton, and xenon [12]–[15]. The atmospheric pressure on the surface of Mars is approximately 6.36 mb (or about 636 pascals) at the planet's mean radius. This number is variable based on the location on the planet, and the season [15]. The average temperature on the Martian surface is about 210 K (-63°C) with extreme values of approximately 184 K to 242 K (-89°C to -31°C) [15].

It is theorized that the temperature range present on Mars may affect any parts being created via additive manufacturing. This is due to Earth based additive manufacturing methods being shown to be influenced by the printing environment's temperatures. There is difficulty in general when choosing the correct machine temperature parameters for polymers in additive manufacturing even when the printing environment is relatively uniform and stable. An example of this is setting the material extrusion temperature, with respect to its melting temperature, in order that the desired heat dissipation, and consequent material layer height occurs with the printed part [16]. Having a manufacturing environment that experiences large temperature variation is thus expected to cause issues with the creation of additive manufacturing parts such as improper material print layer height, or other manufacturing processes [16], [17]. This is an element to in situ part creation research that must be kept in mind when creating test parts and performing material property analysis.

1.2. Using Regolith for In-Situ Manufacturing

1.2.1. Regolith Utilization for Material Creation

A way to address these challenges associated with the materials required for extraterrestrial habitats/mission parts is with in-situ part manufacturing with regolith. In-situ manufacturing using Martian regolith takes away much of the need to send large amounts of material from Earth to a body in space as it makes use of the material already on planet [3], [8]. As such, this saves the time and material cost that would be associated with the transport of Earth based materials.

A manufacturing method potentially capable of creating regolith-based materials on site is additive manufacturing. Additive manufacturing allows for the direct creation of a part or structure without the need for molds. This saves material costs given that molds do not need to be sent to the planet, and time costs as the additive manufacturing can be completed with automation, or

remote control. The benefit of not needing a direct human presence for the main manufacturing of the habitats/mission critical parts is that it saves more time, and material when planning missions to extraterrestrial bodies. The construction of the celestial body surface habitats/parts with long creation time costs can take place well in advance of any astronauts arriving on planet with robotic rovers that do not need as much shielding from the environment on that extraterrestrial body. It is theorized that regolith created structures would also be able to shield against the environment of bodies like Mars [6], [18]. This includes both the atmosphere and the radiation conditions that can be expected to be experienced on the planet. Once again, the benefit of this is the reduction of necessary Earth based materials for the creation of a properly constructed long term surface mission habitats.

Additive manufacturing can also be utilized when the astronauts arrive on the extraterrestrial body's surface. Certain new/replacement parts would be able to be created via in-situ additive manufacturing given that, again, molds are not necessary for part creation. This would allow for flexibility of part design if the mission parameters were altered and save time if a used part were to require a replacement.

1.2.2. Regolith Simulant Utilization for In-Situ Material Creation Previous Studies

1.2.2.1. General Material Creation from Regolith/Regolith Simulant

In order to increase in-situ building material radiation blocking potential, and/or decrease the mass of Earth-based material required to make usable in-situ building material, the general concept of material creation using Martian or Lunar regolith is one that has been explored in the past. In previous work, it has been demonstrated that it is indeed possible to utilize at least regolith simulant, or synthetic planetary regolith aimed at replicating one or more features of some reference sample from said planetary body [19], for material creation purposes. Past studies have

created material samples using methods such as polymerization, geopolimerization, and even the synthesis of an additive manufacturable regolith simulant "ink" used in 3D printing [20]–[22]. Each of these processes produced materials with regolith simulant that had varying mechanical properties for different, unique applications. While most of these material making methods appeared to not be suitable for in-situ manufacturing on the surface of Mars at this time, they exhibited the potential for the variety of different material applications that could be possible with regolith simulant, and potentially regolith.

1.2.2.2. Mixing Regolith Simulant with Polymers

The idea of utilizing a regolith with a polymer binding agent for the purpose of material creation has also been previously explored. The concept was usually driven by the goal to create a material that could serve as a passive galactic cosmic radiation shield around a theoretical surface habitat, though the reduction of Earth based material required for successful building material was also recognized as a benefit. In addition to acting as a binder, the addition of a polymer used in these studies was shown to increase regolith simulant's ability to shield against sources of radiation [23], [24]. This exhibited that the use of a polymer in in-situ manufacturing with regolith may have additional benefits beyond structural considerations by addressing one of the earlier mentioned challenges with long term surface space missions on extraterrestrial bodies; radiation. This illustrated the potential for use polymers along with regolith in the future development of in-situ manufacturing for space exploration. This also brought up the additional consideration of how to provide a supply of polymer on-site at an extraterrestrial body.

1.2.2.3. Extraterrestrial Body In-Situ Polymer Creation

A few papers have conceptualized ideas for in-situ polymer creation. While their findings may not be directly comparable to the mechanical characteristics that are later shown in this study, they did provide information related to the choice of polymer in this paper.

The researched methods of in-situ polymer creation attempted to perform a creation process using primarily on-site resources, again reducing the required amount of material to be shipped from Earth to make usable material at the mission site. The general consensus was that the importation of hydrogen, or water, may be necessary to create the necessary volumes of polymer on a planetary body for material utilization [23], [25], [26]. A few of the sources did cite that it may be possible to extract the necessary hydrogen, or water, from the available regolith on-site [26], [27]. The amount of hydrogen required for the creation of a theorized in-situ polymer would depend on the proposed creation process and polymer type being made.

One starting point for in-situ Martian polymer creation proposed by multiple sources was what is known as the Sabatier process [23], [25], [27]. The process was an outlined pathway and chemical reaction of converting carbon dioxide (CO_2) and hydrogen (H_2) into methane as discovered by a chemist named Sabatier as shown in Figure 1.

$$CO_2 + 4H_2 \rightarrow CH_4 + 2H_2O$$
$$2H_2O \rightarrow 2H_2 + O_2$$
$$CO_2 + 2H_2 \rightarrow CH_4 + O_2$$

Figure 1. Sabatier Chemical Reaction Pathway Outline, Reproduced from Reference [23]

The basic idea behind this reaction was to heat CO_2 from the Martian atmosphere and $4H_2$ to form water ($2H_2O$), use electrolysis to turn the water into $2H_2$ and oxygen (O_2), and then convert CO_2 and the $2H_2$ into O_2 with the byproduct of methane (CH_4). From this methane, it has been theorized that polyimide can be produced. The theory was that the methane could be converted

into benzene, and then dianhydride and diamine monomers using in-situ, and limited Earth imported processing resources. The final products would then able to be theoretically used to synthesize polyimide for the primary purpose of regolith polymer radiation shielding material [23].

Another proposed in-situ polymer whose creation was theorized to be possible with the Sabatier process was polyethylene [27]. This method again began with methane created via the Sabatier process, and then a conversion of it into polyethylene. One source achieved experimental success with this method of in-situ polymer creation and proposed the source of hydrogen as in this case being produced from water extracted from Martian regolith. In the study, polyethylene was experimentally produced from theoretical available resources on the surface of an extraterrestrial body, Mars. The source outlined the creation of polyethylene as being done by converting methane (CH_4) into ethylene (C_2H_2) via a catalytic oxidation at 800-900°C, and then producing polyethylene from the C_2H_2 using catalytic linking of the C_2H_2 monomers as performed in a slurry reactor with Ziegler-Natta catalysts [27]. According to this source, 100g of polyethylene was created using the outlined process in a laboratory setting from materials and elements theoretically available on Mars. Again, the primary purpose for creating the material was driven by an investigation for its use as radiation shielding material as mixed with regolith simulant [27]. The study demonstrated that in-situ polymer creation was theoretically possible and provided encouragement that research into additional in-situ polymer synthesis had potential for feasibility.

An additional process proposed for a Martian in-situ polymer was using what is known as the Fischer-Tropsch process [26]. This process, followed by catalyzed polymerization, was cited as being able to create polypropylene from primarily, or even entirely, in-situ resources of raw hydrogen (H_2) and carbon dioxide (CO_2). The outlined process from this study listed its source of hydrogen as coming from either importation, or extraction from Martian regolith. The eventual

hypothetically created polypropylene was recommended by the source, as compared to other potential in-situ polymers including polyethylene, to be used as a general building material in the creation of a long-term Martian habitat given its general material properties, and manufacturability in-situ [26]. This suggested another potential in-situ polymer creation method that had a chance at near complete in-situ creation capability for the specific use as a general building material.

1.2.2.4. Additive Manufacturing of Regolith Simulant Mixed with Polymer

In addressing additive manufacturing, regolith polymer material part production via additive manufacturing has also been investigated in the past. At a university in Singapore, the basic principles of such part creation were demonstrated using additive manufacturing equipment, and materials that were theorized to be available on and around an established surface Martian habitat [28].The specific materials it used were regolith simulant and a polymer created using chitosan derived from an arthropod cuticle (dried shrimp). While not completely in-situ for an initial long term mission on the planet, the source's resulting "biolith" parts demonstrated flexural strengths ranging from approximately 0.75 MPa to 1.5 MPa (following ASTM D790 Standard Test Method for Flexural Properties of Unreinforced and Reinforced Plastics and Electrical Insulating Materials), and compressive strengths from approximately 2.5 MPa to 3.5 MPa (no standard available/listed) [28]. Research such as this demonstrated the concept of a regolith polymer material being able to be potentially utilized via additive manufacturing with supporting numerical data.

An additional source experimented with the idea of additive manufacturing a potential regolith polymer mix utilized Martian regolith simulant, a polymeric binder, and water to create a slurry that could be molded and shaped in a similar manner to clay or concrete ceramics. The research study was able to successfully create ceramic parts with slip casting and other

conventional ceramic creation techniques as well as powder bed and layer wise slurry deposition via 3D printing [29]. This unique approach from the traditional concepts of additive manufactured proposed in previous studies demonstrated that additional manufacturing techniques and material elements beyond the conventional could be potential avenues of interest for this topic.

Another source that focused on a more traditional concept of regolith polymer material part production via additive manufacturing was completed in July of 2020. In investigating the ability to recycle polymers used in part creation on the surface of the Moon for resource conservation, this source successfully created 3D printed parts using polylactide (PLA) and lunar regolith simulant (CLRS-1) [30]. The resulting parts underwent tensile and bending tests according to ISO 527:2:2012 (Plastics–Determination of Tensile Properties–Part 2: Test Conditions of Molding and Extrusion Plastics) and ISO 178:2010 (Plastics–Determination of Flexural Properties). The mechanical property data values collected from these tests are shown in Figure 2 and Figure 3 along with Table 2 and Table 3.

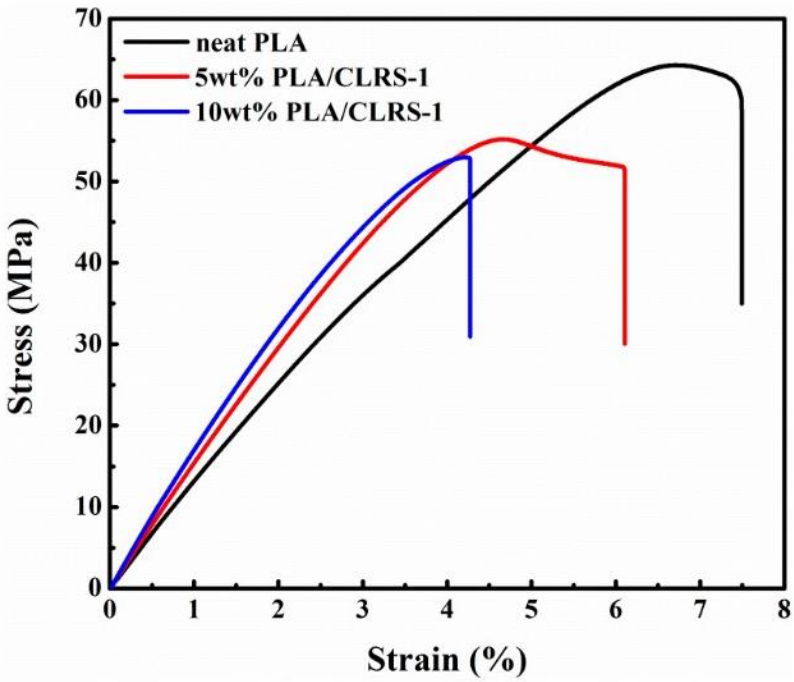

Figure 2. Source Example of Tensile Stress-Strain Curves of 3D Printed Parts Created from PLA/CLRS-1 (Lunar Regolith Simulant) and Neat PLA, Reproduced from Reference [30]

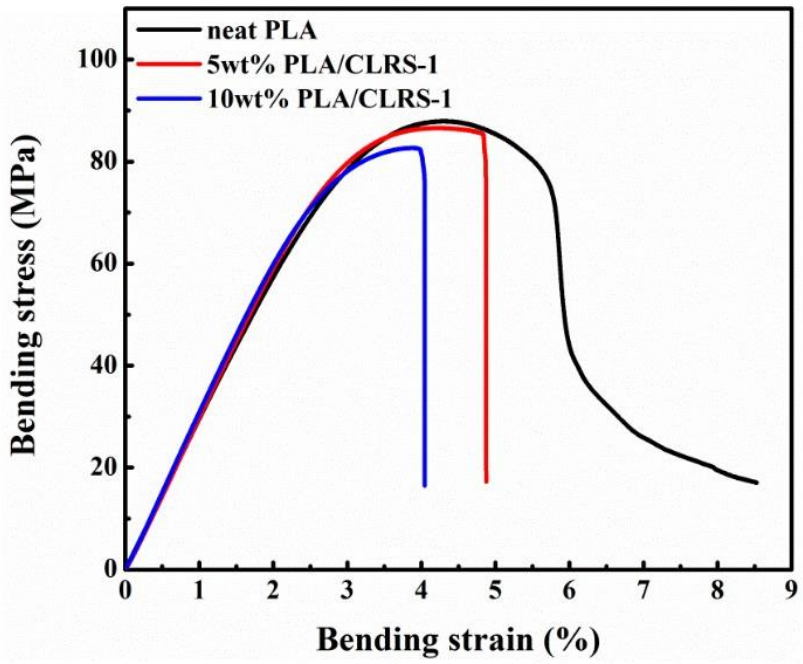

Figure 3. Source Example of Bending Stress-Strain Curves of 3D Printed Parts Created from PLA/CLRS-1 (Lunar Regolith Simulant) and Neat PLA, Reproduced from Reference [30]

Table 2. Tensile Numerical Results of 3D Printed Parts Created from PLA/CLRS-1 (Lunar Regolith Simulant) and Neat PLA, Reproduced from Reference [30]

Samples	σ_{max} (MPa)	Percent Relative Difference	ε_b (%)	Percent Relative Difference
Neat PLA	64.3 ± 3.3	-	7.49	-
5 wt% CLRS-1	55.2 ± 2.8	-14.2	6.11	-18.4
10 wt% CLRS-1	53.0 ± 2.8	-17.6	4.27	-43.0

Table 3. Flexural Numerical Results of 3D Printed Parts Created from PLA/CLRS-1 (Lunar Regolith Simulant) and Neat PLA, Reproduced from Reference [30]

Samples	σ_{max} (MPa)	Percent Relative Difference	E (GPa)	Percent Relative Difference	ε_b (%)	Percent Relative Difference
Neat PLA	88.0 ± 3.0	-	2.84 ± 0.22	-	-	-
5 wt% CLRS-1	86.6 ± 7.0	-1.55	2.96 ± 0.14	4.23	4.87 ± 0.55	-
10 wt% CLRS-1	82.7 ± 3.3	-5.98	3.05 ± 0.15	7.39	4.05 ± 0.46	-

Another recent study completed in September of 2021 experimented with the creation of Martian regolith simulant composite parts. This source investigated varying the weight loading percentages of a single Martian regolith simulant in the base polymer to see the impacts it had on various material properties such as radiation blocking potential and tensile properties. The source also investigated the viability of some of the created Martian regolith simulant composite materials to be utilized in filament fed additive manufacturing [31]. The tensile data from these specific tests and an image of the tensile parts are shown in Figure 4 and Figure 5 respectively.

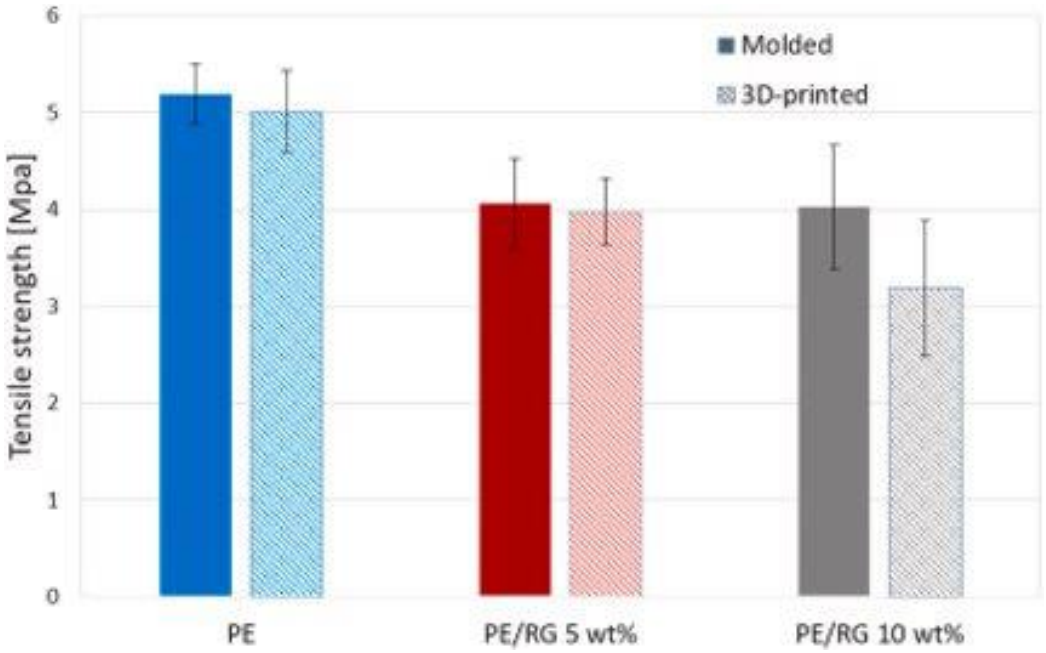

Figure 4. Source Example of Tensile Strength of Molded and 3D Printed PE, PE/RG 5 wt% and PE/RG 10 wt% Specimens (DIN EN ISO 527-2-5A), Reproduced from Reference [31]

The results shown in Figure 2 through Figure 5 and Table 2 through Table 3 provided numerical data to begin to describe the potential mechanical characteristics of parts created in-situ on the Moon and Mars via additive manufacturing. They also illustrated a difference in material performance of created parts based on the amount of regolith simulant used compared to the amount of polymer used.

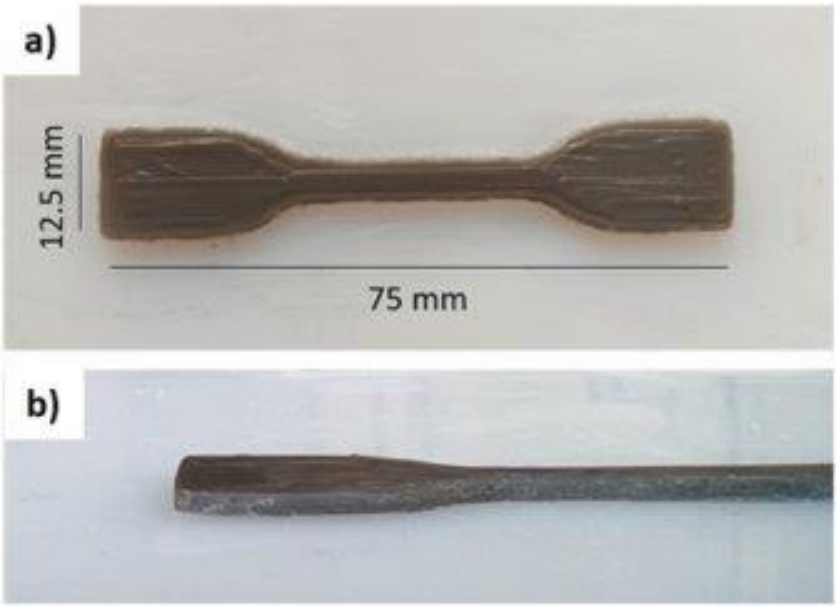

Figure 5. Source Example of (a) Top and (b) Lateral View of Tensile Specimen (DIN EN ISO 527-2-5A) of PE/RG 5 wt% Composite Fabricated by 3D Printing, Reproduced from Reference [31]

In general, the data shown in Figure 2 through Figure 5 and Table 2 through Table 3 suggested that increasing the weight loading percentage of regolith simulant in the used polymer decreases the material strength characteristics of the created parts. Such information was an important inclusion in the constantly growing material database associated with the future of space exploration on extraterrestrial bodies. Understanding what kinds of material properties that can be expected from any theoretically created in-situ material provides engineers and scientists data that can help in long-term mission design. It also raises the question of what other material characteristics are possible based on the ratio of regolith (or regolith simulant) to polymer.

1.2.2.5. Specific Regolith Simulant Validity Concern Highlight

An important note in studies related to space based in-situ material creation is the validity of the raw materials. Specifically, the accuracy of any collected data depends heavily on the accuracy of any used regolith simulant. Some regolith in-situ part creation studies have utilized a

singular or different type of regolith simulant than that to be used in this study. In addition, a certain regolith simulant used by a number of these sources had properties that have since been questioned in terms of their validity in representing regolith [20]–[22], [24], [27], [32]. In particular, the use of JSC-1A regolith simulant in past studies caused concern as to the compatibility and validity of a study's results due to its known high, and unrealistic amount of water content [33]. This must be kept in mind when utilizing data from these sources for the purposes of the supporting of, or comparison to findings/conclusions of this paper's research.

1.2.2.6. Closing Literature Comments

In general, the previously completed research related to the subject of utilizing regolith for material creation from these sources provided items of background information, and specific pieces of material data that were helpful in approaching this research. The previous studies demonstrated the potential for regolith simulant to be used to create building material for a theoretical surface missions to extraterrestrial bodies such as the Moon and Mars, polymers to be used as binding and increased radiation blocking agents in regolith simulant composite parts, certain polymers to be created in-situ on the surface of Mars using the raw materials that have been detected on the surface of the planet, and the possibility of single type regolith simulant based polymeric composite materials to be additive manufactured into load bearing test parts using varying amounts of regolith simulant filler to reduce the amount of polymer required for the creation of mechanical parts. This data from the previous research gave a greater context to the data collected, and conclusions made from this study.

An aspect of this general topic that did not appear to have received much research by previous studies was if the type of regolith simulant on a single extraterrestrial body had an

impact on any created materials' mechanical properties, especially when parts were created using additive manufacturing techniques. It was this aspect that this research focused on.

CHAPTER 2. OBJECTIVES

2.1. Goals of Research

The primary short-term goal of the research was to document the material property data of regolith simulant-based polymeric composite parts using varying types of Martian regolith simulants, or source locations, and manufacturing techniques. This involved creating parts with Earth based injection molding, and fused granulate fabrication (FGF) additive manufacturing to simulate in-situ part creation for the categorization of the created polymeric composite materials.

Achieving the short-term goal of this research was the first step in realizing the primary long-term use goal of the research, which was providing data that would help in the eventual designing of a rover/machine that could be sent to an extraterrestrial body to collect regolith, process regolith (extract polymer base components/create polymer/mix regolith with polymer) and create building materials from regolith for the purpose of human habitat construction, and later mission required part production.

The data collected for the secondary long-term goal of the research was to serve as a baseline material database for future projects and research involving material creation with regolith simulants. Such a database, while limited by the accuracy of the regolith simulants, would provide material property values that could be compared to when creating different materials from/incorporating regolith simulant. In the far future, the database of values could be used in a comparison to parts created utilizing actual regolith in-situ.

2.2. Objectives of Research

In-situ resource utilization on extraterrestrial bodies will be required to provide the most economical, and time efficient missions to the planet. This technology, and the technology of the infrastructure to stay on the surface of Mars for any significant amount of time, will also require

additional research and development before the transportation of astronauts for long term surface missions can take place [9], [10], [34].

Based on the available data, regolith has the potential to be an in-situ resource that could be used for multiple applications. This includes habitat building, water extraction, and fuel creation [10], [35]. As stated before, the technology for how to accomplish this on Mars is still in development. This research focused on the material applications of regolith. Specifically, the study looked at creating, and testing composite materials from thermoplastic polymers and a variety of Martian regolith simulant (MRS) fillers. It also investigated the ability to create sample parts from these Martian regolith simulant composites (MSCs) using injection molding (IM) and FGF additive manufacturing (AM).

The resulting material properties and processes involved in this process were anticipated to depend on the type of regolith simulant selected (simulating regolith taken from different locations on the extraterrestrial body), and the amount of MRS loaded into the neat polymer. The benefit of such research was anticipated to be the documentation of a metric for the material potentials of regolith sources to be eventually used for the creation of material processing/creation rovers utilizing regolith, and extraterrestrial in-situ additive manufacturing standards.

2.2.1. Experimental Goals

- Create part samples from neat polymer and regolith simulant filled polymer composites using Earth based manufacturing techniques
- Create part samples from neat polymer and select regolith simulant filled composites using additive manufacturing techniques
- Characterize material properties of the neat polymer and composite materials utilizing ASTM standards

2.2.2. Analytical Goals

- Determine effect of MRS loading on material properties
- Determine effect of MRS source location on material properties

2.2.3. Intended Outcomes

- Data collected from usable part samples indicates which MSC has suggested best strength material characteristics at largest wt. % loading of MRS over part samples created with other types of regolith simulant
- Data collected from usable part samples indicates which MSC has suggested most consistent material characteristics (lowest standard deviation) at largest wt. % loading of MRS over part samples created with other types of regolith simulant
- Additive manufacturing techniques used in study are shown to be able to consistently produce usable neat PP, and MSC parts
- Data collected from additive manufactured parts provides insight to the compatibility of data collected from parts made using Earth based manufacturing techniques

CHAPTER 3. MATERIALS AND PROCESSING

3.1. Materials

The raw materials used in this research were selected based on what each element of the study required. These raw materials underwent a series of initial tests to check that their properties qualified for the study.

3.1.1. Neat Polymer

The polymer used in this research was polypropylene. It was selected based on its potential for in-situ extraterrestrial application as compared to other types of polymers. The specific benefits that this type of polymer offered were its general material properties, availability for testing, and potential for in-situ creation [26]. This polymer was used in the creation of the part samples made from the polymer and MRS for the purposes of testing the regolith simulant material characteristics. The specific type of polypropylene used was COPYLENE® CH014 homopolymer polypropylene from Bamberger Polymers and Phillips 66. This particular polypropylene was chosen as it was a neat homopolymer and had a listed mass flow index of 1.3 g/10 minutes which was anticipated to beneficial for extrusion/compounding and additive manufacturing.

Polymer that was already created using Earth based manufacturing techniques was used in this research instead of lab created polymer from the theoretical base elements that could be extracted from regolith/regolith simulant and other available in-situ resources available on Mars. This was done as it was anticipated that any amount of successfully extracted polymer from the regolith simulant and other in-situ resources available on Mars completed in a laboratory setting would be small in comparison to the amount necessary to use in the creation of regolith simulant based polymeric composite test parts.

3.1.2. Martian Regolith Simulants

As of the time of this research, no sample of Martian regolith has been brought to Earth for study/research. The study made use of MRS as a substitute for Martian regolith. The simulants used were developed by the CLASS Exolith Lab of the University of Central Florida [36], [37]. Table 4 through Table 15 detail the particle size information, minerology, and bulk chemistry of the simulants.

Table 4. MGS-1 Particle Size Information, Reproduced from Reference [37]

MGS-1 Particle Size Information	
Particle Size Range [mm]	0-1
Mean Particle Size [μm] (by Volume)	105
Bulk Density [g/cm^3] (Depending on Compaction Level)	~1.29

Table 5. MGS-1 Minerology (weight percent, as mixed), Reproduced from Reference [37]

Mineral	**Wt. %**
Plagioclase	27.1
Basaltic glass	22.9
Pyroxene	20.3
Olivine	13.7
Mg-sulfate	4.0
Ferrihydrite	3.5
Hydrated silica	3.0
Magnetite	1.9
Anhydrite	1.7
Fe-carbonate	1.4
Hematite	0.5

Each MRS was designed to simulate a particular type of Martian regolith as varied by physical location on the surface of the planet. MGS-1 was designed to simulate Rocknest windblown soil, MGS-1C simulated MGS-1 enriched with smectite, MGS-1S was created to simulate MGS-1 enriched with polyhydrated sulfate gypsum, and JEZ-1 simulated the anticipated materials in the Jezero Crater deltas in advance of the 2020 NASA Mars rover [37].

Table 6. MGS-1 Bulk Chemistry (weight percent, as measured by XRF), Reproduced from Reference [37]

Oxide	Wt.%
SiO_2	45.57
TiO_2	0.30
Al_2O_3	9.43
Cr_2O_3	0.12
FeO_T	16.85
MgO	16.50
CaO	4.03
Na_2O	3.66
K_2O	0.43
P_2O_5	0.37
SO_3	2.63
MnO	0.1

Table 7. MGS-1S Particle Size Information, Reproduced from Reference [37]

MGS-1S Particle Size Information	
Particle Size Range [mm]	0-1
Mean Particle Size [µm] (by Volume)	119
Bulk Density [g/cm^3] (Depending on Compaction Level)	N/A

Table 8. MGS-1S Minerology (weight percent, as mixed), Reproduced from Reference [37]

Mineral	Wt. %
Gypsum	40.0
Plagioclase	16.4
Basaltic glass	13.7
Pyroxene	12.2
Olivine	8.2
Mg-sulfate	2.4
Ferrihydrite	2.1
Hydrated silica	1.8
Magnetite	1.1
Anhydrite	1.0
Fe-carbonate	0.8
Hematite	0.3

Table 9. MGS-1S Bulk Chemistry (weight percent, as measured by XRF), Reproduced from Reference [37]

Oxide	Wt.%
SiO_2	29.3
TiO_2	0.30
Al_2O_3	6.4
Cr_2O_3	0.1
FeO_T	11.3
MgO	16.2
CaO	14.8
Na_2O	2.1
K_2O	0.5
P_2O_5	0.3
SO_3	18.7
MnO	0.1

Table 10. MGS-1C Particle Size Information, Reproduced from Reference [37]

MGS-1C Particle Size Information	
Particle Size Range [mm]	0-1
Mean Particle Size [µm] (by Volume)	N/A
Bulk Density [g/cm^3] (Depending on Compaction Level)	N/A

Table 11. MGS-1C Minerology (weight percent, as mixed), Reproduced from Reference [37]

Mineral	Wt. %
Smectite	40.0
Plagioclase	16.4
Basaltic glass	13.7
Pyroxene	12.2
Olivine	8.2
Mg-sulfate	2.4
Ferrihydrite	2.1
Hydrated silica	1.8
Magnetite	1.1
Anhydrite	1.0
Fe-carbonate	0.8
Hematite	0.3

Table 12. MGS-1C Bulk Chemistry (weight percent, as measured by XRF), Reproduced from Reference [37]

Oxide	Wt.%
SiO_2	56.1
TiO_2	0.2
Al_2O_3	16.9
Cr_2O_3	0.0
FeO_T	8.2
MgO	12.6
CaO	2.0
Na_2O	1.9
K_2O	0.5
P_2O_5	0.4
SO_3	1.2
MnO	0.0

Table 13. JEZ-1 Particle Size Information, Reproduced from Reference [37]

JEZ-1 Particle Size Information	
Particle Size Range [mm]	0-1
Mean Particle Size [µm] (by Volume)	38
Bulk Density [g/cm^3] (Depending on Compaction Level)	1.54

Table 14. JEZ-1 Minerology (weight percent, as mixed), Reproduced from Reference [37]

Mineral	Wt. %
Olivine	32.0
Plagioclase	16.0
Basaltic glass	13.5
Pyroxene	12.0
Mg-carbonate	11.0
Smectite clay	6.0
Mg-sulfate	2.4
Ferrihydrite	2.1
Hydrated silica	1.8
Magnetite	1.1
Anhydrite	1.0
Fe-carbonate	0.8
Hematite	0.3

Table 15. JEZ-1 Bulk Chemistry (weight percent, as measured by XRF), Reproduced from Reference [37]

Oxide	Wt.%
SiO_2	44.2
TiO_2	0.2
Al_2O_3	11.3
Cr_2O_3	0.3
FeO_T	9.5
MgO	25.9
CaO	3.5
Na_2O	1.9
K_2O	0.3
P_2O_5	0.6
SO_3	2.1
MnO	0.1

The specific makeup of each of the used MRSs was based off data collected from previous information gathering missions to Mars including the MSL Curiosity rover [37]. An image that provided a general visual representation of some the variation detected in Martian regolith composition on the Martian surface is shown in Figure 6.

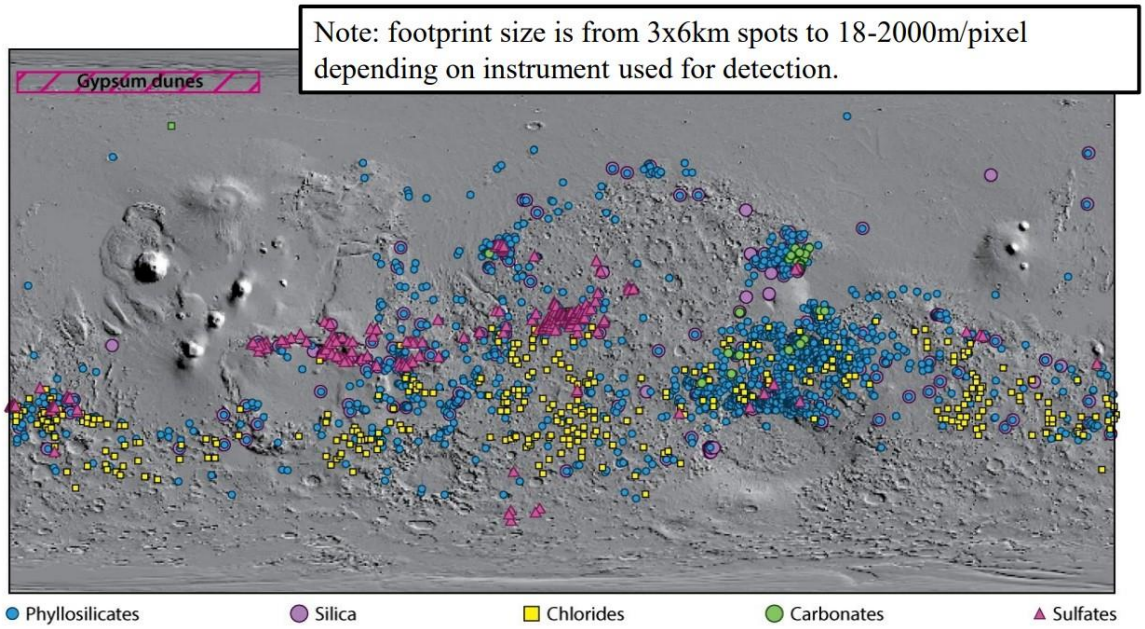

Figure 6. Mineral Detection Compilation for Mars Image from NASA Associated Mars Water In-Situ Resource Utilization (ISRU) Planning (M-WIP) Study as Cited by Exolith Lab, Reproduced from Reference [38]

3.1.3. Pre-Sample Regolith Simulant Material Analysis

The MRSs used in material test part creation were analyzed in advance of sample creation. This was done to provide data that would aid in determining the correct experimental settings for the machines to be used to create the material samples and indicate any potential areas of issue regarding the MRSs' ability to go through manufacturing processes.

3.1.3.1. Preliminary Thermogravimetric Analysis of Martian Regolith Simulant

The general MRS, MGS-1, that was the basis for all the MRSs utilized in this research was subjected to a Thermogravimetric Analysis (TGA). This involved loading small samples (50-100 mg) of the general extraterrestrial body's simulant (MGS-1) into a TA Instruments Q500 TGA and heating it from room temperature (~22°C) to a temperature of 500°C at a rate of 10°C per minute. The testing environment for each type of simulant was varied for certain tests from being a completely inert gas (Nitrogen) to 40% Nitrogen, and 60% room air.

The goal with each of these tests was to gain data that directly characterized each type of simulant's response to an increase in heat. This was anticipated to provide information as to if there would be any material degradation during any thermal based manufacturing processes. The tests would also provide data useful in determining if the additive manufacturing material creation process could potentially be used by astronauts inside as well as outside of an extraterrestrial habitat.

Figure 7 and Figure 8 display the results of the tests performed on the MRS MGS-1 in an environment of 100% Nitrogen, and an environment with a mixture of 40% Nitrogen and 60% room air.

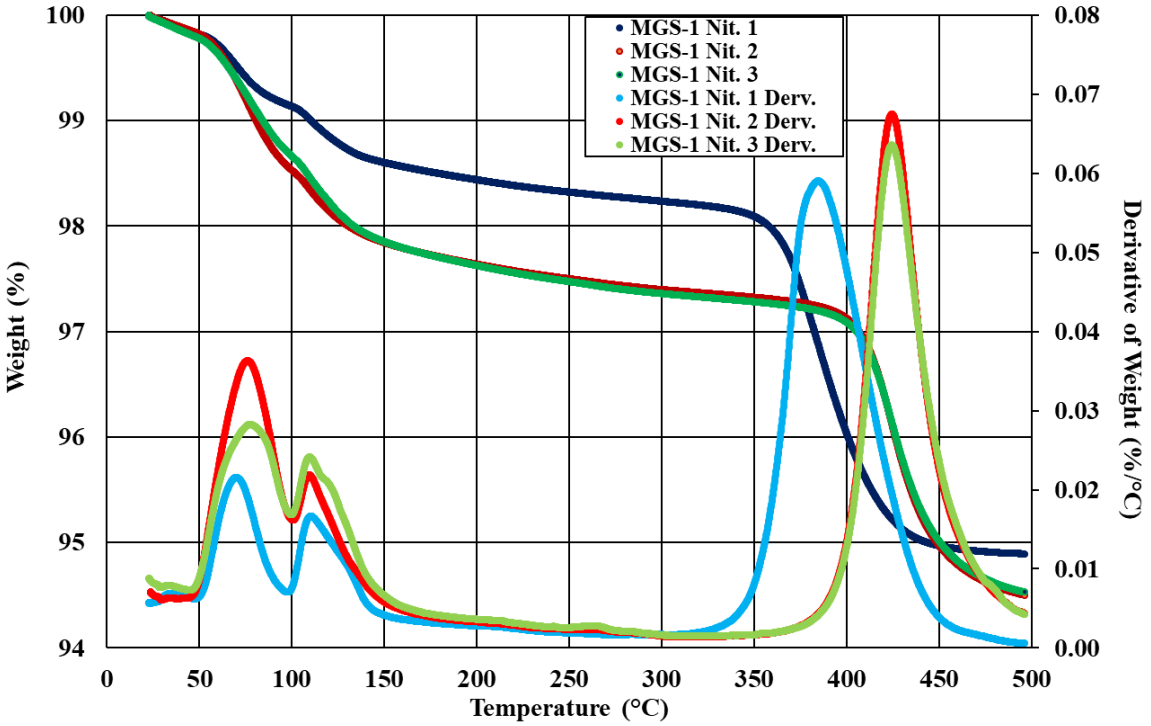

Figure 7. TGA Test Results Overlay MGS-1 in 100% Nitrogen Environment

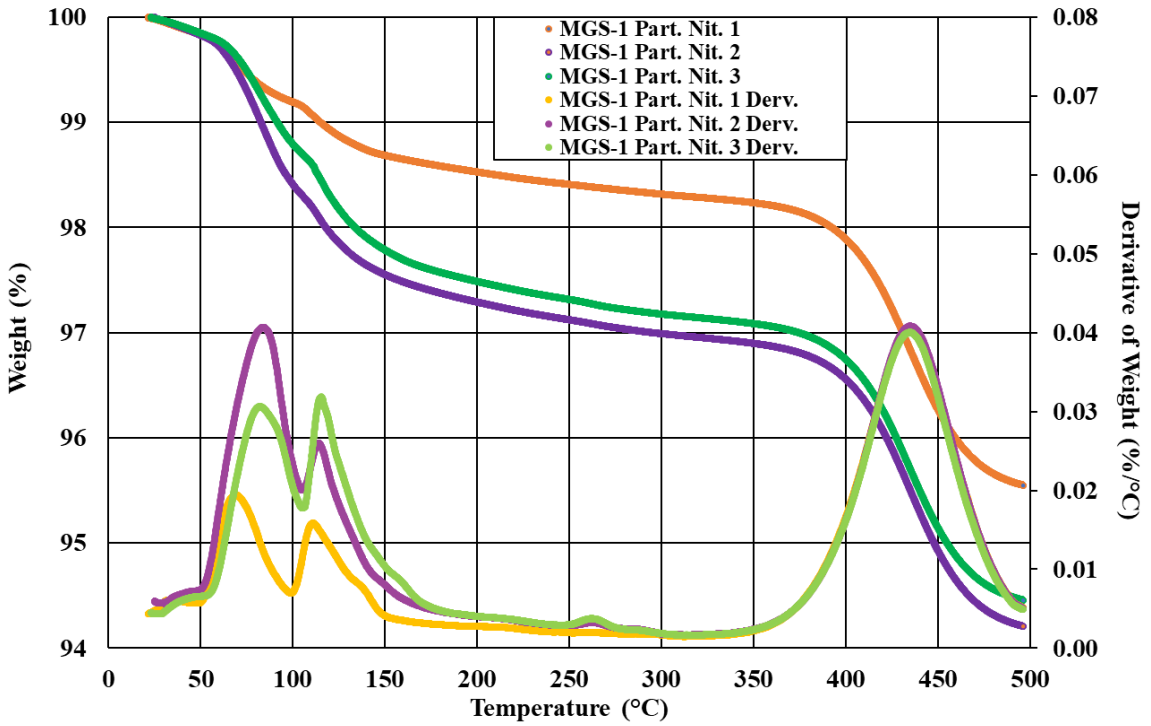

Figure 8. TGA Test Results Overlay MGS-1 in 40% Nitrogen, 60% Room Air Environment

Figure 7 and Figure 8 suggested that the MGS-1 simulant appeared to experience approximately 5% weight percent mass loss from being heated up to 500°C as tested in both atmospheres. This result indicated that this MRS, and its constituents, would be able to be used in material creation methods involving thermal processing with little concern for impact on created parts' material properties from constituent degradation due to heat.

An initial, brief thermal decomposition study of the MRS individual constituents was completed to offer an explain of what mass loss was seen in Figure 7 and Figure 8. The initial mass loss at about 100°C was theorized to be due to some moisture present in the samples at the time of testing evaporating from that temperature as all MRS TGA samples received no drying prior to being tested after being removed from the sealed storage/shipping bag. This was supported by the boiling point of water being approximately 100°C, as well as by previous work done in material and mineral thermal decomposition studies [39]–[41]. It was also possible that MRS constituent hydrated silica saw some thermal decomposition into water and silica at this temperature [40]–[42]. Another one of the present constituents was olivine which was suggested to be capable of experiencing a release of oxygen at temperatures around 200°C when elements of carbon or hydrogen are present (both of which were present in one or more of the other constituents) [43]–[45]. This was theorized to be the possible reason for the gradual mass loss seen in Figure 7 and Figure 8 from 150°C to 350°C. Of the other present minerals in MGS-1, ferrihydrite and Fe-carbonate were found to have sources that suggest they were both capable of experiencing thermal decomposition in the temperature range (approximately 350°C to 500°C) in which the second drop in mass took place [46]–[50]. At these temperatures, Ferrihydrite can decompose into hematite [46], and Fe-carbonate can decompose into magnetite [48], [50]. The releases of these decompositions include water (H_2O) [46] and carbon dioxide/other oxides [50] respectively. In

addition to the information found on the raw constituents, the overall MGS-1 was noted in its technical and safety data sheets as being capable of releasing a number of volatiles as a response to heat, specifically when combusted. These volatile releases were cited as carbon monoxide, carbon dioxide, sulfur monoxide, sulfur dioxide and methane [37]. All of these items were theorized to provide likely candidates for the mass loss seen in the tested samples of MGS-1 as a response to heat.

The presented sources in the initial thermal decomposition investigation provided evidence to suggest what most likely took place during the second drop in mass during the thermogravimetric study of MGS-1. In order to determine which minerals experienced more/less thermal decomposition and released how much of a particular thermal decomposition byproduct or volatile release was created during this second major drop in mass, additional experimentation specifically dedicated to this topic would be required. It was predicted that the low amount of overall mass loss would translate to a negligible amount thermal decomposition of constituents in terms of their overall impact on the quality of any created materials, and release of any potentially hazardous volatile releases for safe operating procedures when working with the created material constituents.

To verify that the weight percent loss of the material did not continue to increase by a significant amount at temperatures higher than 500°C, an additional TGA test was performed on a sample of MGS-1. The test performed took place over a temperature range of approximately 22°C to 1000°C with a heating rate of 10°C per minute in an environment of 100% Nitrogen. Figure 9 displays the results from this test.

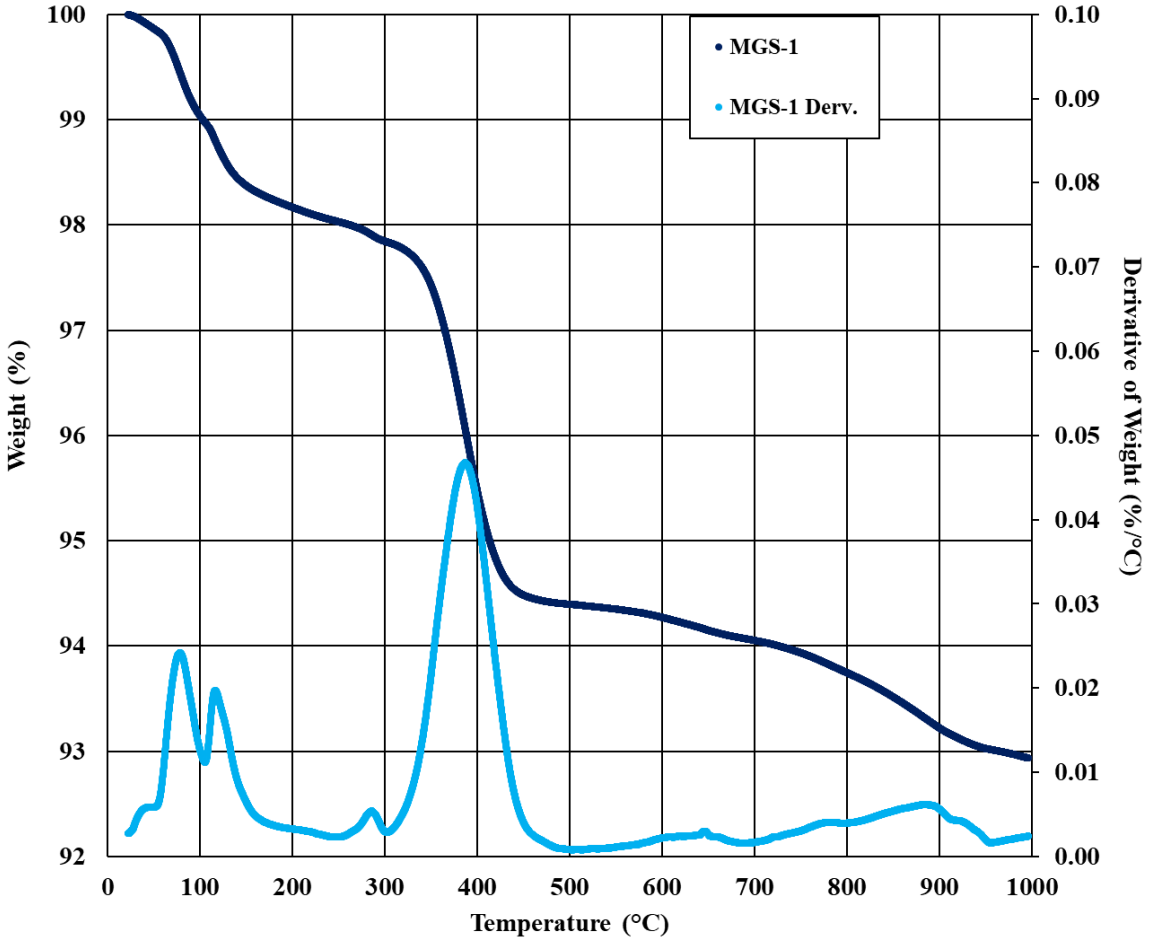

Figure 9. TGA Large Temperature Range Test Results MGS-1 in 100% Nitrogen Environment

Figure 9 indicated that the total MGS-1 weight percent mass loss was approximately 7% as experienced over a temperature range of 22°C to 1000°C. This weight percent mass loss seen in the regolith simulant suggested that even when the maximum temperature seen by this regolith simulant is increased to 1000°C from 500°C, the resulting material degradation would not affect created parts' material properties made by material creation methods involving thermal processing operating near this temperature. This provided further support to the idea that the MRSs could be relied upon when incorporated into the neat polymer to provide consistent sample parts when processing the material with thermal based manufacturing techniques.

3.1.3.2. Thermogravimetric Analysis Material Breakdown Study Special Note

An original purpose for performing a thermogravimetric analysis on the regolith simulant was to investigate the mass loss seen in the material. The goal was to find a temperature at which a large amount of percent mass loss was experienced in a material sample which would indicate the need for pre-processing of the regolith simulant to remove any volatility in the material's overall structure. Any severe material breakdown was predicted to be detrimental to any parts made of the created MSC material via additive manufacturing.

The idea for the mass loss investigation came from a source that presented data that showed more than 20% mass loss seen in an MRS after a similar thermal test [3]. Figure 7 through Figure 9 above show that the same level of percent mass loss seen in this source was not achieved with this regolith simulant. Figure 7 through Figure 9 also suggested that the amount of percent mass loss seen in the samples was not significant enough to suggest volatile behavior of the material, or constituent material breakdown, that would cause improper part creation via the proposed additive manufacturing process and its manufacturing temperatures.

An investigation of the cited source revealed a MRS with known high concentrations of water was used for its study. The high amount of water present in this MRS was cited as being a potential source of error in replicating the characteristics of true Martian regolith [33]. This suggested that the results of the original source were not enough to serve as a basis for its own study.

The information gathered from this investigation was still useful for the purposes of adding context to this research. The thermogravimetric analysis results provided data that was helpful in characterizing/documenting the raw regolith simulant to be used in material creation. The results also gave direct evidence that suggested the creation of parts using regolith should be relatively

unchanged when comparing the results from an inert gas environment, and an environment in which oxygen was present (as would be seen in an extraterrestrial astronaut habitat).

3.1.3.3. Regolith Simulant Mohs Hardness Analysis

The highest value of Mohs hardness of the used regolith simulants was analyzed before material processing. The purpose was to verify that the MRS material did not contain constituents with hardness values that would require specialized processing equipment. The investigation started with finding the Mohs hardness value of each constituent that made up the MRS along with its weight percentage in the MRS. The constituent(s) with the highest Mohs hardness value along with its hardness value and weight percentage were then recorded in a table. Following this process, all of the regolith simulants used were found to contain the values shown in Table 16.

Table 16. Martian Regolith Simulant Constituent Highest Mohs Hardness Values and Weight Percentages

Regolith Simulant Type	Highest Hardness Value Mineral	Hardness (Mohs)	Weight Percentage (%)
MGS-1	Olivine	7	13.7
	Hydrated Silica	7	3.0
MGS-1C	Olivine	7	8.2
	Hydrated Silica	7	1.8
MGS-1S	Olivine	7	8.2
	Hydrated Silica	7	1.8
JEZ-1	Olivine	7	32.0
	Hydrated Silica	7	1.8

The highest Mohs hardness value for all of MRSs as compared to the rest of the hardness values found for all of each simulant's other constituents was 7.0 [37], [51], [52]. In comparison, fiber glass has a Mohs hardness value of approximately 5 to 7 [53] and can be processed on standard plastic processing equipment. Given that the highest Mohs hardness values of the MRSs were comparable to fiber glass, the raw constituents of the MRSs for this study were considered safe for use in the available material processing equipment.

3.2. Processing

The test specimens made from MSCs were created using conventional and additive manufacturing techniques. This allowed the test polymeric composite materials to be made according to ASTM standards for material testing and comparison. The processing procedures used are outlined in the following section.

3.2.1. Twin Screw Extrusion

The MRSs and polymer were compounded in a Leistritz Micro-18/GL-40D, co-rotating twin-screw extruder to produce MSC pellets. The MRS weight percentage (wt.%) loading values used in the polymeric composite materials were 10 wt.%, 20 wt.%, 30 wt.%, and 40 wt.% for each simulant type/source location. The process in producing the simulant composites involved mixing the predetermined mass amounts of polymer and MRS in sealed plastic bags by hand in batches of approximately 1 kg. The mixed raw materials were then compounded using the extruder and an auxiliary pelletizer to create pelletized MSCs. The general extruder temperature profile used was 210, 216, 221, 227, 232, 232, 232, 232, 227°C from the feeder section to the die. The screws rotated at 200 revolutions per minute (RPM) during all MSC production. The pelletized simulant composite was dried in a convection oven for approximately 12 hours at a temperature of 80°C after extrusion/pelletizing was completed to remove as much surface moisture from the pellets as possible before used for any sort of part creation process or material analysis.

For additive manufacturing, a similar process to what was described in the previous paragraph was used to create MSCs. The differences in the process were the creation of MSCs being only done with select MRSs, and an increase of the batch sizes from 1 kg to approximately 2.5 kg.

3.2.2. Injection Molding

Injection molded test samples made from simulant composite pellets were created using a FCA FA-100 SV servo hydraulic 100-ton injection molding machine. The injection molder utilized a single screw with a series of heating zones and an injection nozzle. The temperature settings of the heating zones from the feeder to the injection nozzle were 221, 227, 232, 232, 227°C. In addition, a mold temperature of approximately 38°C was maintained using an auxiliary oil-based mold heater attached to the injection molder. The machine settings, specifically the cushion value, saw minor alterations as needed for certain MRS loading values. The shapes of the injection molded samples were tensile dog bones and rectangular flexural bars with thicknesses of approximately 3.2 mm according to ASTM standards.

The reason for the use of an Earth based injection molding process to produce sample parts for this research was to efficiently obtain material data about the various simulant composites from which general comparisons could be made. The anticipated result of these comparisons was the indication of simulant source locations and wt. % loading levels that would produce usable test parts, and the most promising material characteristics for part creation when mixed with a polypropylene.

3.2.3. Additive Manufacturing

A re:3D, Terabot X additive manufacturing printer (TBX) was utilized for the creation of MSC samples. The TBX used was classified as a fused granulate fabrication printer (FGF), meaning that it used pelletized material for its feedstock in the creation of additive manufactured parts. The use of an additive manufacturing printer in this study was critical to experimenting the feasibility the project's results. According to one source, "The most important technological development that must be made for the creation of an in-situ Martian habitat is an autonomous 3D

assembler" [26]. This is due to a lack of conventional infrastructure for the creation of materials in-situ on Mars. The equipment necessary to perform conventional material creation on any extraterrestrial body is, at the time of writing this study, prohibitively expensive from a monetary and resource standpoint. Thus, additive manufacturing would be the recommended approach to material/habitat creation on extraterrestrial bodies as it would allow for a relatively small mass of equipment to be sent to said body and still allow for high variability in terms of creatable part types. This encourages that any MSC part created for material experimentation and categorization be made at some point using an additive manufacturing machine.

A general cutaway image of a FGF additive manufacturing machine is shown in Figure 10. The image from Figure 10 contains multiple numbered elements that each highlight an aspect of the FGF machine. At element one, a gravity fed hopper is used to input raw polymer pellets into the machine. The pellets are moved by gravity until reaching the extrusion screw, element two, which moves, shears, and mixes the polymer pellets through the extrusion barrel. Element three points to the extrusion barrel with heating elements through which the polymer pellets move through to be melted and mixed prior to reaching the print nozzle. At the print nozzle, element four, the melted and mixed polymer is extruded out onto either the print bed, element five, or previously deposited polymer. In cases where parts being created require support for their overall structure, the creation of support or infill material highlighted by element six is occasionally present as a part of an additive manufactured part [54]. The TBX used for this research utilized the same general procedure outlined in Figure 10 for its FGF.

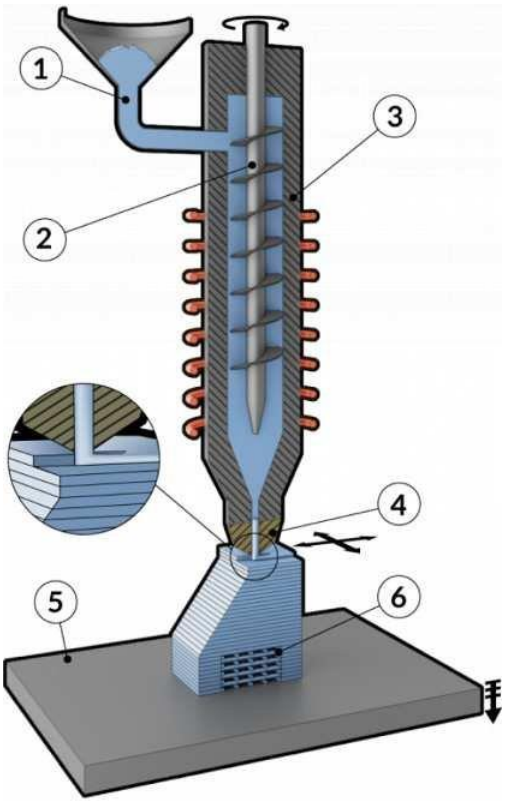

Figure 10. General FGF AM Machine Diagram with Numbered Elements, Reproduced from Reference [54]

Using the data collected from the injection molded parts, a select number of MRS source locations and wt. % loading levels were chosen to be used in the creation of additive manufactured sample parts. It was anticipated this process would provide results more accurate in their representation of part manufacturing in-situ on an extraterrestrial body and allow for created part material characteristic comparisons with MSC parts created via Earth-based injection molding. The reasons for not producing MSC parts via additive manufacturing for all the different MRS wt. % loading levels and source locations were the anticipated time requirements of the additive manufacturing process being beyond those available for this research and the possibility of certain MSC materials showing indications of not being able to be used for part creation via additive manufacturing. The selected MSC materials for additive manufacturing were those that contained 40 wt. % of MGS-1 and MGS-1C. The lower wt. %s of MRS were not selected for AM as they

did not offer the highest potential for mass savings during Martian surface missions. The sulfate based MRS was eliminated due to material behavior that was anticipated to be challenging for successfully creating AM parts. The Jezero based MRS was eliminated due to its material properties being similar or less than the other candidate materials, and time constraints on the research. A later section went into more detail regarding the selection process for AM materials. The specific settings used with the Terabot X printer were recorded in Table 17 through Table 19.

Table 17. TBX Machine Settings Used for Neat PP Part Creation

	Izod Type A	**Flexural**	**Tensile**
Nozzle Size (mm)	0.8	0.8	0.8
Heat Zone 1 (°C)	267 (±2)	267 (±2)	267 (±2)
Heat Zone 2 (°C)	200	200	200
Heat Zone 3 (°C)	165	165	165
Bed Temperature (°C)	105	105	105
Bed Adhesive	Magigoo PP	Magigoo PP	Magigoo PP
Feedstock Print Rate (mm/min.)	1300	1300	1000
Script E# Calibration	E60	E60	E60
Print Environment	Enclosed Print Area with Openings to ~22°C Atmospheric Earth Air	Enclosed Print Area with Openings to ~22°C Atmospheric Earth Air	Enclosed Print Area with Openings to ~22°C Atmospheric Earth Air
Infill Percentage	100	100	100
Minimum Number of Specimens	6	5	5

The creation of sample parts was considered successful if the parts were consistent in size, and shape according to ASTM standards. It should be noted that these parameters were only considered valid for parts created in an environment of standard Earth atmosphere with a temperature of ~22°C. This followed the process of recording the specified information as recommended for any future incorporation of this data in a standard.

The additive manufactured parts created were tested according to the same/similar respective ASTM standards as with the MSC injection molded sample parts. This was done to collect data on

the candidate additive manufactured sample parts that could allow for some comparison to the data collected from the injection molded sample parts of the same MRS wt. % loading and source location.

Table 18. TBX Machine Settings Used for MSC-40G Part Creation

	Izod Type A	**Flexural**	**Tensile**
Nozzle Size (mm)	2.85	2.85	2.85
Heat Zone 1 (°C)	267 (±2)	267 (±2)	267 (±2)
Heat Zone 2 (°C)	200	200	200
Heat Zone 3 (°C)	165	165	165
Bed Temperature (°C)	105	105	105
Bed Adhesive	Magigoo PP	Magigoo PP	Magigoo PP
Feedstock Print Rate (mm/min.)	200	200	200
Script E# Calibration	E46-47	E45	E43
Print Environment	Enclosed Print Area with Openings to ~22°C Atmospheric Earth Air	Enclosed Print Area with Openings to ~22°C Atmospheric Earth Air	Enclosed Print Area with Openings to ~22°C Atmospheric Earth Air
Infill Percentage	100	100	100
Minimum Number of Specimens	6	5	5

Table 19. TBX Machine Settings Used for MSC-40C Part Creation

	Izod Type A	**Flexural**	**Tensile**
Nozzle Size (mm)	2.85	2.85	2.85
Heat Zone 1 (°C)	267 (±2)	267 (±2)	267 (±2)
Heat Zone 2 (°C)	200	200	200
Heat Zone 3 (°C)	165	165	165
Bed Temperature (°C)	105	105	105
Bed Adhesive	Magigoo PP	Magigoo PP	Magigoo PP
Feedstock Print Rate (mm/min.)	200	200	200
Script E# Calibration	E45	E43-44	E41
Print Environment	Enclosed Print Area with Openings to ~22°C Atmospheric Earth Air	Enclosed Print Area with Openings to ~22°C Atmospheric Earth Air	Enclosed Print Area with Openings to ~22°C Atmospheric Earth Air
Infill Percentage	100	100	100
Minimum Number of Specimens	6	5	5

3.2.3.1. Martian Regolith Simulant Particle Size Distribution Through Nozzle Analysis

A major component of creating polymeric particulate composite test parts via additive manufacturing was taking into account the particle size distribution of the used MRS. Understanding this was important in selecting an appropriate nozzle size to use when creating 3D printed parts. The MGS-1 SDS sheet from Exolith Labs listed that the simulant had a mean particle size of 90 µm, median particle size of 60 µm, and a particle size range from >0.04 µm to 600 µm [37].

In theory, the particle size distribution of MGS-1 contained enough large particles to be concerning for proper material flow during 3D printing through small nozzle sizes. It was anticipated that large and small particle consolidation at the nozzle tip could result in a reduced, or completely halted composite material flow for the smaller printer nozzles available for TBX (specifically 0.8 mm and 1.75 mm diameter nozzles). The chance of this occurrence was predicted to become greater with high weight loading percentages of MRS in the PP such as in the case of 40 wt. % loadings of MRS.

In practice, the initial MSC material with 40 wt. % MRS extrusion through the TBX using a 0.8 mm diameter nozzle resulted in a clogged nozzle that stopped polymeric composite material flow and lead to motor skipping on the machine. Given general particle size distribution and high weight loading percentage of the MRS in the PP, it was anticipated a similar occurrence was also possible with a 1.75 mm diameter nozzle. The 1.75 mm diameter nozzle was also not available at the time of collecting research data. As such, a 2.85 mm diameter nozzle was installed for printing the MSCs with 40 wt. % of MRS. This nozzle allowed for proper polymeric composite material extrusion with the TBX as utilized for 3D printing test parts.

3.2.3.2. Neat Polymer Part Creation Nozzle Size Analysis

The creation of the additive manufactured parts with neat PP required the use of a smaller nozzle size, 0.8 mm, from that used for polymeric composite material printing. The reason for this was that printing neat polymer parts with the 2.85 mm nozzle was found to be impossible for this particular PP. Parts created via additive manufacturing with the neat PP used in this research were found to generally experience horizontal and vertical warping behavior that made created test parts unusable if not properly accounted for during printing. The warp preventing print addition used to make usable test parts with neat polymer was a brim attached to the first and second layer of the part. The addition of a brim both kept the part from warping off the print bed and warping in directions horizontal to the bed.

Neat PP parts created with the 2.85 mm diameter nozzle were unable to be created with a brim as the brim was unable to be cleanly removed from the part edges after printing unlike in the case of composite materials printed via the 2.85 mm diameter nozzle. Printing neat PP parts via the 2.85 mm diameter nozzle without the addition of a brim resulted in unusable test parts due to extreme warping of the parts off the print bed, and in the direction horizontal to the print bed. Thus, the additive manufactured test parts created with neat PP were created using the 0.8 mm diameter nozzle instead of the 2.85 mm diameter nozzle.

CHAPTER 4. EXPERIMENTAL PROCEDURES

4.1. Injection Molded Regolith Simulant Composite Creation Test Matrix

A test matrix was utilized in investigating and producing the material characteristics of polymer mixed with regolith simulant. It compared the simulant theoretical source location and wt. % loading in a polymer part. The test matrix is shown in Figure 11.

		Simulant Source Location			
		MGS-1	**MGS-1S**	**MGS-1C**	**JEZ-1**
Simulant Wt. % Loading	**10%**				
	20%				
	30%				
	40%				

Figure 11. Martian Regolith Simulant Material Test Matrix

The resulting table called for a total of 17 materials (16 MSCs and one neat polymer) to be created and utilized for test part production with each material. Figure 11's displayed matrix provided the general framework with which collected material data (tensile strength, elastic modulus, flexural strength, flexural modulus, impact toughness, melt flow index, immersion density, heat deflection temperature, glass transition temperature, and coefficient of thermal expansion) was organized and compared. The collected data formatted with this general framework was anticipated to display potential trends produced by the MRS wt. % loading, and if a particular MRS source location had better material characteristics than other MRS source locations when used to create MSC parts.

4.2. Regolith Simulant Composite Test Matrix Sample Part Production Pathway

The production of sample parts outlined in the test matrix was done according to a general pathway. The raw materials (neat PP and MRS) were mass measured and mixed by hand utilizing an electronic scale and gallon plastic bags. The raw PP and MRS mixtures were then extruded and

pelletized in to MSC pellets. The created MSC pellets were then used to create sample parts either through injection molding or additive manufacturing according to ASTM standards. A visual representation of this general process is shown in Figure 12.

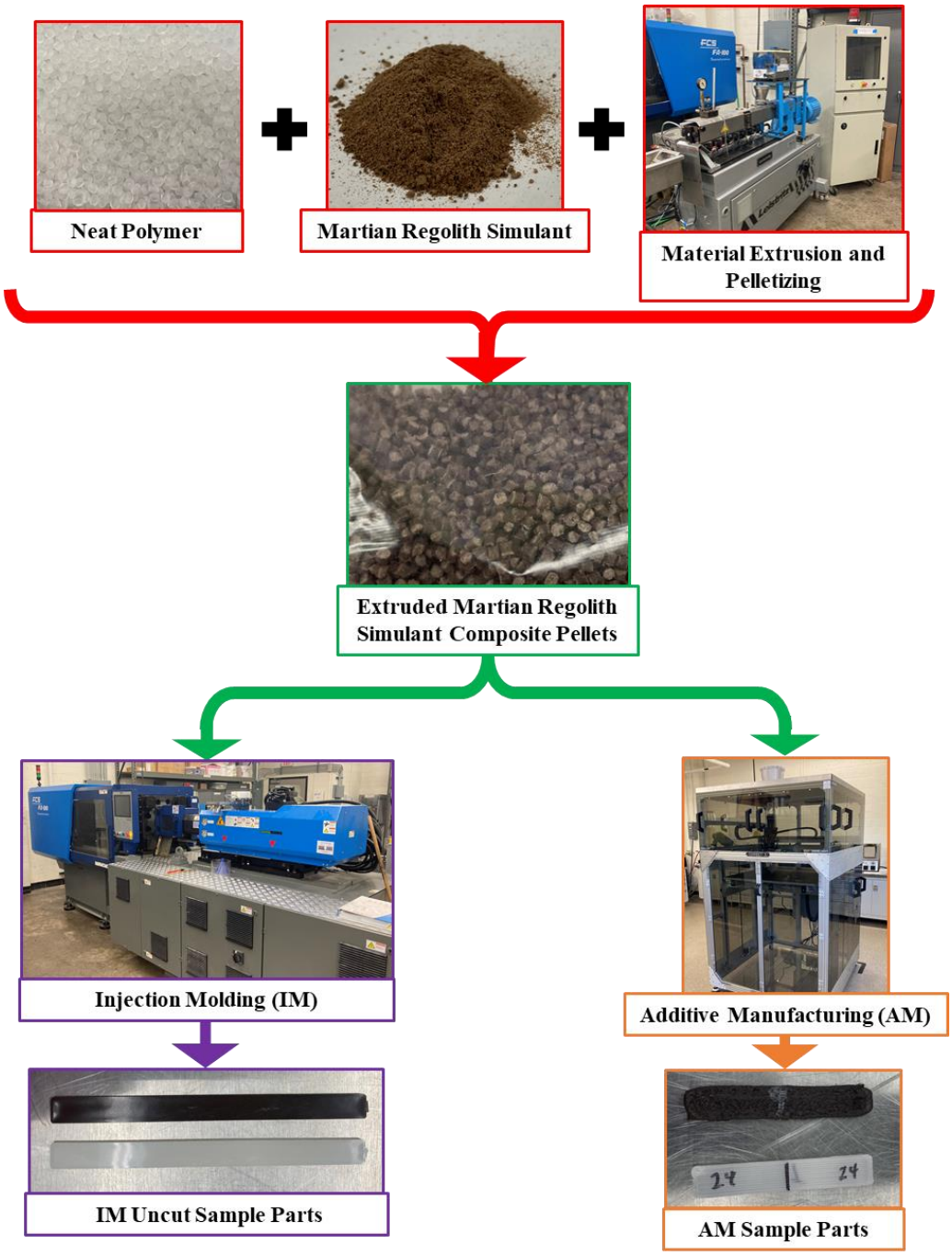

Figure 12. Test Matrix Sample Part Production Pathway Visual Representation

4.3. Regolith Simulant Composite Raw Material Characterization

The created MSC material pellets went through raw material characterization tests that were anticipated to be independent from the part manufacturing processes used after material extrusion for part creation. The two tests completed for this were melt flow index testing, and density testing.

4.3.1. Melt Flow Index Procedure

Melt flow index testing was completed using an MP600 Titan Olsen Extrusion Plastometer (melt flow index) tester. The tests with the machine were done according to the ASTM standard D1238 for neat polypropylene. The used mass on the piston rod was 3.7 kg in response to the low melt flow index listed for the neat polypropylene used in the study. The main purpose of the results was to allow for comparison of the MFI values for all the polymeric composites.

The raw material pellets used in each test run were dried in an oven for at least 12 hours prior to testing. The material pellets were given a melt time in the tester of 420 seconds. The capture distance used in each test was 0.25 in (~0.64 cm) with a start of test occurring with an arm position of 1.811 in (~4.60 cm). The raw data collected from each test was the mass of material extruded during the capture distance, as measured with an Ohaus Adventurer mass balance, and the amount of time, in seconds, it took for the measuring arm to move the capture distance. The desired data from the test was the melt flow index in units of grams per 10 minutes.

The values desired from the MFI tests were the melt flow indices of the polymeric composite pellets. This value was found by taking the measured mass value (in grams) of material extruded during the specified capture distance, dividing it by the amount of time (in seconds) it took for the capture distance to be traveled by the measuring arm, and multiplying the resulting value by 600 seconds to obtain the units of grams per 10 minutes.

4.3.2. Immersion Density Test Procedure

The densities of MSC injection molded and additive manufactured parts were found using a Mettler Toledo density determination kit. The parts used for testing were broken half pieces from Notched Izod impact testing. Test samples were conditioned for a least 24 hours before testing in the test room.

At least six test specimens were tested per sample. The "dry mass" of each specimen was measured using an Ohaus Adventurer mass balance. The kit and mass balance were then configured to find the density of solids according to the 33360 listed procedure provided by the kit. The liquid used for testing was 91% isopropyl alcohol based on the listed specific gravity of the neat Copylene CH014 of 0.902 specific gravity. The "wet mass" of each specimen was then measured by the mass balance in the previously mentioned 33360 configuration. The measurements taken for this "wet mass" were the displayed mass value on the mass balance and the temperature of the used liquid (91% isopropyl alcohol) as measured with the kit provided liquid thermometer.

The immersion density test raw results of specimen dry mass, wet mass, and liquid temperature recorded during testing were used to calculate the density of each test specimen. The primary equation utilized was the Mettler Toledo kit provided density equation, Eq. 1, for solid mass density determination.

$$\rho_{solid} = \frac{A}{A-B} * \rho_{liquid} \qquad \text{Eq. 1}$$

The density of the used test liquid (91% isopropyl alcohol) was determined based on the measured temperature of the test liquid at the time of testing and concentration of the IPA as read in a density vs. temperature calculation chart for IPA [55]. The appropriate density for the recorded test temperature was used along with Eq. 1 to calculate each test specimen's density.

4.4. Characterization of Injection Molded (IM) Regolith Simulant Composites

Parts created using conventional injection molding manufacturing techniques underwent a series of material tests to characterize the material properties of each part's respective material.

4.4.1. IM Tensile Strength and Elastic Modulus Procedure

At least five tensile samples of each polymeric composite were subjected to a tensile test according to ASTM standard D638-14, the Standard Test Method for Tensile Properties of Plastics. The material properties to be found with this test were the tensile strength and elastic modulus. The test utilized an Instron 5567 load frame and 30kN load cell. A 1-inch MTS extensometer model number 632.11B-20 was also used for strain recording during the beginning of the test. The extensometer was removed from the sample being tested after reaching an elongation of 1.5%. The samples were each tested with a crosshead rate of 5 mm/min until the specimen no longer carried load or rupture occurred in the gage length region. The desired tensile material property values for each injection molded material were found with computer calculated values using the raw data from the test, and the Bluehill load frame program. Microsoft Excel was used to convert each specimens' dimensions, machine applied force, and extensometer raw data into a stress-strain curve. For each specimen, the slope of the linear portion of the stress-strain curve data was then taken as the tensile modulus value. The calculated tensile modulus values of all of the tested IM specimens were used to calculate an average tensile modulus value for the samples of each polymeric composite material. The program took material sample specimen's dimensions and maximum stress values to calculate an average maximum tensile strength value.

4.4.2. IM Flexural Strength and Modulus Procedure

At least five flexural samples of each polymeric composite were subjected to a three-point bend flexural test according to ASTM standard D790-17, the Standard Test Methods for Flexural

Properties of Unreinforced and Reinforced Plastics and Electrical Insulating Materials. The material properties to be found with the test were the flexural strength and modulus. The test utilized an Instron 5567 load frame and 2kN load cell. The samples were each tested with 3.2 mm diameter support and loading pins. The samples were all subjected to an increasing flexural load until part failure, or a strain of 5% was reached. If part failure did not occur before a 5% strain was reached, the flexural strength was taken as the stress achieved at 5% strain on the sample part. The desired flexural material property values for each injection molded material were calculated using the Bluehill load frame program. The program took the sample specimens' dimensions, calculated crosshead rate, and raw extension data to produce an average flexural modulus (automatic) value. The program also took the sample specimen's dimensions and maximum stress values at 5% strain to calculate an average maximum flexural strength value.

4.4.3. IM Izod Impact Toughness Procedure

At least six rectangular sample parts of each polymeric composite were subjected to a notched Izod impact resistance test in accordance with the ASTM standard D256-10, the Standard Test Methods for Determining the Izod Pendulum Impact Resistance of Plastics. The impact toughness of each material was investigated with this test. The test used an Izod pendulum impact apparatus following the ASTM procedure "A" with a pendulum impact energy of 2.75 Nm (force of approximately 4.52 N from a drop height of 0.61 m). Each specimen was notched according to the D256-10 ASTM standard before being impacted. If a sample did not see crack propagation from the pendulum impact greater than 90%, it was considered a non-failure. The impact toughness for each specimen of injection molded material was calculated using the recorded impact energy and cross-sectional area at the created notch on the specimen.

4.4.4. IM Glass Transition Temperature Dual Cantilever DMA Procedure

The glass transition temperature of the polymeric composites was found through dynamic mechanical analysis (DMA) completed using a Q800 TA Instruments DMA tester. The clamp used was the dual cantilever clamp with a minimum of three specimens created from injection molded flexural bars trimmed according to D7028 ASTM standard. Specimens were cooled to a temperature of -60°C then heated at a rate of 5°C/min. to 100°C. The specimens underwent a cyclical strain of 0.05% (within the viscoelastic region of the material) at a frequency of 1 Hz throughout the heating process. The desired data sources were the storage modulus (MPa), the loss modulus (MPa), and the tangent delta with respect to temperature. The glass transition temperature (T_g) was taken as the temperature value that corresponded to the inflection point of the storage modulus data nearest to a tangent delta peak. Figure 13 shows an example of a plot with data formatted to determine T_g. In Figure 13, the T_g of the tested specimen would be recorded as 24.11°C.

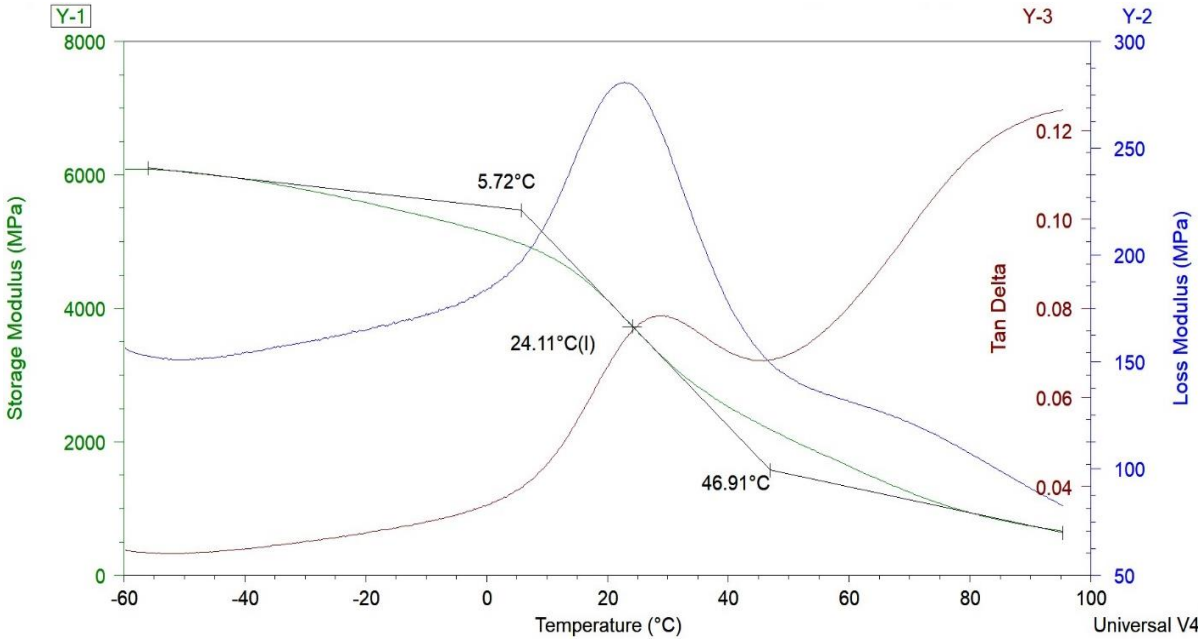

Figure 13. Example Plot Using Neat PP Specimen 1 for Determining T_g

4.4.5. IM Heat Deflection Temperature Test Procedure

Heat deflection temperature (HDT) testing on the polymeric composites was completed using a Q800 TA Instruments DMA tester. The clamp used was the 3-point bending clamp with a minimum of three specimens created from injection molded flexural bars trimmed according to a TA approved modified version of the ASTM D648 standard. A constant force was applied to the specimens in an amount according to the equations provided by the modified ASTM D648 standard. While the static force was applied, the specimen was equilibrated at 30°C, then heated at a ramp rate of 2°C/min until the desired deflection (≈10 mm) was seen by the sample while the static force was applied. The exact value of the desired deflection was calculated from the equations provided in the modified ASTM D648 standard. The data gathered from the HDT test was the deflection of the specimen with respect to the temperature. When the desired deflection was achieved during the test, the corresponding temperature was taken as the HDT.

4.4.6. IM Coefficient of Linear Thermal Expansion Test Procedure

Coefficient of linear thermal expansion (CLTE) testing on the polymeric composites was completed using a Q800 TA Instruments DMA tester. The clamp used was a thin film clamp provided with the tester. A minimum of three test specimens were created from injection molded tensile bars trimmed according to the E831 ASTM standard. The specimens placed in the clamp and equilibrated to a temperature of 30°C with a static force of 0.0000 N. The specimens were then heated at a rate of 5°C /min. to 150°C. The CLTE tests completed on the MSCs measured the change in deflection of the specimen with respect to temperature. The slope of the linear portion of the data's resulting curve was taken as the value for CLTE. The particular temperature regions of linear portion for each specimen tested was selected using a visual inspection of the plot created

from change in deflection of the specimen with respect to temperature. The units of the collected CLTE values were mm/mm/°C.

4.5. Additive Manufactured Regolith Simulant Composites

Additive manufactured test specimens were created from the MSC pellets in order to simulate a manufacturing technique that would likely be used in-situ on the surface of Mars. The creation of such specimens also allowed for a comparison of the material characteristics seen in specimens made using injection molding with the same materials.

4.5.1. Additive Manufactured (AM) Regolith Simulant Composite Candidates

Select MRS types and wt. % loadings were chosen to use for additive manufacturing tests based on the data collected from the injection molded parts. The specific items looked for in a candidate MSC was the used MRS constituent makeup as compared to the other used MRSs, the amount of decrease seen (if any) in mechanical properties due to wt. % loading of the regolith simulant in the polymer, the amount of decrease seen (if any) in mechanical properties due to the regolith simulant type in the polymer, the melt flow index results for each of the regolith simulant composites as compared to the other created MSC materials, and general material processing notes made about particular wt. % loadings or used MRSs during part creation of the regolith simulant composite parts.

4.5.2. Additive Manufactured Regolith Simulant Composite Characterization

The candidate MSCs and neat polymer were used to create test specimens via additive manufacturing techniques. The test specimens were tested according to comparative ASTM standards to injection molded materials to provide general, and comparative data on the additive manufactured parts. The print direction used in creating each part was done lengthwise, or in the direction of the longest measurement of the part shape ends conventionally known as a zero-degree

part print orientation. This was done as a previous research study suggested that print pattern direction has an impact on part strength characteristics, and a zero-degree orientated printing pattern provides the highest average values for tensile strength as compared to other print pattern orientations [56].

4.5.2.1. AM Tensile Strength and Elastic Modulus Procedure

At least five tensile samples created from the select additive manufactured polymeric composites and neat polymer were subjected to a plastics tensile test based on ASTM standard D3039, the Standard Test Method for Tensile Properties of Polymer Matrix Composite Materials. The D3039 standard allowed for the machine specific testing desired data, settings, and procedures to be the same as completed with the IM tensile specimens outlined in section 4.4.1.

4.5.2.2. AM Flexural Strength and Modulus Procedure

At least five flexural samples created from the select additive manufactured polymeric composites and neat polymer were subjected to a three-point plastics flexural test based on ASTM standard D790-17, the Standard Test Methods for Flexural Properties of Unreinforced and Reinforced Plastics and Electrical Insulating Materials. The completed tests' procedure followed the same steps as in section 4.4.2.

4.5.2.3. AM Izod Impact Toughness Procedure

At least six rectangular sample parts created from the select additive manufactured polymeric composites and neat polymer were subjected to a notched Izod impact resistance test for plastics based on the ASTM standard D256-10, the Standard Test Methods for Determining the Izod Pendulum Impact Resistance of Plastics. The procedure outlined in section 4.4.3 was followed in the notched Izod impact resistance tests for the AM parts.

4.6. Regolith Simulant Composite Material Statistical Analysis

4.6.1. Analysis of Variance (ANOVA) Test

A two factor Analysis of Variance (ANOVA) test using a 95% confidence interval was completed with each of the averaged material characterization results collected from the injection molded characterization tests. The null hypothesis tested was that there was no relation between a particular material property and one of the varied parameters of the MSC (source location and weight loading percentage). The goal was to provide numerical support to suggest the impact of varying either the MRS source location or wt. % loading on the material results. This was done to provide additional insight into any visually presented results in plots.

A one factor ANOVA test using a 95% confidence interval was completed with the raw, individual specimen material characterization results of each created material collected from the additive manufactured material characterization tests. The use of the raw, individual specimen material characterization results was done as there were not enough varied parameters and data points to complete the one factor ANOVA test with averaged values from additive manufactured parts. The null hypothesis tested was that there was no relation between a particular material property and the varied parameter of the MSC's MRS source location. The goal was to provide numerical support to suggest the impact of varying the MRS source location on the material results. This was done to provide additional insight into any visually presented results in plots.

4.7. MSC Material Result and Surface Finish Variation Investigation Procedure

An investigation was conducted on the used MRSs in response to certain material behaviors seen in the MSC material/created parts during injection molding and additive manufacturing. Its primary focus was to obtain information on the thermal response of each MRS and provide

evidence-based suggestions as to the likely candidates for weight percent mass loss of the MRSs due to heat.

4.7.1. Regolith Simulant TGA Simulant Source Location Investigation Procedure

TGA tests were run on samples of MGS-1C, MGS-1S, and JEZ-1 in addition to the initial TGA tests performed on samples of MGS-1. These tests were completed by loading 50-100 mg samples of each simulant into a TA Instruments Q550 TGA. The undried samples were subjected to a temperature ramp from room temperature (~22°C) to a temperature of 500°C at a rate of 10°C per minute in an environment of 40% Nitrogen and 60% room air.

4.7.2. Regolith Simulant Temperature Cycling Investigation Procedure

A TGA test was completed to investigate the response of MGS-1, the MRS used as the basis for all the other types of MRS, to cyclical heating. Specifically, the test was set up to capture data from temperature ramps and holds that would generally be experienced by the MRS during MSC part production. The test was completed on a TA Instruments Q550 TGA with an approximately 116 mg sample of MGS-1. The test had multiple stages. Stage one was a temperature ramp from room temperature (~22°C) to a temperature of 250°C at a rate of 10°C per minute immediately followed by a temperature hold at 250°C for two minutes. The sample was then allowed to cool down to room temperature (~22°C). Stage two was a temperature ramp from room temperature (~22°C) to a temperature of 500°C at a rate of 10°C per minute. The test environment for all stages was 40% Nitrogen and 60% room air with the exception of the sample cooling back down to room temperature which was done in open air.

4.7.3. Created Part Microscopy Procedure

Microscopy was used to investigate the internal structure of MSC parts made of 40 wt. % MGS-1 when injection molded and additive manufactured. The use of sample parts of MSC made

of 40 wt. % MGS-1 was done as MGS-1's constituents were used as the basis for all of the other used MRSs, and the presence of 40 wt. % MRS in the MSC parts was predicted to increase likelihood of displaying images that could be utilized in offering explanations to certain seen material behaviors by the MSCs when loaded with increasing amounts of MRS.

The used samples were originally half of tested parts from notched Izod impact testing. The samples were cut in half then cleaned with isopropyl alcohol (91% IPA) and left to dry. Isopropyl alcohol (91%) was also used to clean two-part, 1.5 in diameter mounting cups. The cleaned mounting cups were sprayed with mold release and left to dry. The sample pieces were placed inside the assembled mounting cups and oriented such that the sample pieces were normal to the bottom surface of the mounting cups. Sample piece orientation was maintained using zip ties lightly secured around each sample piece and raised above the bottom surface of the mounting cup. A two-part epoxy resin kit was selected for sample mounting. The epoxy was mixed with the kit included disposable mixing equipment and a laboratory scale. The mixed epoxy was then poured over the oriented sample pieces of MSC and placed in a vacuum pump chamber for approximately three minutes set at approximately 25 inHg. The samples were then removed from the vacuum chamber, lightly covered, and left to cure at room temperature and pressure for a minimum of six hours. After curing was complete, the mounts were removed from the mounting cups.

The epoxy mounted samples were polished using an Allied High Tech Products' Metprep 3, PH-3 Grinding/Polishing System. A series of polishing materials and machine settings were used to polish the sample to a degree in which viewed images of the MSC samples were free of visible scratches. The polishing materials and machine settings are outlined in Table 20. The stage

cycles present in Table 20 were repeated as needed depending on the remaining visible scratches left from the previous stage's polishing procedure.

The polished epoxy mounted samples were observed with a Carl Zeiss Axiovert 40 MAT inverted digital microscope fitted with a Carl Zeiss ZEN Core microscope to computer imaging device and software. The desired image quality was an image that displayed no visible scratches on its surface at the used magnification. The captured images were utilized to make observations on the internal structure of the MSC samples and the interface between the used constituents.

Table 20. MSC Epoxy Mounted Sample Microscopy Polishing Materials and Machine Settings

Polishing Stage	**Pre-Polish**	**1**	**2**	**3**	**4**
Polishing Material	600 grit	800 grit	1200 grit	1 µm poly diamond abrasive	0.04 µm colloidal silica abrasive
Paper / Carrier Type	Silicon Carbide	Silicon Carbide	Silicon Carbide	Polishing Cloth P	Polishing Cloth A
Suspension	N/A	N/A	N/A	Glycol	Suspension
Lubricant	Water	Water	Water	Green Lube	Wetting Water
Platen Speed (RPM)	300	300	300	150	100
Platen Direction	Same as sample holder	Same as sample holder	Same as sample holder	Same as sample holder	Same as sample holder
Sample Holder Speed (RPM)	150	150	150	150	150
Force Setting (N)	26	26	26	22	18
Stage Cycle Time (min)	Until sample surface reached	1	1	3	2

CHAPTER 5. RESULTS AND DISCUSSION

5.1. Regolith Simulant Composite Raw Material Analysis

The created MSC materials underwent tests that did not require test part manufacturing or were anticipated to be independent of the used part manufacturing process. The results from these tests, melt flow index and density testing, are shown in the following section.

5.1.1. Melt Flow Index

Figure 14 shows the MFI values for each material type created as varied by MRS source location and weight loading percent.

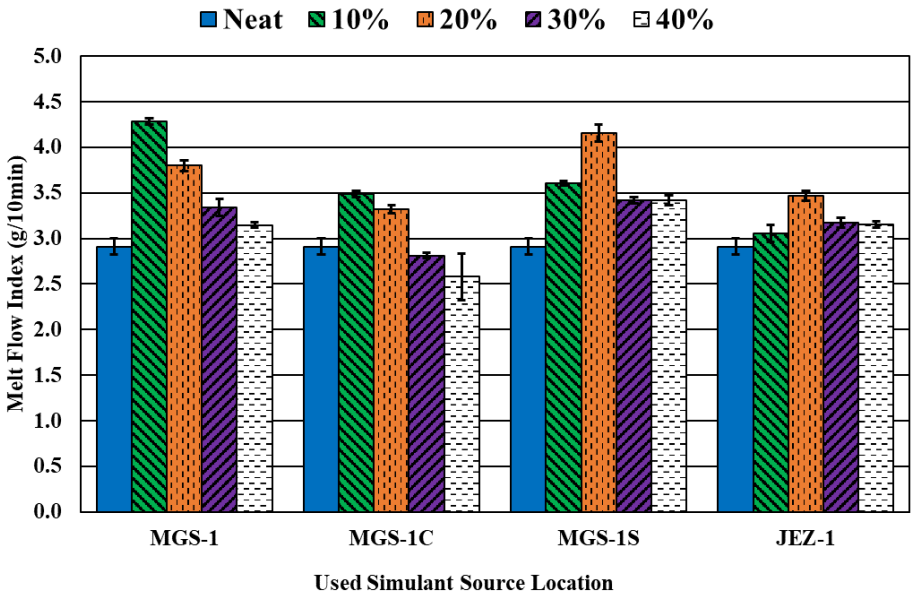

Figure 14. Melt Flow Index Properties of Neat PP and MSCs Varying by Source Location and Weight Percent Loading

The MFI values in Figure 14 did not show any definitive trends in the bar graph in terms of when the MRS source location and MRS wt. % loading parameters were varied. This suggested that both elements to the MSC creation had an impact on the resulting MFI value. The ANOVA test on the MFI values supported this conclusion by showing there was enough statistical evidence to suggest that MRS source location and wt. % loading influenced the MFI values of the MSC

materials with F-values of 5.02 and 4.78 respectively. The collected F-values were close enough to the critical F-value of 3.86 to imply that the degree of influence of both parameters was low.

A previous study suggested that a higher MFI value of a material is a favorable material flow behavior for additive manufacturing. The source also stressed that a high MFI value alone is not enough to definitively indicate high print quality of a given material [57]. This suggested that the created MSCs with higher MFI values, such as MSC with 10 wt. % MGS-1 and MSC with 20 wt. % MGS-1S, had favorable material flow behavior for additive manufacturing. However, this information did not definitively prove if such materials would work for part creation via additive manufacturing as it did not take into consideration the materials' other characteristics. It was therefore decided that the results from the MFI tests would be used alongside/after the consideration of other material factors when selecting candidate materials for additive manufacturing.

The desired wt. % loading of MRS to be used in MSC part creation was 40 wt. % as it provided the highest amount of theoretical mass reduction for polymer Earth shipment or Mars in-situ creation. Thus, the MFI results for MSCs at 40 wt. % MRS were considered for direct value comparison. The 40 wt. % MRS loaded MSC material with the highest measured MFI was that which used MGS-1S at a value of 3.42 g/10 min. The next highest MFI value was that from MSC material loaded with 40 wt. % JEZ-1 at 3.15 g/10 min. The MSC loaded with 40 wt. % MRS with the smallest standard deviation in MFI values was that which used MGS-1 at 0.029 g/10 min.

5.1.2. Immersion Density Test

5.1.2.1. Injection Molded Parts' Density

MSC injection molded test parts were subjected to immersion density testing. The averaged values from these tests were recorded and displayed in Figure 15.

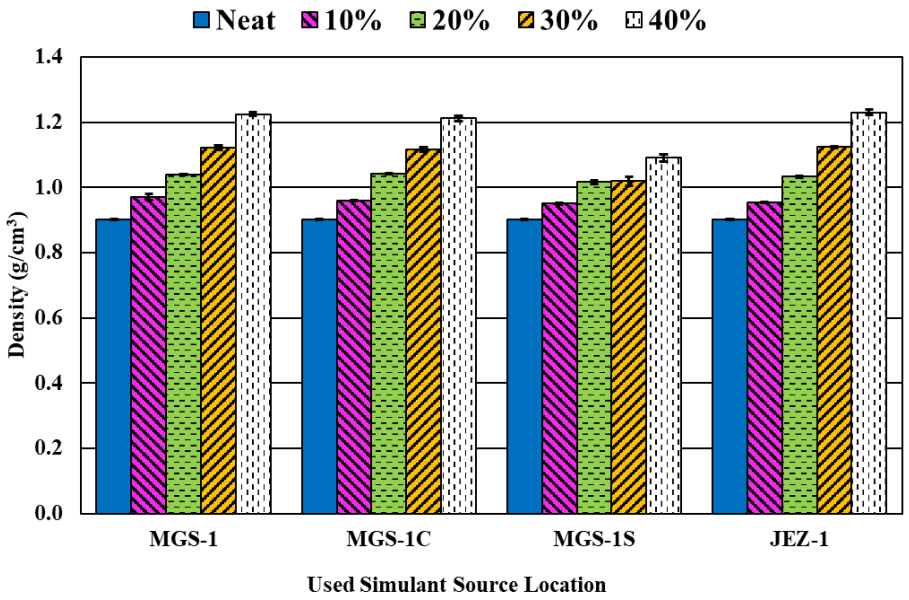

Figure 15. Immersion Density Values of Injection Molded Neat PP and MSC Parts Varying by Source Location and Weight Percent Loading

Figure 15 showed that the density data collected from the injection molded specimens had a few notable features. The density of the MSC parts seemed to increase as the wt. % loading of MRS increased from neat PP parts. This general trend also seemed to occur for all of the MSC parts regardless of the source location of used MRS. This result was expected as the MRSs were anticipated to have a higher density than the neat PP which would translate to higher density values as the amount of MRS used in the neat PP was increased for the created MSCs. There was one MRS type that showed a slight difference in its resulting MSC parts' overall increase in density values compared to the other created MSCs. Figure 15's displayed density values for MSCs with MGS-1S were generally lower than the other MSCs at similar wt. % loadings of MRS, especially at higher wt. % MRS loadings. This observation of the bar chart data provided potential evidence of the type of MRS used in the MSCs having an impact on MSC density values.

The ANOVA tests, with a critical F-value of 3.86, provided further insight into the visual observations made from Figure 15. With an F-value of 4.92, there was enough statistical evidence to suggest that there was interaction between the MRS source location used in the MSCs and the

MSCs' density values. There was also enough statistical evidence to support that the wt. % loading of MRS in an MSC part influenced its value of density as the calculated F-value was 42.01. Between the two varied parameters, the higher F-value seen for the wt. % loading of MRS compared to the F-value seen for MRS source location suggested that the parameter with the higher degree of influence in this case was wt. % loading of MRS in the MSC parts.

As usable MSC test parts were able to be made from all wt. % loading of MRSs, and for the largest theoretical polymer mass savings, the MSCs made with 40 wt. % of MRS were considered for density value comparison. The highest value seen in an MSC material made with 40 wt. % of MRS was that which utilized JEZ-1 at 1.23 g/cm^3. The MSC loaded with 40 wt. % MRS with the lowest standard deviation was that which contained MGS-1 at 0.0055 g/cm^3.

5.1.2.2. Additive Manufactured Parts' Density

A series of immersion density tests were performed on additive manufactured candidate MSC materials. Figure 16 shows the collected values from these tests.

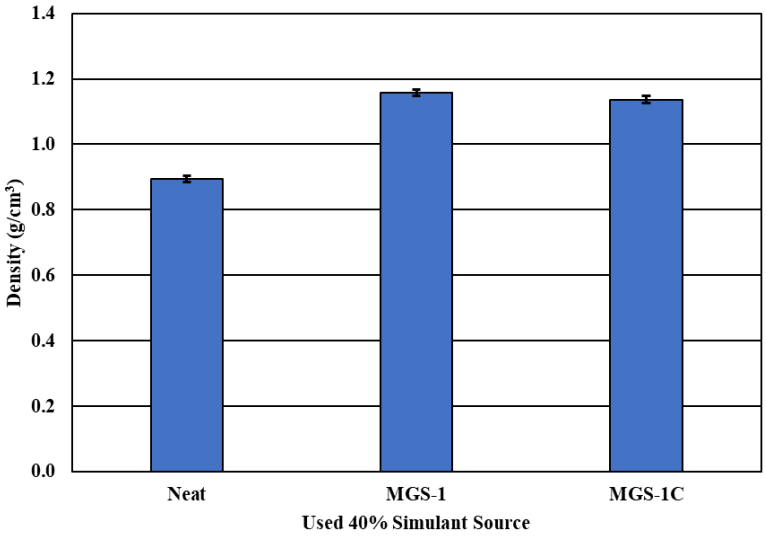

Figure 16. Immersion Density Values of Additive Manufactured Neat PP and MSC Parts Varying by Source Location

An increase in recorded density was observed for candidate MSC materials from neat PP parts in Figure 16. This followed the general trends of increasing density values with increasing MRS wt. % loading seen with the injection molded MSC parts' densities from Figure 15. The bar graph plotted data in Figure 16 did not seem to strongly indicate if the type of MRS used in the MSC parts was influential on the density values. The ANOVA test performed on the data, with a critical F-value of 4.75, provided further insight into this. The additive manufactured MSC density data had a corresponding F-value of 12.93 which indicated there was enough statistical evidence to suggest that there was interaction between the MRS source location and MSC density. This also lined up with the conclusions drawn from the data present in Figure 16 for injection molded MSCs.

A loading of 40 wt. % MRS in MSC parts provided the highest potential mass savings for MSC parts made during a Martian surface mission. In addition, usable test parts were able to be created from MSCs loaded with 40 wt. % MRS. Thus, AM MSCs loaded with 40 wt. % MRS were considered for density value comparison. The AM MSC material with the highest value for density and lowest value for standard deviation appeared to be MSC containing 40 wt. % MGS-1 with values of 1.16 g/cm^3 and 0.0108 g/cm^3 respectively.

5.2. Analysis of Injection Molded Regolith Simulant Composites

The material property results of the regolith simulant composites created from conventional injection molding manufacturing were recorded and processed to show comparison between the different material creation conditions as outlined in the test matrix.

5.2.1. IM Tensile Strength and Elastic Modulus

The averaged tensile strength values shown in Figure 17 through Figure 20 for the used MSC materials seemed to be impacted more by the MRS wt. % loading compared to the MRS source location. A general decrease in tensile strength value was seen in the MSC materials as the

wt. % loading of MRS increased from 10%. This seemed logical as the presence of MRS in the PP was thought to take the place of potentially load bearing polymer chains in the sample parts.

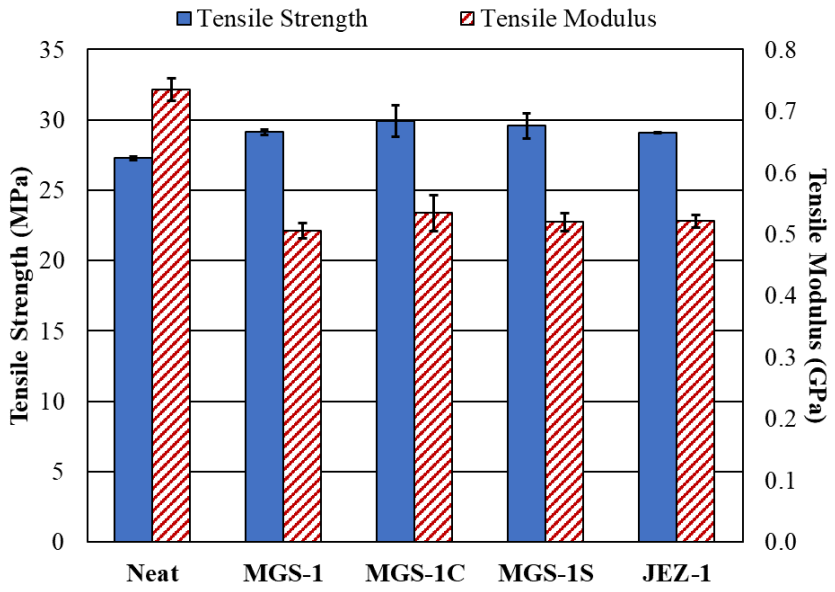

Figure 17. Tensile Properties of Injection Molded Neat PP and 10% MRS Weight Percent Loaded PP

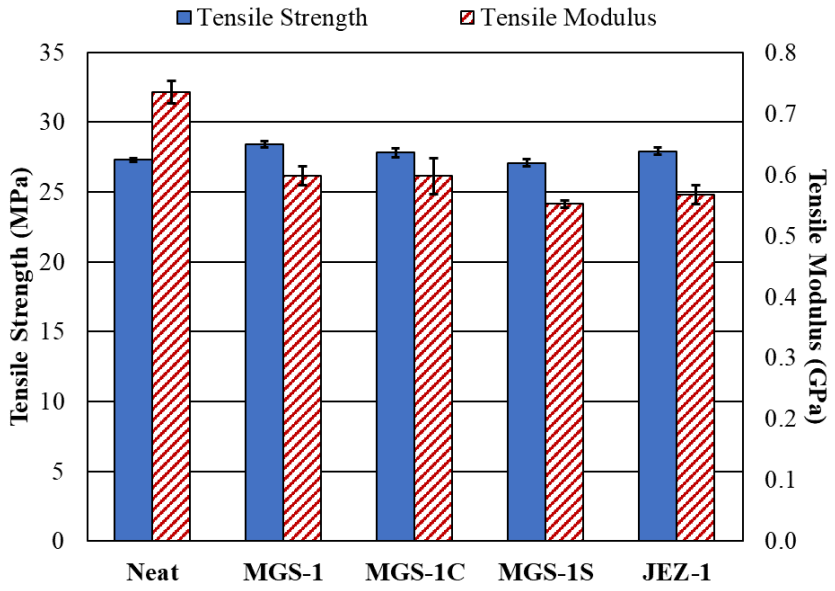

Figure 18. Tensile Properties of Injection Molded Neat PP and 20% MRS Weight Percent Loaded PP

Figure 17 showed an exception to this with a slight increase in tensile strength when wt. % loading of MRS went from 0% in the neat PP to 10% of each MRS type. This slight increase was

thought to be potentially due to the MRS particles causing early disentanglement, and thus early unidirectional alignment, of some of the polypropylene molecular chains during the test. Such unidirectional alignment would be expected to eventually occur within all of the PP based test sample parts during tensile testing. The presence of the MRS particles was thought to in this case provide points at which the polymer chains could become caught on particles and become aligned in the direction of applied load at a smaller axial extension than that seen in neat PP test sample parts [58]. The effect was predicted to become less influential once more MRS was mixed into the PP taking the place of the load bearing polymer chains.

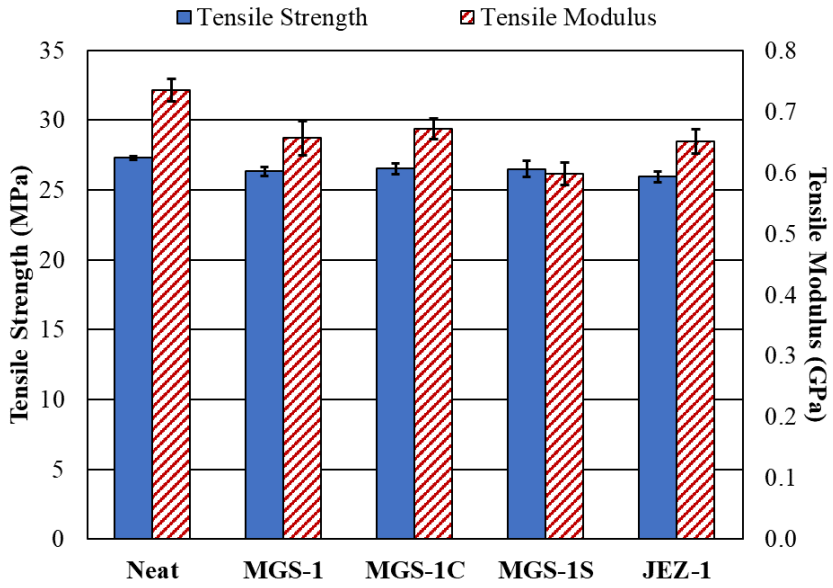

Figure 19. Tensile Properties of Injection Molded Neat PP and 30% MRS Weight Percent Loaded PP

The two factor ANOVA results provided support to the conclusion based on the observation of the data trends of the wt. % loading of MRS in each MSC having more of an impact on tensile strength values than the MRS source location. The critical F-value for the tensile ANOVA tests was 3.86. With an F-value of 0.12 for a 95% confidence interval, there was not enough statistical evidence found to suggest that the MRS source location had interaction with the

tensile strength of MSC parts. In contrast, there was enough statistical evidence to suggest that the MRS wt. % loading had interaction with the tensile strength of MSC parts with an F-value of 78.36 for a 95% confidence interval.

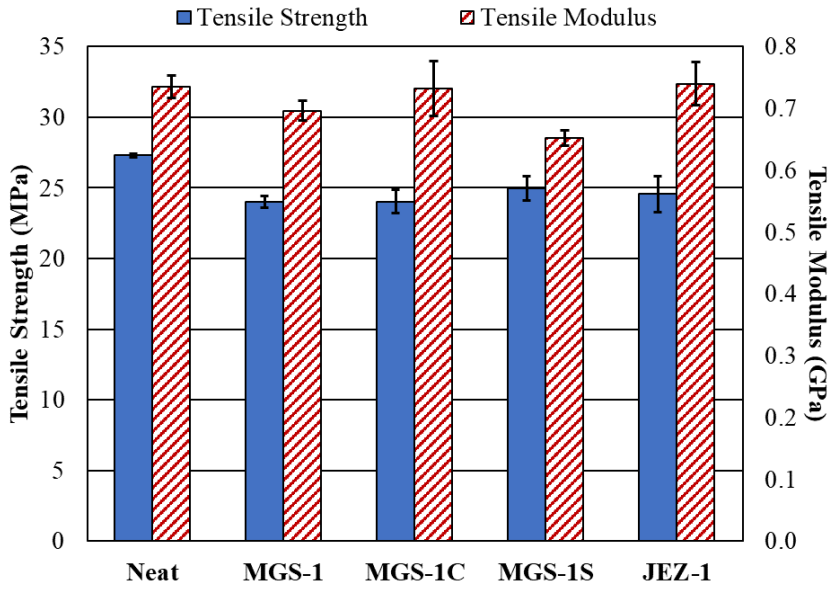

Figure 20. Tensile Properties of Injection Molded Neat PP and 40% MRS Weight Percent Loaded PP

The average tensile modulus values of the created MSC parts shown in Figure 17 through Figure 20 were observed to likely be impacted by both the wt. % loading of MRS in each MSC and the source location of the used MRS. While there was a general increase in tensile modulus values as the wt. % loading of MRS increased, the particular amount of increase was slightly different between each MRS source location used in the MSC parts. Another noteworthy element seen in Figure 17 was the initial decrease in tensile modulus from neat PP parts to MSC parts loaded with 10 wt. % of each MRS. This was once again theorized to be caused by the previously mentioned early unidirectional alignment of some of the polypropylene molecular chains during the tensile tests.

The predictions of interaction of tensile modulus with each varied parameter based on the data trends shown in Figure 17 through Figure 20 received support from the completed two factor

ANOVA tests. MRS source location, with a F-value of 4.98 for a 95% confidence interval, had enough statistical evidence to suggest that this parameter impacted the value of tensile modulus in MSC parts with the F-value's relatively low amount of difference from the critical F-value suggesting this impact was to a low degree. A F-value of 62.21 for a 95% confidence interval provided statistical support to the idea of the MSC parts' tensile modulus values being influenced by the amount of wt. % loading of MRS.

As all wt. % loadings of MRS in neat PP created usable MSC test parts, the MSCs with the highest wt. % loadings of MRS were focused on for comparing the tensile properties. The tensile property that had evidence to suggest interaction between MRS source location and the property was tensile modulus. The MSC material that had the highest value for tensile modulus was MSC that used Jezero MRS with a value of 0.740 GPa. The MSC material that had the lowest standard deviation for tensile modulus values was MSC that used Sulfate MRS with a value of 0.0120 GPa. The MSC material with the second lowest standard deviation in for tensile modulus was the MSC that used Global MRS with a value of 0.0157 GPa.

5.2.2. IM Flexural Strength and Modulus

The flexural modulus data displayed in Figure 21 through Figure 24 seemed to make general sense given the tested materials. It was predicted that the MSCs would see at least increased flexural modulus values as the MRS wt. % loading was increased as the presence of the MRS particles in the PP were anticipated to inhibit polymer chain movement, and thus result in stiffer material behavior. Figure 21 through Figure 24 appeared to have data to support this. It is worth noting that all the tested MSC parts did not fracture after being subjected to the maximum flexural strain of 5%. This was thought to be due to the used PP's inherent material resilience to flexural loads. The lack of fracture also provided merit to the results of increased flexural strength

values of MSC parts with increasing amounts of MRS wt. % loading. Since there was no part fracture, the MSC parts would be expected to have higher values for flexural strength by the time of reaching the maximum strain value of 5% as with each increase in MRS wt. % loading, there was an increased modulus value as well.

The flexural results for the created MSCs reported in Figure 21 through Figure 24 appeared to follow relatively steady trends of increasing values for both flexural strength and flexural modulus as the wt. % loading of the MRS in PP increased for all the MSC materials used. This supported the idea that the MRS wt. % loading in the MSC parts had influence over the parts' flexural strength and flexural modulus values. By contrast, the level of impact of the used MRS source location on flexural strength and flexural modulus appeared to be low to non-existent based on the trends in the bar graphs. That being said, Figure 21 through Figure 24 displayed a higher increase in flexural strength of MSCs made with MGS-1C than the other MSC materials. This gave potential evidence of some interaction between a MSC's used MRS source location and flexural strength.

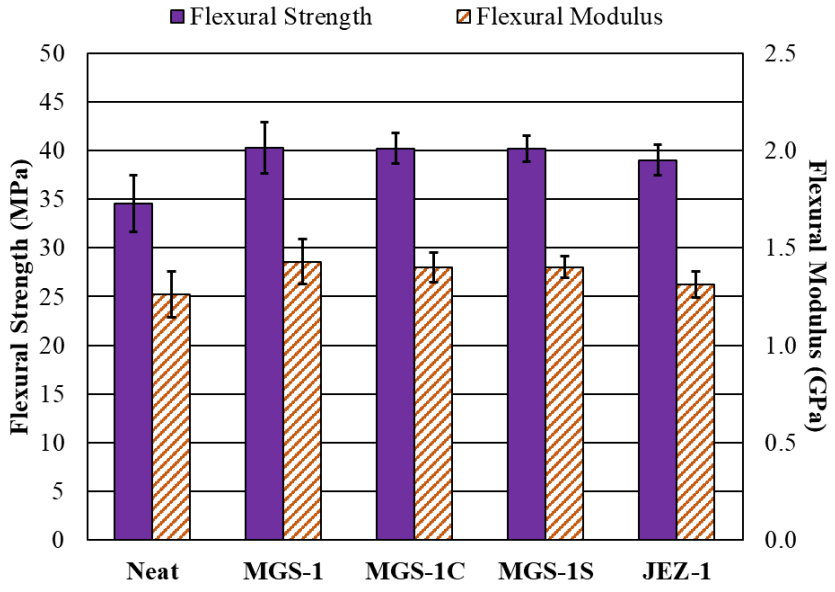

Figure 21. Flexural Properties of Injection Molded Neat PP and 10% MRS Weight Percent Loaded PP

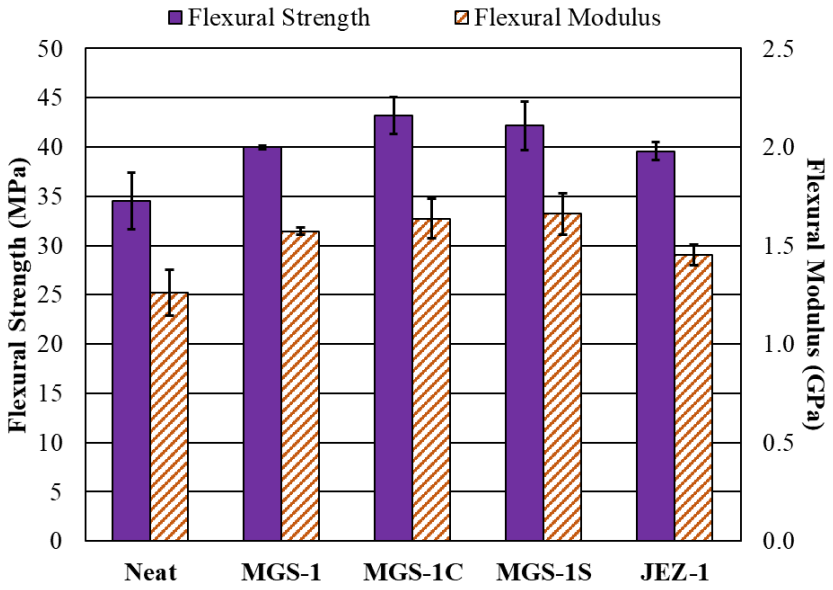

Figure 22. Flexural Properties of Injection Molded Neat PP and 20% MRS Weight Percent Loaded PP

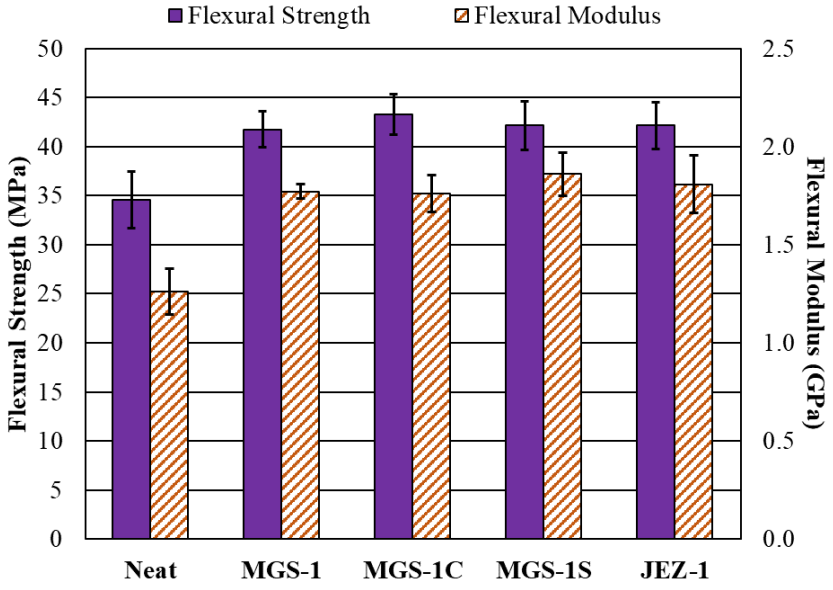

Figure 23. Flexural Properties of Injection Molded Neat PP and 30% MRS Weight Percent Loaded PP

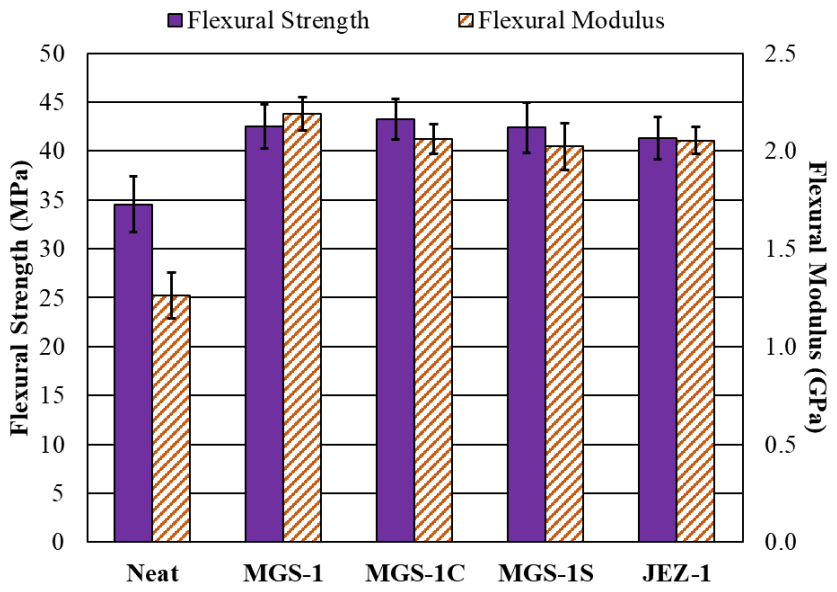

Figure 24. Flexural Properties of Injection Molded Neat PP and 40% MRS Weight Percent Loaded PP

With a critical F-value of 3.86, the ANOVA results for flexural strength and flexural modulus provided enough statistical evidence to suggest that MRS wt. % loading was influential in impacting both material characteristic values with a F-value of 9.82 for flexural strength and a F-value of 83.51 for flexural modulus. These results matched the bar chart observation based conclusions made from Figure 21 through Figure 24. The ANOVA results for these material characteristic values did not have enough statistical evidence to show interaction between flexural modulus and MRS source location with a F-value of 1.41. However, the results did have enough evidence to reject the null hypothesis of no interaction between flexural strength and MRS source location with a F-value of 5.27, which lead to the same bar chart observation based conclusion made from the higher increase in flexural strength of MSC made with MGS-1C than the other MSC materials seen in Figure 21 through Figure 24. The ANOVA results regarding MRS source location influence on flexural strength also provided evidence to support the idea that the degree of influence by this varied parameter on flexural strength was to a relative low degree given that its calculated F-value was relatively close to the F-critical value.

All of the created flexural parts, regardless of MSC MRS wt. % loading and source location, were able to be tested with standardized testing techniques. Between the two flexural material properties investigated, the flexural strength values of MSC parts were found to be impacted by the MRS source location used in the MSC material. Based on this, the MSC at 40 wt. % loading of MRS that had the highest value of flexural strength at 43.2 MPa and the smallest value in flexural strength standard deviation at 2.09 MPA was that which used MGS-1C.

5.2.3. IM Izod Impact Toughness

Figure 25 presented impact toughness data for the created MSCs which appeared to decrease in value from neat PP as the wt. % loading of MRS in each MSC increased. This general trend was observed to occur for all of the MSCs created regardless of MRS source location. A decrease in impact toughness value due to the inclusion of a particulate in a neat polymer seemed a reasonable result as the inclusion of the particulate took the place of the impact resisting neat polymer for the same relative cross-sectional area seen between parts. The MSCs made of MGS-1C and MGS-1S did show slight variation from the general decrease in impact toughness values as MRS wt. % loading increased in the form of larger drops between particular MRS wt. % loadings compared to the other created MSCs. These larger drops can be seen in Figure 25 between 20 and 30 wt. % clay MRS, 10 and 20 wt. % sulfate MRS, and 20 and 30 wt. % sulfate MRS. This observed variation suggested the potential for the type of MRS used in the MSCs to be influential of created part impact toughness.

The completed ANOVA results for impact toughness provided enough statistical evidence, with an F-value of 26.23 compared to the critical F-value of 3.86, to support that the wt. % loading of MRS in each MSC impacted part impact toughness. The ANOVA test run to investigate if impact toughness was influenced MRS source location produced an F-value of 2.70 which did not

provide enough statistical evidence to suggest interaction between the two factors. This dismissed the original idea based on the observations of the trends in the bar graph's data that MRS source location influenced MSC impact toughness values.

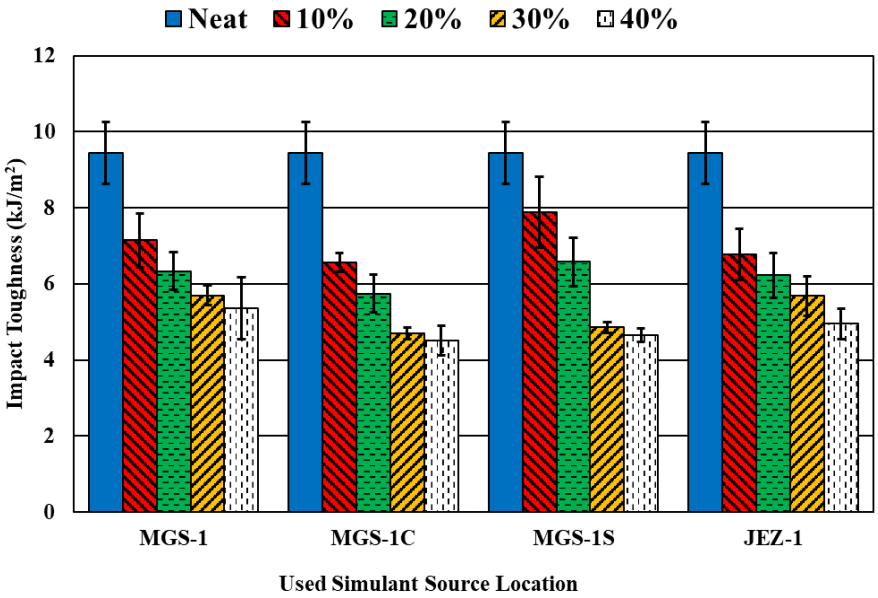

Figure 25. Notched Izod Impact Toughness of Injection Molded Neat PP and MSC Parts Varying by Source Location and Weight Percent Loading

The MSCs with 40 wt. % MRS were considered for impact toughness value comparisons as usable test parts were able to be created from the material. Based on the ANOVA results, the impact toughness values of the MSCs were not able to be compared with respect to the type of MRS used as not enough statistical evidence was found to show that MRS type influenced the impact toughness values. The average impact toughness value for these parts at 40 wt. % MRS was approximately 4.9 kJ/m^2. In terms of the consistency of results, MSC parts made with MGS-1S were found to have the lowest value of standard deviation at 0.17 kJ/m^2 for all 40 wt. % MRS loaded MSCs. MSC parts made with MGS-1C had the second lowest value of standard deviation at 0.39 kJ/m^2.

5.2.4. IM Glass Transition Temperature Dual Cantilever DMA

The results from the process followed for obtaining the glass transition temperatures of the tested IM polymeric composite materials are shown in the Figure 26. The observed data trends shown in Figure 26 suggested that there was little change in the value of T_g as both the type of MRS and MRS loading wt. % was varied in the MSC materials. The little amount of change in T_g that occurred in the MSC materials compared to the neat PP material was positive and negative in direction. The nature of the overall amount and direction of what change in T_g values was present compared to MRS wt. % loading appeared to depend upon the MRS source location used in the MSCs. For example, the MSC made with MGS-1C MRS appeared to have smaller average values of T_g as compared to MSC made with MGS-1S MRS. This suggested that MSC T_g was in some capacity influenced by MRS source location. That being said, it is worth stressing that overall change observed in the T_g of MSC materials from the neat PP was low with presented standard deviation bars of the averaged values almost completely overlapping each other. This suggested that said influence of MRS source location on polymeric composite T_g was to a low degree if present at all.

The collected ANOVA results for MSC T_g provided enough statistical evidence to imply that the MRS source location had an impact to some degree on the value of MSC T_g with a F-value of 7.06 compared to the critical F-value of 3.86. This aligned with the previous suggestion of MSC T_g being influenced in some capacity by MRS source location as based on the observations of the data trends seen in Figure 26. The results did not show enough evidence to show interaction between MSC T_g and MRS wt. % loading with a collected F-value of 1.41.

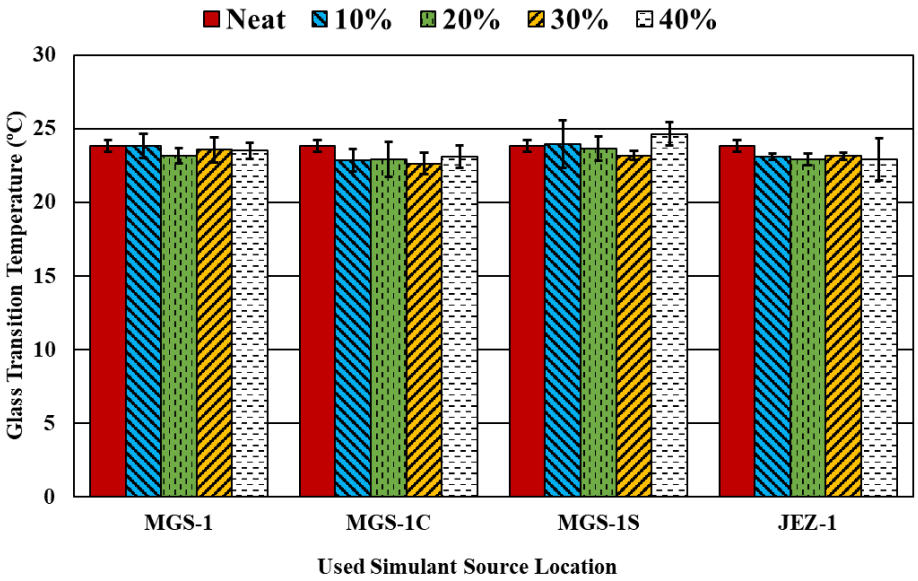

Figure 26. Dual Cantilever DMA Glass Transition Temperature of Injection Molded Neat PP and MSC Parts Varying by Source Location and Weight Percent Loading

The original expectation for the value of T_g for polymer test parts when filled with increasing amounts of a particulate filler was for it to decrease from that measured with neat polymer test parts. This expectation came from the idea of the increasing amounts of MRS in the MSC parts taking the place of neat PP within a test part which would make the part have a decreased amount of polymer chains capable of bearing load and thus resisting any applied bending stresses. While the instances in which the value of T_g increased from that measured from neat PP test parts challenged this expectation, as seen in Figure 26, their occurrence was not without precedence. A past study found values of T_g for polymer matrix particulate composite parts that increased as the concentration of a filler material (glass beads and Attapulgite clay) was increased in the parts. The source suggested that this was likely due to the particles' interaction with the polymer reducing the "molecular mobility and flexibility of the polymer chains in the vicinity of the interfaces" [59]. A similar phenomenon to that seen in this source was thought to be possible with the created MSC test parts in this research. The presence of the MRS particles could have reduced polymer chain mobility of the used PP, raising the parts' values of T_g, while

also taking the place of bending stress resistant PP polymer chains in the created test parts, lowering the parts' values of T_g. The end result of these two proposed competing effects from the used MRS particles in the matrix PP material would in theory be a near net zero change in the value of T_g of an MSC test part as compared to a neat PP test part. Based on this idea, the near net zero change in values of T_g in MSC test parts would also be expected to continue as the wt. % loading of MRS increased in the MSC material since the two proposed competing effects from the used MRS particles in the matrix PP material would in theory both continue to counter each other's impact on any test part's value of T_g. This provides a possible reason as to the observation of a relatively low changes in T_g values between the created material test parts in Figure 26 as both the MRS source location and wt. % loading was varied between materials. What small changes in T_g values were present could have been due to one of the proposed impacts of the MRS particulates in the matrix PP material having slightly more influence compared to the other proposed impact of the MRS particulates in the matrix PP for those particular test parts.

The T_g values for the MSC materials were found to not have enough statistical evidence to suggest influence by wt. % loadings of MRS which lined up with the observed data trends in Figure 26, and the previously theorized impact of the two proposed competing effects from the used MRS particles in the matrix PP material in causing a near net zero change in the value of T_g of an MSC test part as compared to a neat PP test part. This, as well as the ability for usable test parts to be created from MSCs of all wt. % loadings of MRS, provided support to focus on MSCs loaded with 40 wt. % of MRS when comparing T_g values. The 40 wt. % MRS loaded MSC with the highest T_g value at 24.6°C was that which used MGS-1S. The 40 wt. % MRS loaded MSC with the second highest T_g value at 23.5°C was that which used MGS-1. A standard deviation of 0.54°C made the MSC that used MGS-1 the material loaded with 40 wt. % with the lowest standard deviation.

5.2.5. IM Heat Deflection Temperature Test

The HDT results shown in Figure 27 were found to increase in value from neat PP as the wt. % loading of MRS increased in value, suggesting that this varied parameter had influence over the value of HDT. The general, steady increasing trend of HDT seen in the MSC parts appeared to occur regardless of the used MRS source location in the MSC parts. This indicated that MRS source location did not impact the value of HDT in MSC parts.

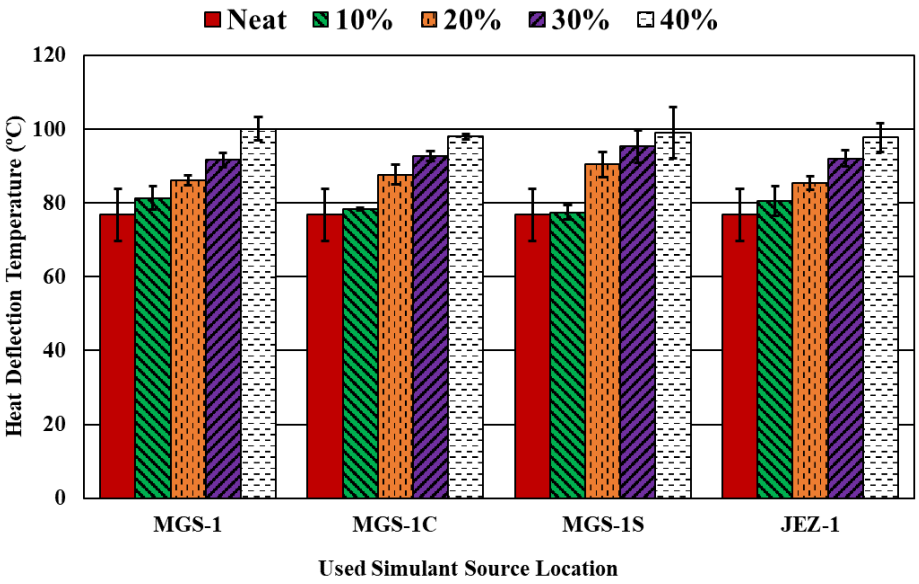

Figure 27. Heat Deflection Temperature Values of Injection Molded Neat PP and MSC Parts Varying by Source Location and Weight Percent Loading

A F-value of 0.63 from an ANOVA test on the MSC HDT results suggested there was not enough statistical evidence to show interaction between the used MRS source location and MSC HDT. In contrast, the ANOVA results did provide enough statistical evidence to suggest that MRS wt. % loading was impactful to MSC HDT with a F-value of 82.18. The ANOVA results for both varied parameters, both with a critical F-value of 3.86, provided additional support to the conclusions drawn from the observations of the data trends seen in Figure 27. As there was not enough evidence present to suggest difference of HDT values based on the MRS source location

used in the MSC parts, there was not a material type family that had more consistent or maximum values of HDT.

These findings seemed logical given that the inclusion of increasing amounts of particulates in a neat polymer would generally be expected to increase any created material test part's resistance of flexibility to a static load requiring additional thermal energy to cause significant deflection of the part.

HDT test parts were able to be created from all the MSC materials. For the best potential of theoretical mass savings, MSC materials with 40 wt. % of MRS were compared in terms of their values for HDT. Statistical evidence did not show enough evidence to suggest interaction between the MRS source location used in an MSC and its HDT. The MSC materials at 40 wt. % MRS thus had an average value of HDT of 98.7°C. The 40 wt. % MRS loaded MSC with the most consistent results was the MSC material made with MGS-1S as it had a standard deviation of approximately 0.76°C, the lowest standard deviation of all of the like MRS loaded materials. The MSC material made with MGS-1 had the second lowest standard deviation for HDT results with a value of approximately 3.09°C.

5.2.6. IM Coefficient of Linear Thermal Expansion Test

In Figure 28, the values for CLTE are displayed for each IM polymeric composite material. The CLTE value for increasing amounts of MRS in the MSC parts decreased from the CLTE value of neat PP parts. In Figure 28, this trend appeared with each group of MSC as differentiated by MRS source location. The implication of these observations was that MRS source location did not impact CLTE in MSC parts while MRS wt. % loading did impact CLTE values. The ANOVA results, with a critical F-value of 3.86, supported these conclusions. A F-value of 59.54 for MRS wt. % loading in the ANOVA test provided enough statistical evidence to suggest MRS wt. %

loading interaction with MSC CLTE. In contrast, the ANOVA test did not show enough statistical evidence to suggest MRS source location interaction with the values of MSC CLTE with a F-value of 1.15.

The results in, and conclusions from, the data in Figure 28 seemed reasonable for predicted standard material behavior. Neat polymer parts had the largest amount of material by weight capable of experiencing significant expansion in the temperature range of the test. The displacement of neat polymer in a created part by stiff filler particles was expected to result in a decrease the part's ability to expand from a change in temperature. The CLTE data collected and displayed in Figure 28 seemed to adhere to the anticipated standard material behavior.

Usable CLTE test parts were able to be made from MSC materials even at the highest wt. % loading of MRS at 40 wt. %. Thus, the MSCs loaded with 40 wt. % MRS were considered for CLTE comparison. The MRS source location for MSC materials was suggested by the ANOVA results to not influence the value of CLTE for the materials. The average value of CLTE for the MSCs loaded with 40 wt. % of MRS was approximately 0.0144 mm/mm/°C. A standard deviation of 0.00017 mm/mm/°C suggested MSC with 40 wt. % JEZ-1 was the material with the most consistent CLTE values compared to similarly loaded MSC materials.

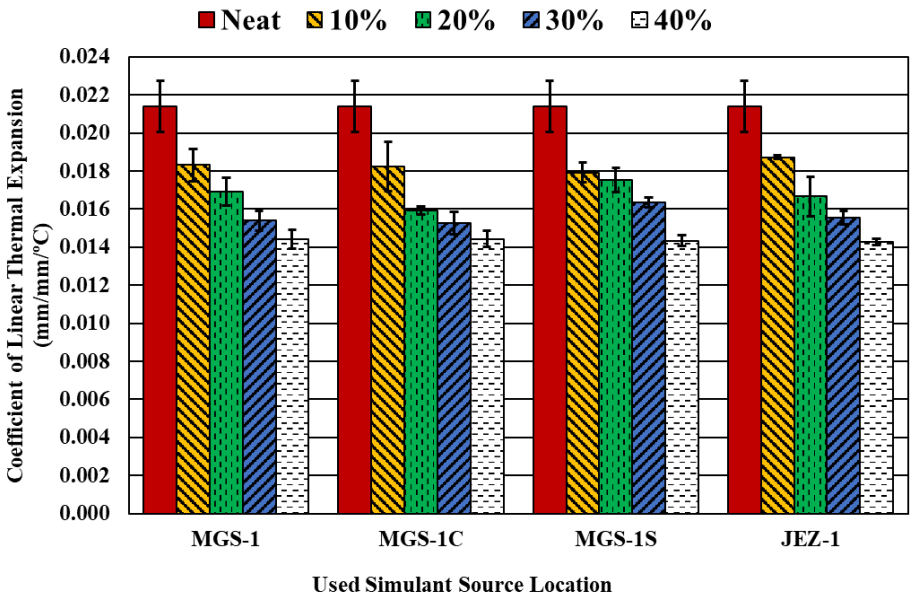

Figure 28. Coefficient of Linear Thermal Expansion Values of Injection Molded Neat PP and MSC Parts Varying by Source Location and Weight Percent Loading

5.2.7. IM Part Result Comparison and AM Candidate Selection

The collected material property data, and general material processing notes were utilized to select the candidate MSC materials to be experimented with in additive manufacturing. The data that was focused on was the MRS makeup as compared to the other used MRSs, the seen general decrease in mechanical strength characteristics as wt. % loading of MRS was increased and type of MRS was varied, the values and consistency of the melt flow index values, and material processing observations made for each MSC.

The MSC material utilizing MGS-1S displayed extreme amounts of expansion during injection molding. This observed behavior was different than that seen with the other created MSC materials, and often resulted in interference with the creation of usable test parts. The interference was in the form of excessive material expansion out of the nozzle, when there was no mechanical part movement, preventing a proper injection nozzle to mold fit, and/or the higher potential for voids assumed to be from the manufacturing process to be present within the created parts. While usable parts were able to be created with the injection molding process, it was anticipated that this

unanticipated behavior would make utilizing the MGS-1S based MSC material difficult to utilize for additive manufacturing. This disqualified all MSCs made with MGS-1S from being selected as candidate materials for additive manufacturing.

It was theorized that loadings of 40 wt. % MRS in an MSC material would result in parts that would be unable to be used according to standard test techniques. This theory was found to be incorrect, and the overall decrease in material strength characteristics was lower for all created MSCs than anticipated when loaded with 40 wt. % of MRS. In some cases, such as in the case of the flexural data showed in Figure 24, the presence of 40 wt. % of MRS increased the strength characteristics of the MSC material as compared to the neat polymer. This suggested that parts made with 40 wt. % of MRS could be manufactured into usable parts without seeing too large an amount of decrease in overall material strength characteristics. This, in addition to the theoretical mass savings for future crewed Martian surface missions, gave reason to consider MSCs with 40 wt. % of MRS for additive manufacturing experimentation.

The MRSs used to create the MSCs each contained specific minerals. While these constituents, and their amounts, varied between each MRS, the MGS-1 MRS was used as the basis for all the other MRSs. This meant that the MGS-1C, MGS-1S, and JEZ-1 all contained the same used minerals as found in MGS-1 with varying percentages for their basic composition of constituents.

The created MSC materials were shown to have different material values impacted by variation of the MRS type for specific material behavior tests. These were tensile modulus, flexural strength, glass transition temperature, and melt flow index. Based on the previous candidate selection criteria, the MSCs in question for comparing material behavior for candidate selection were those that contained MGS-1C and JEZ-1 loaded at 40 wt. % MRS. The MSCs made with 40

wt. % MGS-1C had on average higher values for tensile modulus, flexural strength, and glass transition temperature than MSCs made with JEZ-1 at 40 wt. % loading. In addition, the melt flow index value for MSC made with 40 wt. % of JEZ-1 was found to be similar to the value found for MSC made with 40 wt. % of MGS-1 while the MSC made with MGS-1C had a melt flow index value that was smaller. This provided support to the idea of not utilizing MSCs with 40 wt. % JEZ-1 as MSCs using MGS-1 were already being considered for use as additive manufacturing candidate materials from a prior selection criterion. From all of the material behavior characteristics, MSCs made with MGS-1C were the recommended materials to consider for candidate additive manufacturing due to their higher material strength values compared to MSCs with JEZ-1 at 40 wt. % loading of MRS, and its difference in melt flow index value to the general MSCs with MGS-1.

Based on all of the data and selection criteria, the candidate MSC materials chosen for additive manufacturing were MSC with 40 wt.% MGS-1 and MSC with 40 wt.% MGS-1C.

5.3. Additive Manufactured Regolith Simulant Composite Analysis

Test parts from the candidate MSC and neat PP materials were created using FGF additive manufacturing. The material properties of these additive manufactured parts were recorded and processed to provide comparison between the used MRS source locations in the MSC parts, and the respective MSC parts' results created using injection molding.

5.3.1. AM Tensile Strength and Elastic Modulus

The tensile results for the AM polymeric composite materials are presented in Figure 29. The tensile strength values of the additive manufacture parts decreased with the inclusion of 40 wt. % MRS in MSCs as compared to the neat PP parts. As seen in Figure 29, the value of tensile strength for the MSCs made with MGS-1 and MGS-1C appeared approximately equal suggesting

that the type of MRS used in an MSC did not impact the polymeric composite's tensile strength. ANOVA results for tensile strength provided support to this suggestion with a F-value of 2.70 versus the critical F-value of 4.96 not providing enough statistical evidence to show interaction between AM part tensile strength and MSC used MRS source location.

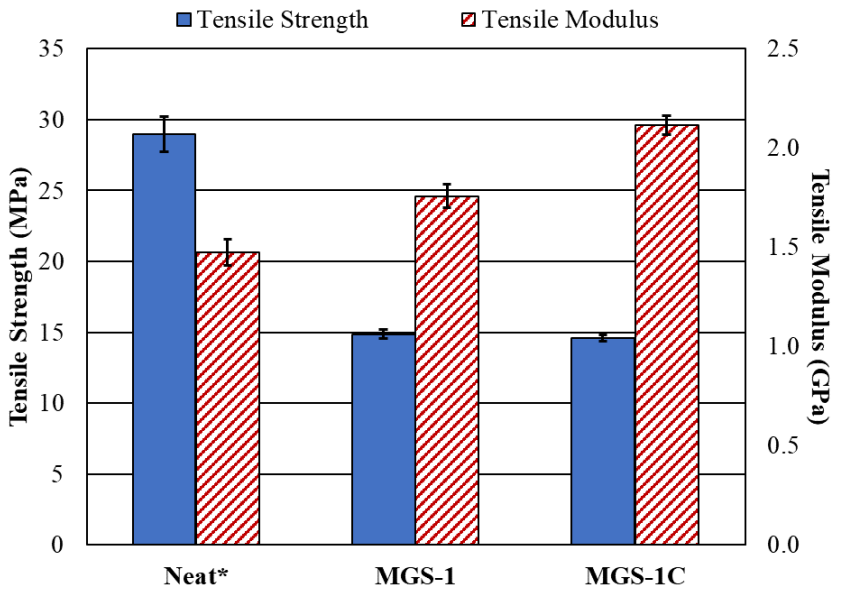

Figure 29. Tensile Properties of Additive Manufactured Neat PP and 40% MRS Weight Percent Loaded PP (* Different Nozzle Size Used During AM)

The tensile strength values for AM MSC parts were suggested to not be influenced by MRS source location based on ANOVA results. Thus, the average value of the AM MSC parts for tensile strength was approximately 14.7 MPa. The tensile strength values that had the lowest standard deviation of 0.23 MPa for AM MSC parts were those from the MSC made with MGS-1C. Figure 29 showed the additive manufactured parts' tensile modulus values increased with the inclusion of 40 wt. % MRS in MSCs as compared to neat PP parts.

The increase of tensile modulus was not similar between the parts made with polymeric composite material utilizing MGS-1 and MGS-1C MRS. This led to the theory that the type of MRS used in MSC production impacted the tensile modulus of created test parts. The ANOVA test for tensile modulus produced a F-value of 124.74 versus the critical F-value of 4.96, providing

enough statistical evidence to suggest interaction between tensile modulus and MRS source location. In this case, the MSC made with MGS-1C had the highest tensile modulus value of the additive manufactured material at 2.11 GPa. It also had the lowest value for standard deviation of the additive manufactured MSC materials at 0.047 GPa.

5.3.2. AM Flexural Strength and Modulus

The flexural data shown in Figure 30 displayed flexural strength values for the MSC materials that were lower than those collected for neat PP parts. In addition, the MGS-1 based MSC material flexural strength value was smaller than the MGS-1C based MSC material flexural strength value. This led to the idea that the flexural strength of MSC parts was influenced by the MRS source location used in the MSC materials. The ANOVA test performed on the data, with a critical F-value of 5.32, supported this idea with a F-value of 19.08, showing statistical evidence to suggest interaction between flexural strength and MSC MRS source location. The MSC material that had the highest flexural strength value was MGS-1C based MSC at 28.7 MPa.

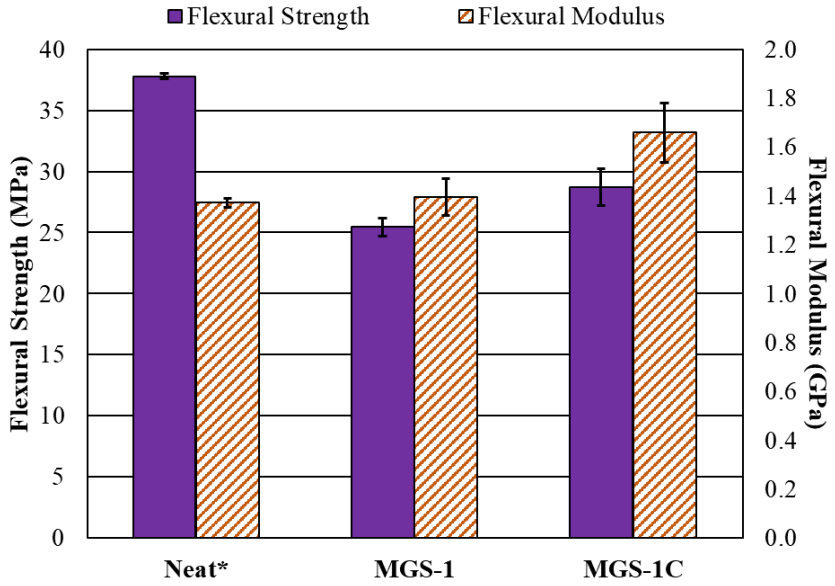

Figure 30. Flexural Properties of Additive Manufactured Neat PP and 40% MRS Weight Percent Loaded PP (* Different Nozzle Size Used During AM)

Flexural modulus values of the additive manufactured materials were found to be larger in MSC material-based parts compared to neat PP material-based parts. ANOVA results for flexural modulus provided enough statistical evidence with a F-value of 17.12 versus the critical F-value of 5.32 to suggest that MRS source location for MSC parts impacted the resulting flexural modulus of the material. This suggestion was supported by Figure 30 as the figure presented increased values for flexural modulus for MGS-1 based MSC and MGS-1C based MSC from neat PP with MGS-1C based MSC having the largest value for flexural modulus at 1.66 GPa. Figure 30 also displayed the standard deviations of each of the averaged flexural modulus values for each material. The MSC material with the smallest standard deviation for flexural strength and modulus was MGS-1 based MSC with values of 1.39 MPa and 0.075 GPa respectively.

5.3.3. AM Izod Impact Toughness

The impact toughness results for the AM polymeric composite samples are presented in Figure 31. Figure 31 showed a minimum decrease of approximately 10 kJ/m^2 in impact toughness for the PP parts when 40 wt. % of MRS was loaded into the material. Between the two additive manufactured materials, MSC global had the larger value of impact toughness at 4.66 kJ/m^2 along with a smaller value for standard deviation at 0.37 kJ/m^2. Since the exact decrease seen for each MSC material tested appeared different based on what MRS source location was in the MSC, it was theorized that this varied parameter had influence on part impact toughness. The results from the ANOVA test run for impact toughness, a F-value of 7.04 compared to the critical F-value of 4.41, revealed that there was statistical evidence to suggest interaction between the used MRS source location and impact toughness value for an MSC material. This supported the original observation of the data present in Figure 31.

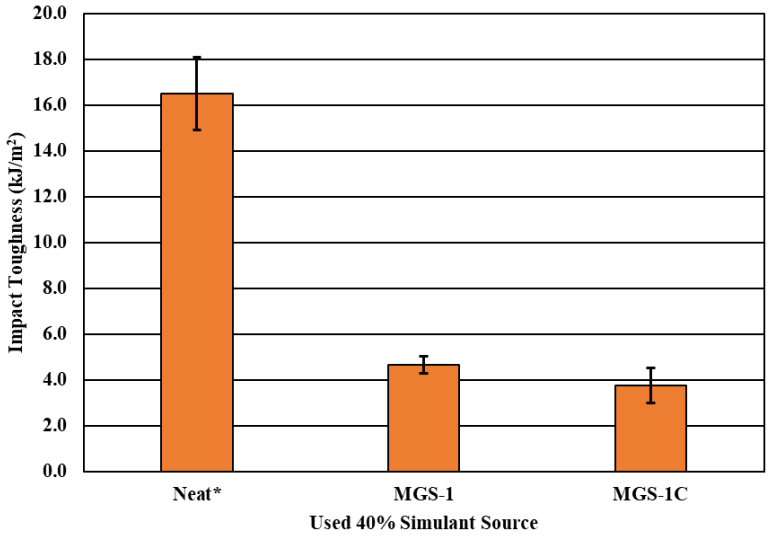

Figure 31. Notched Izod Impact Toughness of Additive Manufactured Neat PP and 40% MRS Weight Percent Loaded PP (* Different Nozzle Size Used During AM)

An important note to be made about the results of the AM MGS-1C based MSC parts was that the standard deviation, 0.76 kJ/m^2, was not within 10% of sample value mean, 3.78 kJ/m^2, as achieved with the other material tests in this study despite a large sample size of 14 specimens. This was the resulting value of standard deviation even after outlying data points were removed from the sample. The spread of the values of impact toughness in the parts' sample suggested that additional test data points would not be able to impact the value of standard deviation to a degree high enough to warrant a reasonable size of additional specimen tests. Thus, the achieved standard deviation from the AM MGS-1C based MSC sample was used as was found from the used specimens for this study.

5.3.4. AM Part Results Comparison to IM Part

A general comparison of the MSC parts made by additive manufacturing and injection molding was done in order to note any significant differences between the parts made from the two manufacturing processes. This was possible as a number of material tests completed on the

MSC parts were either the same, or relatively similar to allow for at least a general comparison of material behavior between parts created using both manufacturing processes.

5.3.4.1. AM Versus IM Part Density Results Comparison

The average densities of the neat PP parts made using additive manufacturing and injection molding were found to be similar in value. This result was expected as the used manufacturing processes were predicted to not change the neat PP material's value of density as their only differences were mechanical, and not chemical in nature. There was also no additives input into the neat PP in the creation of test parts providing more support for little to no change to have been seen in density values between the test parts made with different manufacturing processes.

The density values of approximately 1.16 g/cm^3 and 1.14 g/cm^3 for AM MSC parts made with 40 wt. % MGS-1 and 40 wt. % MGS-1C respectively were found to be slightly smaller than the average densities of the corresponding IM MSC parts made with 40 wt. % MGS-1 (1.22 g/cm^3) and 40 wt. % MGS-1C (1.21 g/cm^3). Both types of parts were made from MSC material that had been compounded/extruded with the same machine parameters and raw constituents. While the difference was relatively small, the decrease in density for parts made via additive manufacturing from parts made via injection molding suggested that the differences seen in the additive manufacturing process from injection molding allowed for the MSC material to behave in a way that resulted in parts with less density. This also provided reason for additional research to be completed to investigate the cause of this observed material behavior between manufacturing techniques.

5.3.4.2. AM Versus IM Part Tensile Results Comparison

The neat PP AM tensile parts were found to have a slightly higher value for tensile strength than those created using the IM process. The tensile strength values for neat PP parts were still

relatively similar regardless of the used manufacturing process, especially when considering the standard deviations for each of the values and the relatively small level of difference between the two values. In contrast, the average tensile modulus value measured from AM neat PP parts was almost double that of the average tensile modulus value measured from IM neat PP parts. This was theorized to be due to the individual strands of material being laid down for each layer of an AM part preventing the opportunity for large amounts of horizontal polymer chain entanglement as compared to parts made with the IM process. If this was the case, then the higher number of mostly vertically (applied force direction) aligned polymer chains could have caused increased stiffness behavior in a test part made from neat PP.

The MSC test parts created with both MRS source locations using the AM process had lower average values for tensile strength compared to test parts made with the IM process and with the same materials. In addition, the MSCs' tensile modulus values were found to be higher for AM test parts as compared to IM test parts. This result was not expected and led to the theory that an unanticipated behavior of the used MSC materials had occurred from the change in material part manufacturing technique. It was thought that additional research into the MSC constituents may provide insight into the change in tensile property values from IM to AM processing.

5.3.4.3. AM Versus IM Part Flexural Results Comparison

Neat PP parts made using the AM process were found to have higher flexural strength and modulus values as compared to those made using the IM process. The reason for this was theorized to be similar to what was thought to cause the increased stiffness in the neat PP tensile specimens. That being that the laying down of individual strands of polymer in each layer of an AM part in the zero-degree orientation resulted in a higher number of mostly aligned polymer chains could have caused increased stiffness behavior in a test part made from neat PP. This theory fit with the

observed increase in flexural strength and modulus as both can be influenced by the overall stiffness of a material.

The flexural test parts additive manufactured from the MSC made with 40 wt.% MGS-1 and MGS-1C had decreased values for flexural strength and modulus as compared to injection molded flexural test parts made from the same materials. It was unknown why this occurred with the MSC materials. This led to the idea that more information was required on the MSC constituents to investigate what could have caused the difference in flexural data collected from each manufacturing process with the MSCs.

5.3.4.4. AM Versus IM Part Notched Izod Impact Results Comparison

The neat PP notched Izod impact test specimens had an averaged impact toughness value that increased by a large margin. This result was unexpected as AM neat PP parts were found to have fairly similar results to their IM neat PP counterparts in terms of tensile and flexural properties. The reason for this increase in impact toughness when additive manufacturing the neat PP was possibly due to the printing process causing micro spaces between lines/layers of material when creating the test parts. These micro spaces between lines/layers of material are not an unknown occurrence as a previous study found when additive manufacturing test parts [56]. It was predicted that the presence of such consistent micro spaces throughout the length of the part from the AM process could explain the increased energy absorption by the test parts made of the neat PP material seen in this research.

The two AM MSC notched Izod impact samples made with both MRS source locations produced data that when averaged was relatively similar in value to the respective averaged IM MSCs' test specimen data. This suggested that the impact toughness of MSC materials was not

majorly influenced by the type of manufacturing process used to create the polymeric composite's test specimens.

5.3.4.5. AM Versus IM Part Shape and Surface Finish Comparison

The shape of the AM tensile specimens was different for all of the materials used in AM part creation. The AM tensile specimens were rectangular as compared to the dogbone shaped specimens created during the IM process. This was done as attempts to create AM dogbone specimens resulted in nozzle retraction at the tapered sections of the created part. This presented a weak point where stress concentrations would cause the AM MSC part to fail outside of the gauge length of the part. Thus, a rectangular specimen was created with the same thickness as the IM specimens according to the D3039 ASTM standard. Rectangular test specimens that fractured outside of the gauge length were considered invalid during testing. The results from the tensile tests following this standard were still comparable to the standard followed for IM tensile parts as the D3039 ASTM standard allowed for the same test parameters to be used during AM tensile testing. This meant that the only difference between the two tests was the general shape of tested parts.

The geometry of the AM neat PP rectangular test parts was relatively similar to that seen with the IM neat PP rectangular test parts. The 0.8 mm nozzle diameter allowed for printing movements by the 3D printer that were able to create parts with a high enough resolution to be nearly identical to the IM created parts. The surface finish of the AM neat PP rectangular test parts was slightly varied from that seen with IM neat PP rectangular test parts. While relatively similar in terms of the material smoothness, the AM printing process created minor, patterned grooves in the test parts where two lines of extruded material met. This was an inherent aspect of the AM

process that could not be changed based on how the layer-by-layer part creation was a key element of the FGF manufacturing process.

The geometry of the AM MSC rectangular test parts was relatively the same as that seen with the IM MSC rectangular test parts. The 2.85 mm nozzle diameter's printing resolution caused the radius of the rectangular AM part corners to be slightly different those achieved in the IM process. This was deemed acceptable as the section of the test specimens anticipated to be under stress during material testing was away from the corners of the test parts.

The surface finish of the AM MSC rectangular test parts was different than that of the IM MSC rectangular test parts. One reason for this was the resolution of the 2.85 mm nozzle diameter's printing resulting patterned grooves where lines of extruded material met. The lines of extruded material were also found to have a porous surface finish left over after being laid down on the part. This was a significant difference from the surface finish achieved with the IM MSC rectangular test parts. The specific reason for this was unknown during part creation. This provided more reason to investigate the used constituents in the MSCs to see if there was an unanticipated reaction occurring within the extrusion zones of the AM machine during part creation.

5.4. MSC Material Result and Surface Finish Variation Investigation

The MSC pellets used in creating injection molded parts saw slight to noticeable material expansion out the machine nozzle between material injections when there was no movement in the machine, especially at higher weight loading percentages of MRSs. The polymeric composite material expansion forced material out of the nozzle resulting in streams of polymeric composite with diameters slightly larger than the machine nozzle diameter. This was originally thought to be normal polymer expansion due to increased heat retention by the MRS particles and was addressed by adding a cushion or small pull back decompression retraction of the injection screw as is

normally done to address similar material behavior in other polymers. The MGS-1S based MSC pellets saw this material expansion behavior to an extreme degree, a degree much higher than the other MSC types, at all weight loading percentages of MRS in PP. When injection molding with this MGS-1S based MSC material, a large decompression retraction of the injection screw before and after each material load between material injections was required to allow for usable part creation. Based on these initial observations of material behavior, it was concluded that the MGS-1S based MSC should not be used in future part creation via injection molding or for additive manufacturing.

The MSC materials that were used in the creation of AM parts were found to exhibit noticeable material expansion out of the machine nozzle even when the extrusion screw was not spinning. This would eventually stop when not enough material was left near the extruder nozzle to expand out of the opening. The action taken to address this was to spin the extrusion screw right before printing to refill the extrusion nozzle, and the printing of a sacrificial part before the printing of test parts. This resulted in predictable, consistent material extrusion during the additive manufacturing of MSC test parts. This material expansion was similar to that seen with the same polymeric composite material when used to make IM parts.

Tested MSC parts created using additive manufacturing were observed to have a rough surface finish most notably seen on sides not in contact with the print bed as shown in Figure 32. This rough surface finish was not able to be removed using different printer settings with the MSC material used. This was in contrast to the smooth surface finished achieved with parts created via injection molding with the same MSC material.

Based on the previously observed MSC material expansion seen during injection molding, the presence of this surface finish on AM test parts was predicted to be from the material expansion

behavior actively continuing during test part creation. The streams of forced out MSC material from the material expansion had diameters slightly larger than the machine nozzle in both manufacturing processes. This material expansion behavior was thought to be due to an unanticipated reaction or gas release from the used MRSs deforming and expanding the matrix neat PP resulting in, what can be most closely described as, the foaming behavior seen in the heated MSC material. Further support for this was found with the immersion density values of additive manufactured MSC parts being slightly less than the respective injection molded MSC parts.

Figure 32. Additive Manufacture MSC-40C Part Surface Finish Example

A brief moisture analysis was completed on the raw candidate MSC material pellets to see if moisture on the pellets after oven drying could have contributed to the foaming behavior seen in the additive manufactured test parts. The moisture test run was on an Arizona Instrument LLC. Computrac MAX 4000XL Moisture Analyzer following its instructions for testing the moisture levels for neat polypropylene. MSC-40G and MSC-40C pellets were dried in an oven at 80°C for at least 12 hours before running the test. The MSC-40G pellet sample of 9.97 g was tested and found to have a measured moisture content of approximately 0.094%. The MSC-40C pellet sample of 8.50 g was tested and found to have a measured moisture content of approximately 0.070%. These values were reasoned to be low in terms of surface moisture levels on the pellets. As the same oven drying parameters used in advance of this test were also used before part creation with

both manufacturing techniques, the moisture test results suggested that surface moisture levels were not high enough to be the reason for the foaming behavior effect seen in the created additive manufactured MSC parts.

The presence of the MSC foaming behavior suggested it was possible that an unanticipated reaction or gas release from the used MRSs created micro voids between the PP and MRS particles in some of the created test parts, particularly those with higher wt. % loadings of MRSs. Before testing, a lack of bonding between the PP and MRS particles was expected due to the poor bonding/adhesion nature of PP [60], [61]. This seemed supported after testing as halves of fractured/broken test parts showed visible large MRS particles still imbedded in the PP in the same relative size and position of divots in the opposite part half as shown in Figure 33 through Figure 36.

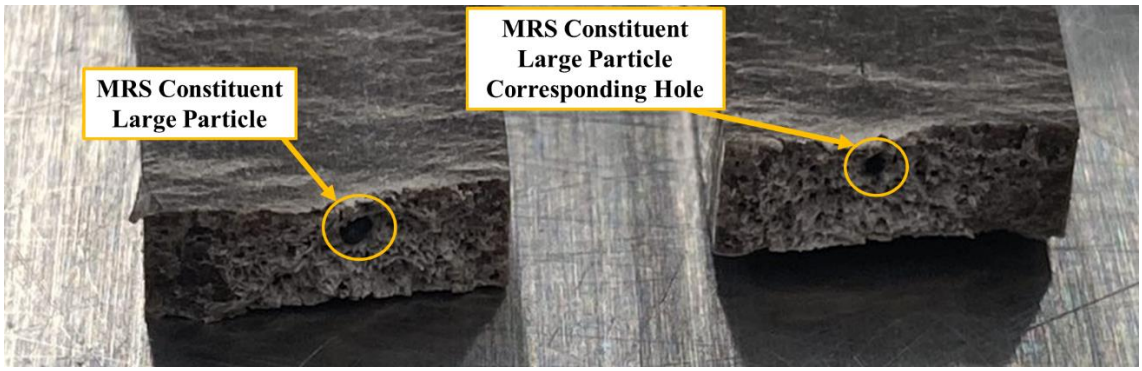

Figure 33. Injection Molded MSC-40C Tested Tensile Fracture Surface View One


Figure 34. Injection Molded MSC-40C Tested Tensile Fracture Surface View Two

This initial information about the constituents used in the creation of the tested injection molded parts seemed to justify the observations made with the resulting part fractures/breaks/failures. In addition, the nature of the manufacturing process itself may have contributed to the observed foaming behavior not being as influential on injection molded parts as additive manufactured parts given the relative velocity of material injection and presence of a rigid mold to provide pressure on material as it was molded compacting the material and expelling any trapped gasses within the part.

Figure 35. Injection Molded MSC-40C Tested Tensile Specimen Fracture Surface View Three

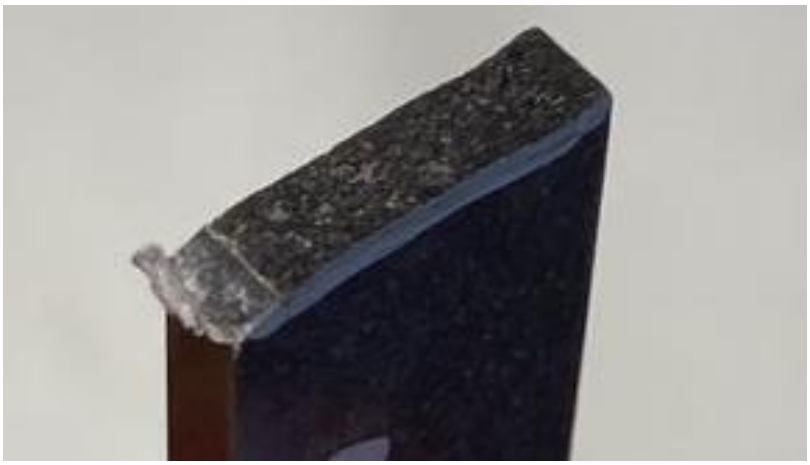

Figure 36. Injection Molded MSC-40C Tested Izod Specimen Fracture Surface

While possibly not being as impactful with injection molded parts, the observations and data made from the additive manufactured parts suggested that the foaming behavior may have

been an indication of an unanticipated, impactful element in the creation of MSC test parts. Based on this, the thought was to investigate from a theoretical standpoint potential gas releases from the used MRSs that could have caused the observed polymeric composite material foaming behavior.

The theoretical investigation of the MRS potential gas releases consisted of a review of the previously completed TGA tests with MGS-1 before test part creation, the completion of a series of additional TGA tests on the other MRS types to provide more temperature-based mass loss data on all of the MRSs, a literature review on the potential releases of the MRS constituents, and microscopy on MSC parts of the same material made using different manufacturing processes. The goal was to provide information that could provide a potential explanation for the observed foaming behavior in this study and narrow the scope for future studies that may further investigate this subject.

5.4.1. Regolith Simulant TGA Simulant Source Location Investigation

A brief thermal decomposition study had been previously completed for samples of MGS-1 as shown in Figure 7 and Figure 8 in section 3.1.3. To reiterate, Figure 7 and Figure 8 showed three wt. % drops seen during the tests of MGS-1. At approximately 100°C there was a sharp drop in the wt. % of approximately 1-2%. From approximately 150°C to 350°C there was a steady drop in the wt. % of approximately 0.75%. Finally, starting at approximately 350°C and ending at 500°C there was a sharp drop in the weight percent of approximately 2.5%. The profiles of these wt. % drops were similar in both Figure 7 and Figure 8 despite the difference in testing environment. This suggested that the presence of an inert atmosphere would not be influential in the thermal breakdown of MRSs compared to one that contained Earth atmospheric air.

After injection molding and additive manufacturing, and testing of the created MSC test parts was completed, the second series of TGA tests were run to learn more about all the MRSs

used in polymeric composite part production. These tests were run on the three types of MRS not previously studied using a TGA: MGS-1C, MGS-1S, and JEZ-1. The test results are shown in Figure 37 through Figure 39.

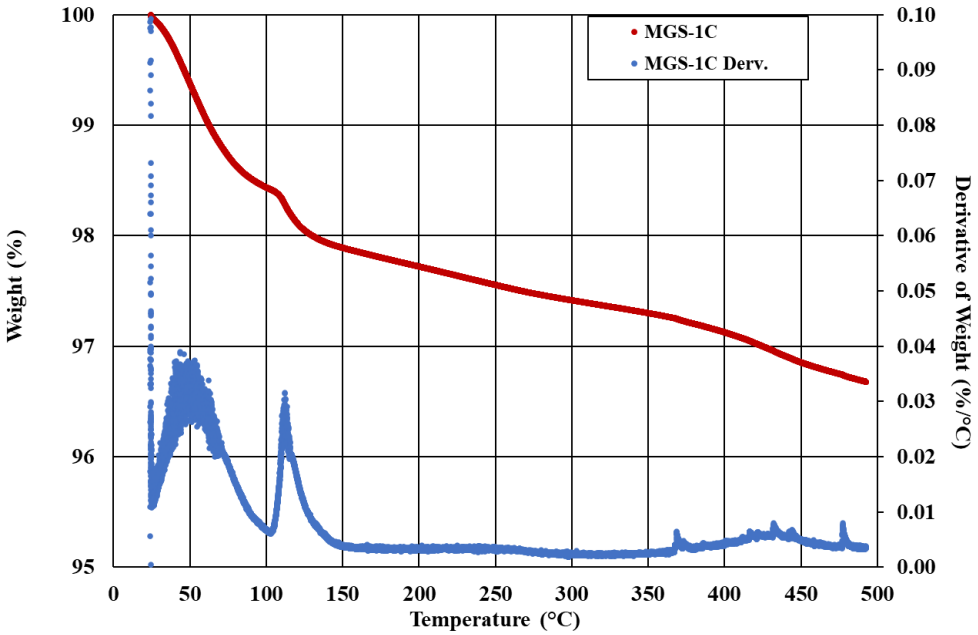

Figure 37. Q 550 TGA Test Results MGS-1C in 40% Nitrogen, 60% Room Air Environment

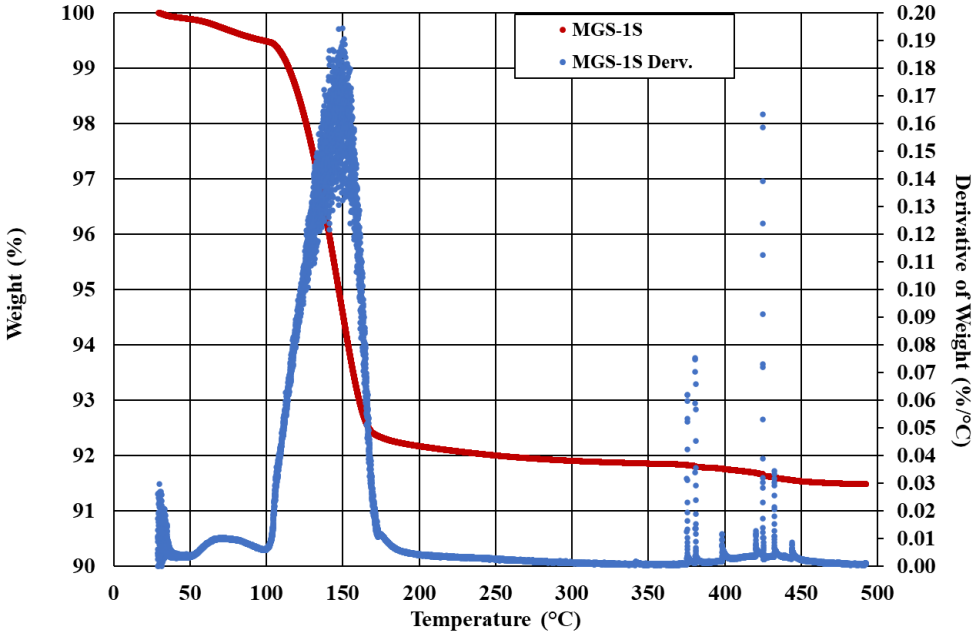

Figure 38. Q 550 TGA Test Results MGS-1S in 40% Nitrogen, 60% Room Air Environment

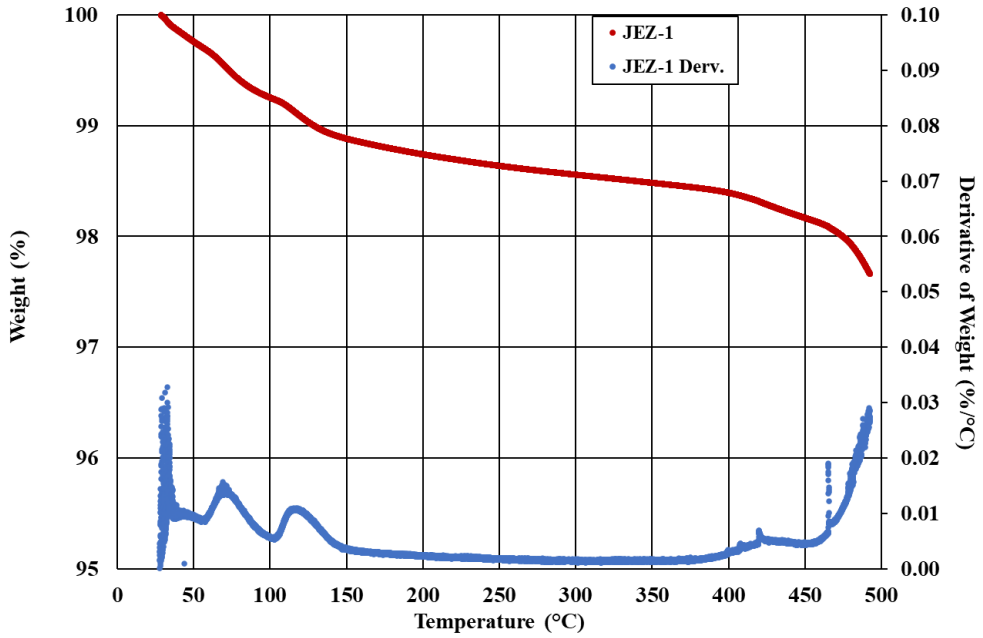

Figure 39. Q 550 TGA Test Results JEZ-1 in 40% Nitrogen, 60% Room Air Environment

The MGS-1C and JEZ-1 MRSs had results with some similarity to the original TGA tests run on MGS-1. As shown in Figure 37 and Figure 39, there were three general weight percentage drops seen during the ramp tests. These were classified as a sharp drop around 100°C, a more gradual, steady drop from approximately 150°C to 350°C, and another drop occurring at around 350°C to 500°C. These similarities made sense as the MGS-1 MRS was used at least as the basis for all three simulants.

Figure 37 and Figure 39 also showed data with a couple differences from the previous data gathered as displayed in Figure 8. In these cases, the gradual, steady weight percent drop from approximately 150°C to 350°C seen in both Figure 37 and Figure 39 appeared approximately 0.5% versus the 0.75% drop as seen with MGS-1 as shown in Figure 8. In addition, the overall weight percentage loss over the temperature ramp for MGS-1C and JEZ-1 was smaller in value, at approximately 2.5% to 3.5%, to the ~5% loss seen with MGS-1. Finally, the weight percent drops at around 100°C and 350°C to 500°C were not as severe in Figure 37 and Figure 39 as compared

to Figure 8. These differences could have been due to the variation in formulation seen in each MRS, or the use of different TGA machines used for each MRS.

Figure 11 displayed results for the MGS-1S Sulfate MRS that displayed significant difference to that seen in Figure 8. First, the overall weight percent loss was larger in value at approximately 8.5% to the ~5% seen for MGS-1 in Figure 8. Second, the primary weight percent loss (~7%) of the MRS was seen at around 110°C to 160°C. This suggested that at least one of the constituents used to make the MGS-1S, that was not in MGS-1, experienced major thermal decomposition in this temperature range.

There was one similarity between the data for MGS-1S and MGS-1. After the main weight percent loss at around 150°C, there is a steady weight percent drop that occurs from approximately 175°C to 375°C as seen in Figure 38. While a slightly shifted temperature range, this general weight percent loss is similar to that which was seen in Figure 8 for MGS-1. As the MGS-1S used MGS-1 as a basis, this could suggest the two MRSs share a similar constituent(s) that experiences steady thermal decomposition/gas release around this temperature range.

5.4.2. Regolith Simulant Temperature Cycling Investigation

An additional TGA test that was completed to learn more about the used MRSs was a temperature cycle test. The intent behind this test was to investigate the response of MGS-1 to repeat temperature ramps and one temperature hold as would generally be seen during MSC part production. The temperature cycle test was completed on a TA Instruments Q550 TGA. A sample of ~116 mg of MGS-1 was subjected to a multi-stage test. The first stage of the test consisted of a temperature ramp from room temperature (~22°C) to a temperature of 250°C at a rate of 10°C per minute. The sample was then held at 250°C for a period of two minutes then allowed to cool back down to room temperature (~22°C). The second and final stage of the test consisted of a

temperature ramp from room temperature (~22°C) to a temperature of 500°C at a rate of 10°C per minute. The test environment for all stages of the test, except during cooling, was a mixture of 40% Nitrogen and 60% room air. Figure 40 through Figure 42 display the data collected from all the stages of the TGA temperature cycle test.

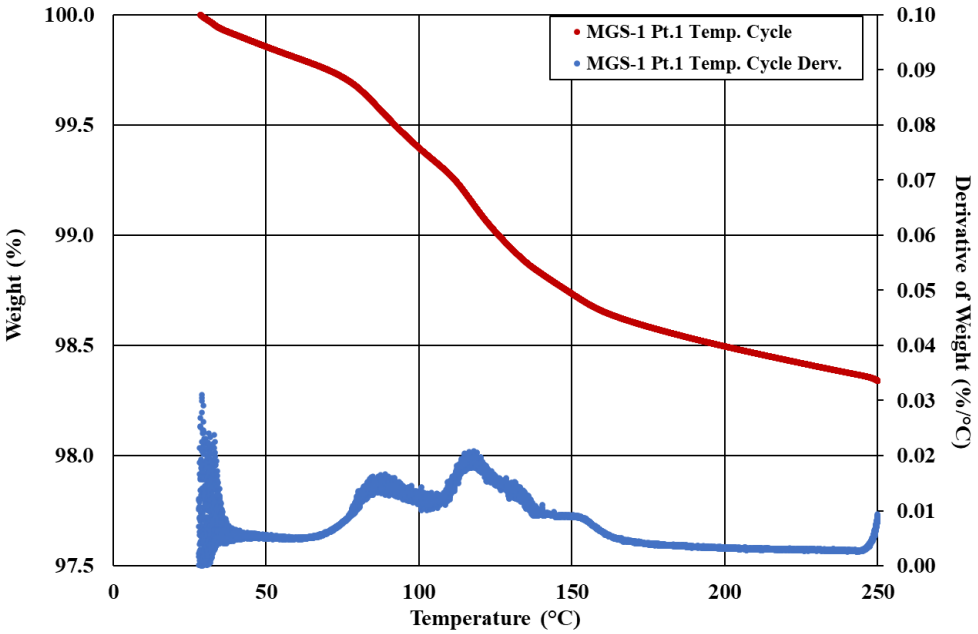

Figure 40. Q 550 TGA Temperature Cycle Test Results MGS-1 in 40% Nitrogen, 60% Room Air Environment Stage 1

Stage 1, as shown in Figure 40, showed results for the thermal response of MGS-1 that was similar to the MGS-1 thermal response displayed in Figure 8. There was an initial drop in weight percent of approximately 1-2% around the temperature 100°C. A gradual weight percent drop is then seen starting near 150°C until the maximum temperature reached in stage 1 of 250°C. This result made sense as the only changed test parameter from the initial TGA parameters used to collect the data shown in Figure 8 was the maximum value of the temperature. The results displayed in Figure 41 from the two-minute temperature hold after the stage 1 temperature ramp suggested that weight percentage change of the MGS-1 sample was negligible during the temperature hold. An unexpected item of data from this section of the test was the exponential

increase in the derivative of the weight percentage towards the end of the temperature hold. The negligible amount of weight percent loss suggested that this change in the derivative of the weight percentage came from a different source. It was theorized that the most likely candidate was the heating element of the TGA turning on at the beginning of this derivative increase to maintain the 250°C temperature that resulted in a constantly increasing value for the measured temperature near the end of this stage in the test. This then caused the calculated value of the derivative of the weight percent to also increase in value towards the end of this stage of the test.

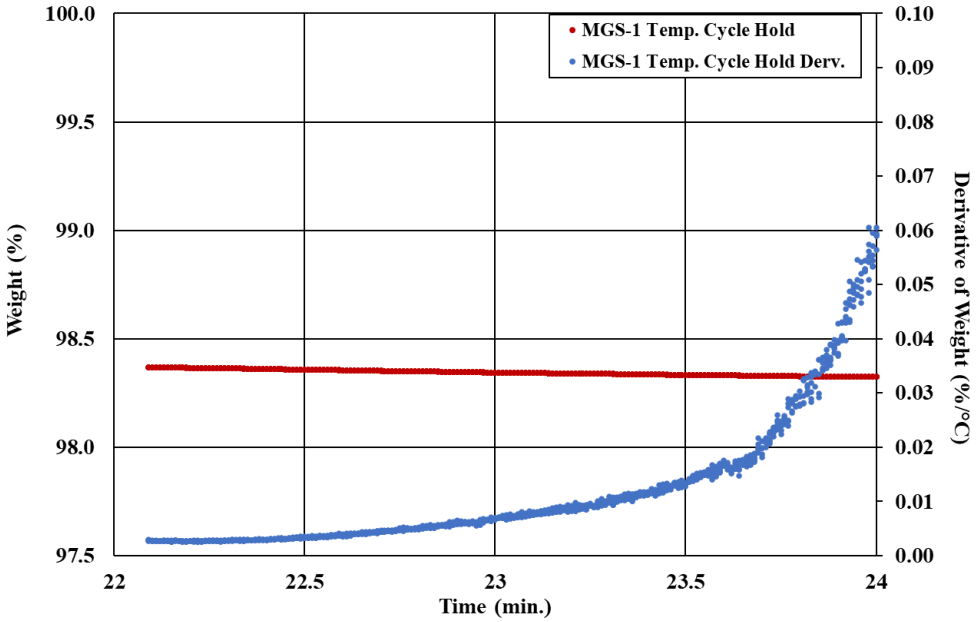

Figure 41. Q 550 TGA Temperature Cycle Test Results MGS-1 in 40% Nitrogen, 60% Room Air Environment Hold Stage at 250°C for 2 minutes

Figure 42 showed the results for the thermal response of MGS-1 during stage 2 of the test. In comparison to the stage 1 data shown in Figure 40, the initial weight percent drop seen at temperatures near 100°C as well as the gradual weight percent drop from 150°C to 250°C appeared to be smaller in value. This was supported by the value of overall mass loss of MGS-1 up to 250°C being approximately 0.05%. After 250°C, the sample of MGS-1 saw an increased rate of weight percent drop until 300°C at which point the rate of weight percent drop became more consistently gradual. An additional "sharp" drop in weight percent began at approximately 400°C and leveled

off around 500°C. In stage 2 of the test, the MGS-1 sample saw decreased overall mass loss at nearly 1.2%. Compared to Figure 8's data, the combined overall mass loss seen in the MGS-1 sample during the entire temperature cycle test was estimated to be 3%.

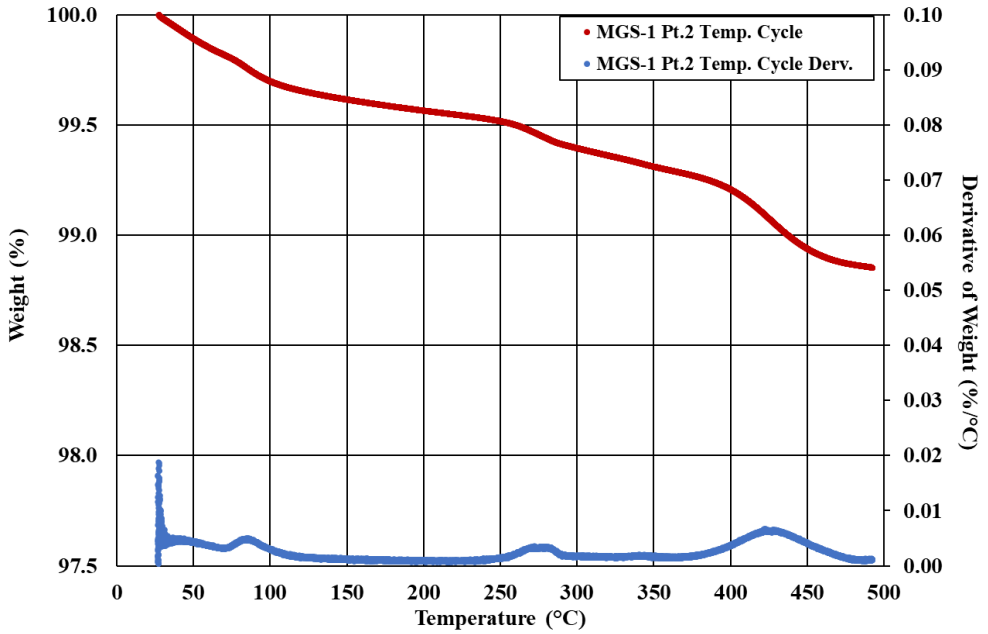

Figure 42. Q 550 TGA Temperature Cycle Test Results MGS-1 in 40% Nitrogen, 60% Room Air Environment Stage 2

The weight percent drop profile and overall value shown in Figure 42 was different from the previous MGS-1 thermal response data collected in Figure 8. The overall amount of mass loss decreased, and the weight percent drop profile behavior appeared more stable. It was thought possible that this was due to the initial stage 1 heating of the sample during the temperature ramp and hold thermally stabilizing the raw MGS-1. This had some support by the small increase of weight percent loss rate seen immediately after 250°C, the maximum temperature reached during stage 1, in stage 2 of the test as well as the overall decrease in mass loss. It was also possible that the use of different TGA equipment could have impacted the thermal response results for MGS-1 collected in Figure 40 through Figure 42 as compared to that collected for Figure 8.

5.4.3. MSC Regolith Simulant Constituent Theoretical Release Investigation

The simulant thermal release literature review aimed at finding research that documented the thermal decomposition and respective release of each individual constituent for each MRS type for the temperature range of the original TGA completed on the MGS-1 simulant (~22°C to 500°C).

The constituents of all of the MRSs that were found to potentially thermally decompose within the original TGA temperature range according to previous research sources are olivine, ferrihydrite, hydrated silica, Fe-carbonate, smectite, gypsum, and Mg-carbonate (assumed natural magnesite).

For olivine, major thermal decomposition of the isolated mineral did not seem to occur until temperatures around 1600°C [44], [62]. Before that temperature, sources suggested that the general presence of some element/impurities such as carbon or hydrogen might result in some oxygen release from the mineral at lower temperatures in the range close to 200°C [43]–[45].

Ferrihydrite was cited as going through dehydration/dehydroxylation when heated to a temperature of 460°C. Through this process, the ferrihydrite can release water during the crystallization of hematite [46], [47], [63].

Hydrated silica can possibly form and release water molecules leaving behind silica [41]. This is because minerals like hydrated silica are noted for having low thermal stability due to containing absorbed water and OH-groups. The minerals are cited as becoming unstable at around 370 K, or approximately 97°C [42].

Fe-carbonate was cited as experiencing thermal decomposition at around 400-600°C [48], [49]. During this thermal decomposition, it can be possible for the Fe- carbonate to decompose into carbon dioxide, other various oxides, and magnetite [48], [50].

Sources suggested that unmodified smectite contains water as absorbed/surface/interlayer molecular water, and as structural water in the mineral itself. The absorbed/surface/interlayer molecular water could be removed at temperatures around 20-380°C while the structural level water could be removed at temperatures around 400-700°C [64], [65].

Gypsum in its pure form could contain upwards of 20% water by mass. This water could be released at temperatures lower than 210°C [66]. One source's experimental results suggested that this dehydration occurs at approximately 120°C causing the formation of anhydrite [67].

Mg-carbonate (assumed/reasoned to be in its natural form of magnesite) can thermally decompose into water, magnesium oxide, and carbon dioxide. Some water loss and some carbon dioxide release was suggested to occur at around 200°C. The temperature range in which the main carbon dioxide is released leaving magnesium oxide was cited to occur at 500-550°C [68]–[70].

5.4.4. Suggested Candidates for TGA Weight Percent Drops in Temperature Range

In Figure 7 and Figure 8, three primary drops in weight percentage were seen in for MGS-1 with a sharp drop at approximately 100°C, a gradual drop from 150-350°C, and a sharp drop starting at approximately 350°C and ending at 500°C. Based on the simulant thermal release literature review, the most likely constituent candidates to have caused these weight percent drops due to thermal decomposition were olivine, ferrihydrite, hydrated silica, and Fe-carbonate. As mentioned in the previous section, hydrated silica can dehydrate at around 100°C, olivine is able to release oxygen at temperatures around 200°C due to the presence of carbon and hydrogen (as found in the simulant), and ferrihydrite and Fe-carbonate are able to thermally decompose at temperatures around 400-600°C with ferrihydrite releasing water and Fe-carbonate releasing carbon dioxide and various oxides.

The company that created the simulant, Exolith Labs, provided an evolved gas TGA for MGS-1 in an updated technical data sheet released near the time of completing this study. Figure 43 shows the data collected from this test.

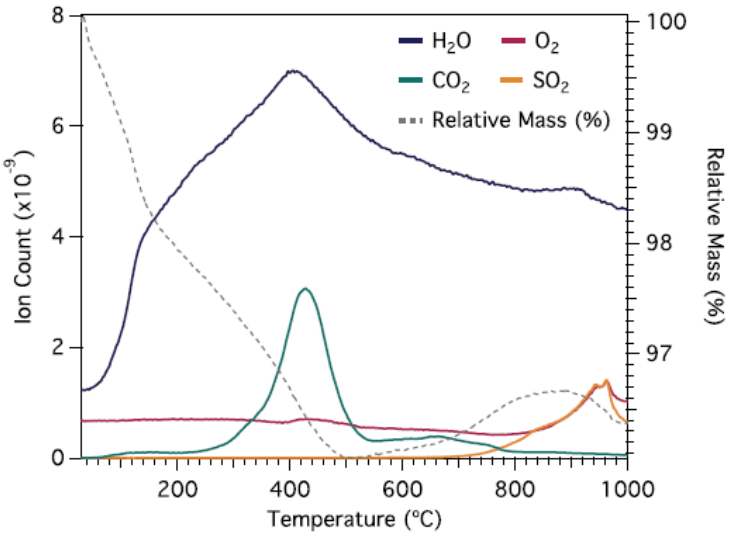

Figure 43. Exolith Labs' Combined Thermogravimetry and Evolved Gas Analysis of MGS-1 Prototype, Performed at SAM-like Conditions, Reproduced from Reference [71]

The data present in Figure 43 seemed to be comparable with the performed TGA results of Figure 7 and Figure 8 along with the findings of the simulant thermal release literature review especially with its detection of water, oxygen, and carbon dioxide at temperatures between 0-500°C. A noteworthy item from Figure 43 was the continual detection of water and oxygen ions that seemed to occur from the beginning of the test (0°C) to the end of the test (1000°C). This was of particular interest when comparing with the gradual weight percent drop of MGS-1 in Figure 7 and Figure 8 from approximately 150-350°C. Based on the simulant thermal release literature review, it was theorized that the steady increasing release of water in this temperature range was possibly from hydrated silica on the tail end of its dehydration and ferrihydrite at the beginning of its dehydration. It was also suggested that the steady release of oxygen in the specified temperature range was due to the thermal decomposition of olivine. These findings, while not definitive, were

promising in terms of providing likely explanations to the weight percent drops seen for MGS-1 during TGA tests.

MGS-1C (Clay MRS) was shown in Figure 37 to experience a similar weight percent loss profile as MGS-1. This made sense as MGS-1C was created using MGS-1 as a base, and thus contained the same base constituents. Therefore, the thermal releases seen in MGS-1 were theorized to be mostly the same as for MGS-1C. The primary difference between the two MRSs was the presence of 40% by weight of smectite in MGS-1C [37]. Based on the simulant thermal release literature review, it was suggested that this constituent was capable of releasing absorbed/surface/interlayer molecular water at temperatures around 20-380°C and structural level water at temperatures around 400-700°C. Figure 37 showed an overall weight percent drop that was smaller than that seen in MGS-1 as in Figure 8 with smaller sharp drop in weight percent occurring at around 400-600°C. It was thought possible that the more gradual weight percent drop profile of the simulant was from the presence of smectite taking the place of the constituents ferrihydrite and Fe-carbonate thus preventing their more significant release of water and carbon dioxide/other oxides near this temperature range. This also suggested that the more gradual weight percent drop behavior of the simulant was due to the steady release of water from the smectite first with the absorbed/surface/interlayer molecular water at temperatures around 20-380°C and then the structural level water 400-500°C.

MGS-1S (Sulfate MRS) had a weight percent drop profile that was different than that seen with MGS-1 in Figure 8 with a majority of its weight percent drop seen at approximately 110-160°C as displayed in Figure 38. This suggested that the difference in formulation of MGS-1S to MGS-1 was the most likely reason for the difference in thermal response data. Indeed, based on the simulant thermal release literature review and Exolith lab data, MGS-1S contained gypsum

which was suggested to be capable of thermally decomposing/dehydrating at approximately 120°C forming anhydrite. According to Exolith Labs, MGS-1S was made up of 40% gypsum with the rest of its composition being the same constituents as MGS-1 [37]. The presence of a relatively high amount of a constituent capable of thermal decomposition at temperatures within in the 110-160°C range as seen in Figure 38 seems to explain the weight percent drop profile shown for MGS-1S. The additional gradual weight percent drop seen from 175-375°C was possibly explained by the thermal decomposition of MGS-1 constituents present in MGS-1S.

Figure 39 displayed a weight percent drop profile for JEZ-1 that was similar to what was seen with MGS-1 in Figure 8 with a few differences. The similar weight percent drop profile of a sharp drop around 100°C, a more gradual, steady drop from approximately 150-350°C, and another drop occurring at around 350-500°C supported the idea that JEZ-1 used the same constituents as MGS-1 as a base.

The differences seen for JEZ-1 were thought to be due to the difference in constituents seen between this MRS and MGS-1. JEZ-1 contained 11% of Mg-carbonate (magnesite), and 6% of smectite which were not present in MGS-1 [37]. Based on the thermal release investigation of the MRS constituents, it is possible that Mg-carbonate was responsible for some of the gradual weight percent drop seen from 150-350°C due to minor releases of carbon dioxide and water. This gradual weight percent drop could also be from some water release from smectite as well similar to that seen with MGS-1C. The weight percent drop seen at 350-500°C was thought to be due to additional releases by Mg-carbonate, specifically the release of carbon dioxide according to some of the literature review sources. The overall weight percent loss of ~3% seen of JEZ-1 in Figure 39, as compared to the ~5% seen for MGS-1 in figure 9, was predicted to be due to the inclusion of Mg-carbonate and smectite in the MRS which displaced previous concentrations of constituents such

as ferrihydrite and Fe-carbonate preventing their predicted higher releases of water and carbon dioxide/other oxides near temperatures around 400-600°C.

JEZ-1 also contained over double the amount of olivine as that seen in MGS-1. Alone, this information would suggest that any thermally based releases from the mineral would increase from that predicted in MGS-1. Figure 39 showed that in the theoretical thermal release temperature range of olivine, as suggested when investigating MGS-1, the total amount of weight percent loss seen was actually smaller in value at ~0.5% as compared to the ~0.75% seen for MGS-1 as seen in Figure 8. Based on this information, it was theorized that the elements of carbon and hydrogen that sources claimed were needed for oxygen release by olivine at these temperatures were not as prevalent in JEZ-1 as compared to MGS-1. This was supported by the amounts of hydrated silica and ferrihydrite in JEZ-1 both being smaller than those in MGS-1. These two minerals were theorized in a previous section to release a small, gradual amount of water over the temperature range in question of 150-350°C, which would reduce the potential presence of the element hydrogen needed for theoretical releases of oxygen by olivine.

Material processing temperatures for the created MSC materials was at its maximum 270°C. Surface moisture of the MRSs and MSCs was removed as each material was always oven dried before material processing to remove such moisture. This was confirmed to be the case by the previously mentioned moisture tests performed on some of the candidate MSC pellets. Thus, thermal release behavior for the MRS constituents between ~100°C to 270°C were thought to be the best candidates for explaining the foaming behavior seen in the MSCs to varying degrees.

5.4.5. Created Part Microscopy

The cross-sectional area of an IM MSC test part with 40 wt. % MGS-1 was viewed with a microscope at 10X, 20X, 50X, and 100X as shown in Figure 44 through Figure 47. The part's

internal structure and constituent interface were investigated for material behavior that would suggest elements of the foaming behavior seen in the created MSCs.

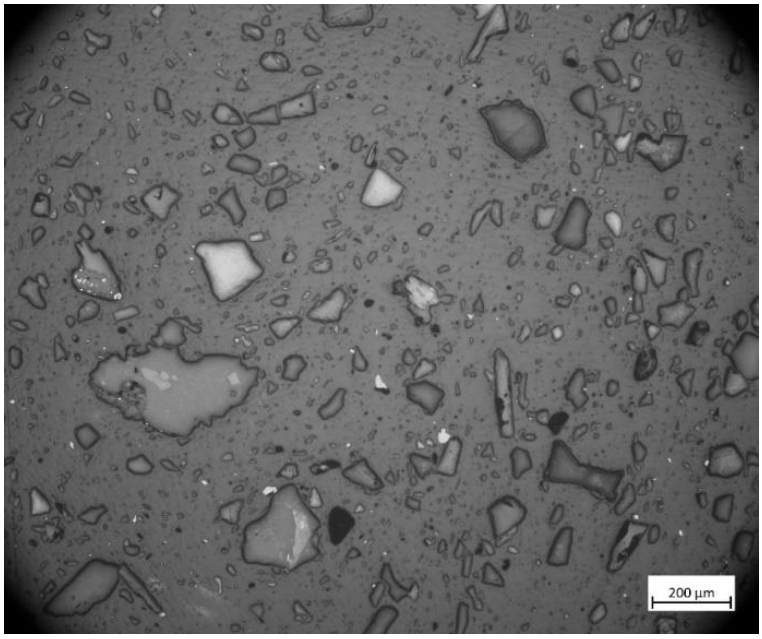

Figure 44. 10X Microscope Cross Section Image of IM MSC Part with 40 Weight Percent MRS

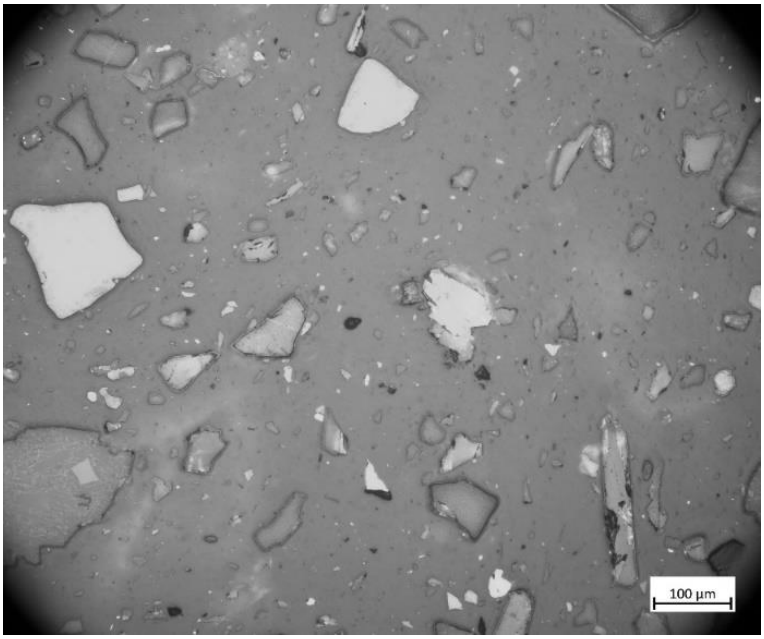

Figure 45. 20X Microscope Cross Section Image of IM MSC Part with 40 Weight Percent MRS

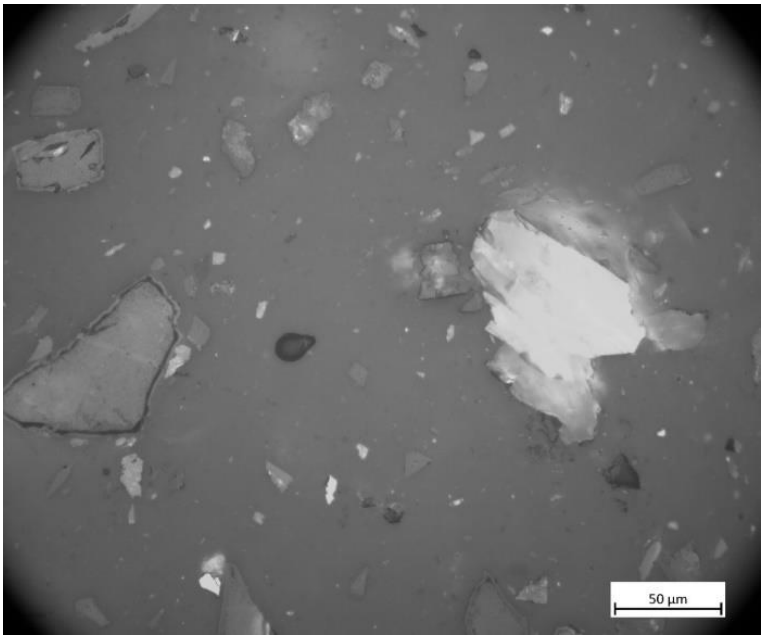

Figure 46. 50X Microscope Cross Section Image of IM MSC Part with 40 Weight Percent MRS

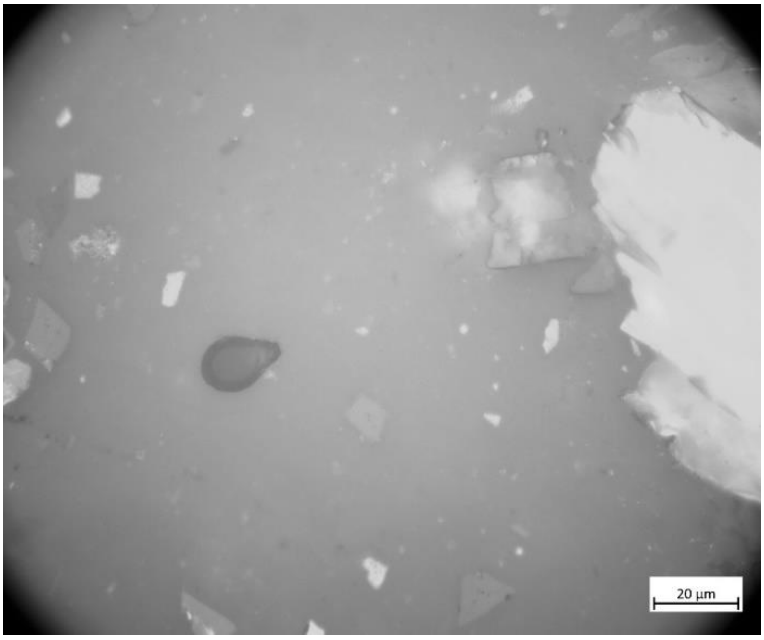

Figure 47. 100X Microscope Cross Section Image of IM MSC Part with 40 Weight Percent MRS

The general dispersion of constituent particles with a variety of shape, size, pattern, and coloration was expected to be seen in the MSC part. This was theorized to be due to the used MRS being made of multiple minerals. Figure 44 through Figure 47 all displayed a large number of varied particulates suspended in the matrix material which seemed to verify this expectation.

Figure 44 through Figure 47 showed several dark spots within the PP. A number of these dark spots were investigated for their potential as voids. Most of the dark spots were found to be dark colored constituent particles while others were suspected to be the former location of constituent particles. The reasoning behind suspecting some of the dark spots being the former location of constituent particles was based on their shape, sharp clean lines in particular, and size being similar to other constituent particles still within the PP matrix. It was assumed that the particles that were once in these spots fell out either during the fracturing/cutting of the part, or during part polishing.

One of the smaller dark spots, approximately 10 μm in diameter was magnified at 100X on the microscope as shown in Figure 47. This dark spot showed the sign of being a former site of a constituent particle from a sharp, angular point as a part of its shape. The rest of its shape was near circular which indicated the presence of a void from most likely the former presence of a released gas. These aspects of the magnified dark spot in Figure 47 provided support to the idea that the constituent particle that was formerly present in this location produced a thermal release as a response to heat after already being within the matrix PP resulting in slight deformation of the matrix material in the immediate vicinity of the constituent particle. It was assumed that the particle once in this spot later fell out either when the part was fractured/cut, or during part polishing. This provided additional support to the idea of specific constituent thermal releases being the reason for the observed MSC foaming behavior. Additional dark spots that were similar to the one seen in Figure 47 did not appear prevalent or larger than 10 μm in diameter in the rest of the IM MSC part.

This result was anticipated for IM MSC parts after observing the foaming material behavior during additive manufacturing. The basis for this prediction was from the nature of the IM manufacturing process used to create the MSC material. The rapid injection of material into a ridge mold most likely moved the material into an environment in which the surrounding pressure either

expelled or prevented major matrix material deformation from any thermal releases of the present constituents in the PP. The images shown in Figure 44 through Figure 47 appeared to verify this idea. This suggested that while the foaming behavior was present or had the potential to be present to some degree in IM MSC parts, its impact on overall material behavior was low as long as the present constituents did not produce thermal releases that caused extreme polymeric composite material foaming behavior.

A microscope at 10X, 20X, 50X, and 100X was used to view the cross-sectional area of an AM MSC part with 40 wt. % MGS-1. Figure 48 through Figure 53 show the images collected from this part. The AM MSC part's internal structure and constituent interface were investigated for similarities to the test part made of the same MSC material with IM processing as well as elements would suggest the presence of the foaming behavior seen in the created MSCs during material processing.

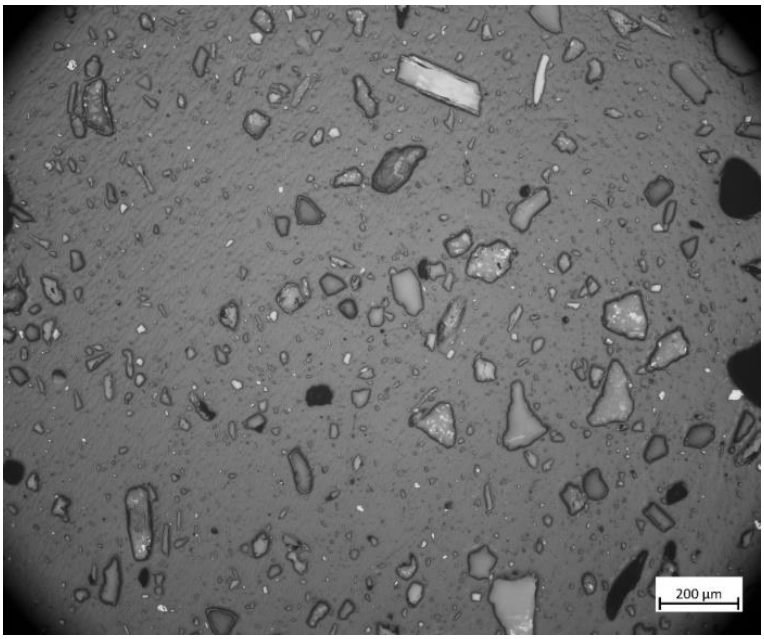

Figure 48. 10X Microscope Cross Section Image of AM MSC Part with 40 Weight Percent MRS Area View One

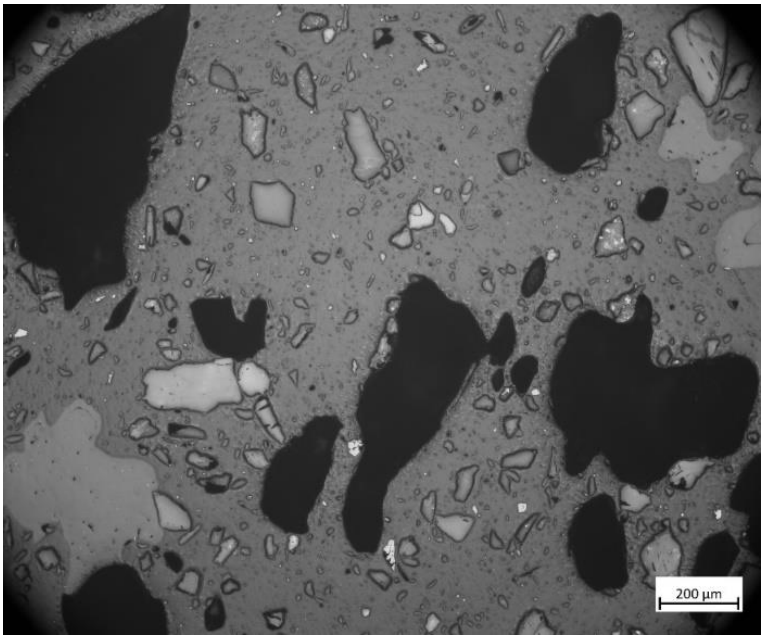

Figure 49. 10X Microscope Cross Section Image of AM MSC Part with 40 Weight Percent MRS Area View Two

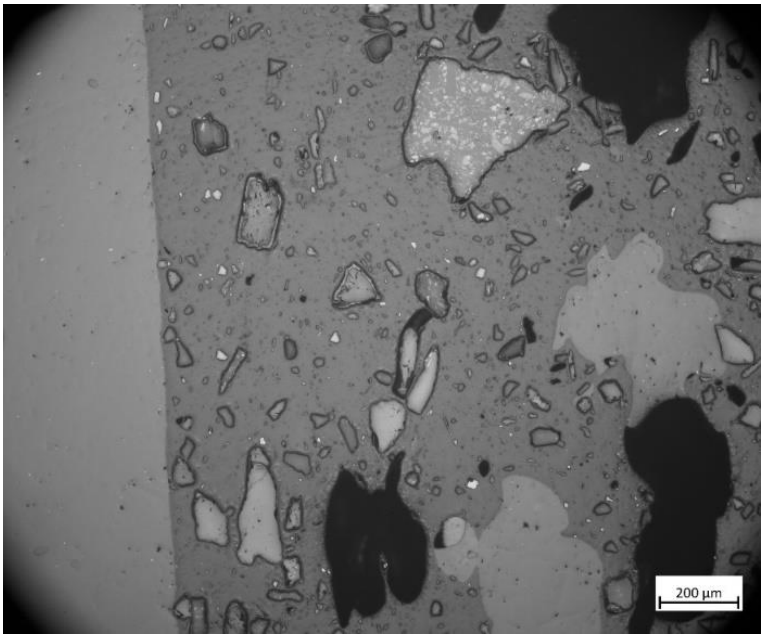

Figure 50. 10X Microscope Cross Section Image of AM MSC Part with 40 Weight Percent MRS Area View Three Showing Epoxy Material Comparison

Figure 48 showed areas of the AM part material that appeared much like the IM part material as shown in Figure 44. These regions contained similar various constituents as suspended in the matrix PP. In some cases, dark regions of the material were dark constituents, or suspected to be the former site of constituent particles due to shapes, sizes, and sharp lines being similar to

the present constituent particles. This result was reasonable given that the same material was used to create the parts magnified in Figure 44 and Figure 48.

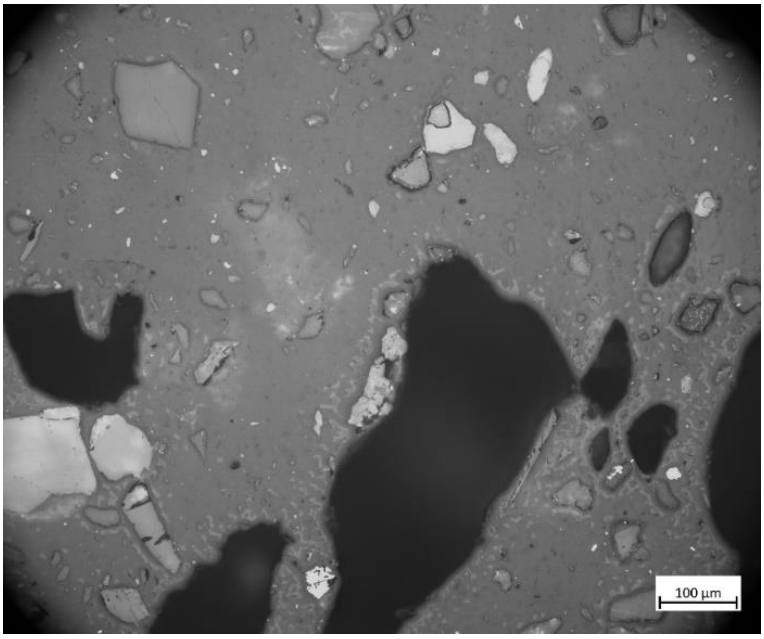

Figure 51. 20X Microscope Cross Section Image of AM MSC Part with 40 Weight Percent MRS

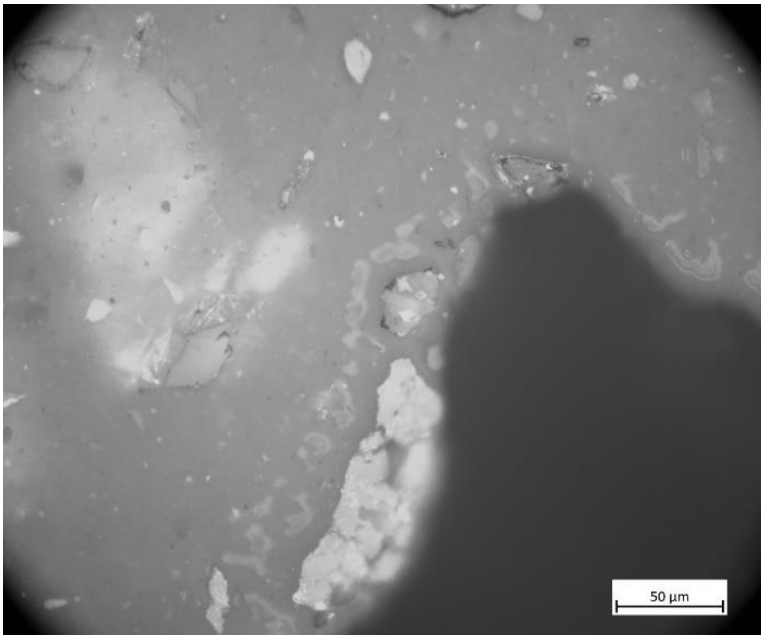

Figure 52. 50X Microscope Cross Section Image of AM MSC Part with 40 Weight Percent MRS

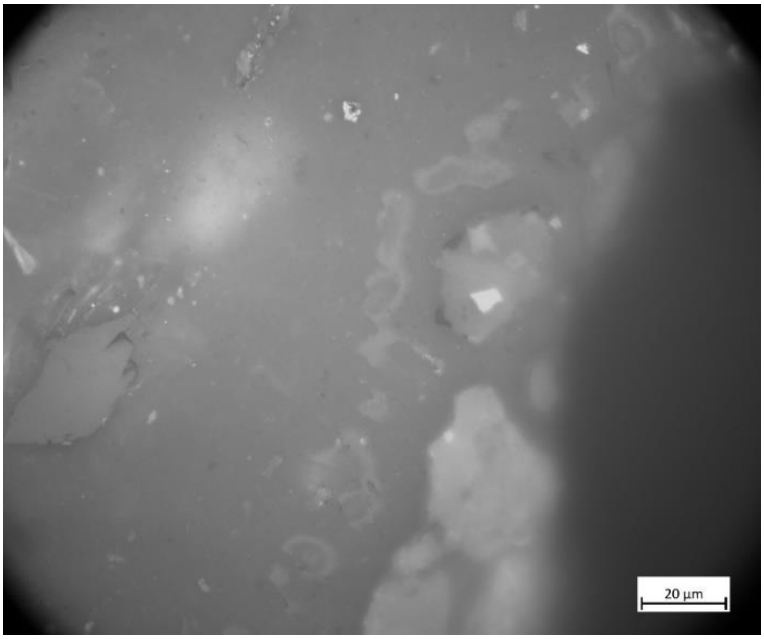

Figure 53. 100X Microscope Cross Section Image of AM MSC Part with 40 Weight Percent MRS

Large dark regions that were not similar in shape to the present constituents and found not to be dark colored constituent particles were also present in Figure 48. Another area view, displayed by Figure 49, of the AM MSC part showed additional, larger dark regions than those seen in Figure 48. These large dark regions were found to be voids given their shape and size difference from the present constituents and based on changing the focus the microscope lens revealing relatively large amount of depth to the dark regions. This was a significant difference from the image of the IM part shown in Figure 44. It also made sense given the constant MSC material foaming behavior seen during test part additive manufacturing, and how well the result seemed to line up with the ideas proposed by the thermal breakdown literature review. Specifically, the thermal breakdown literature review suggested thermal releases from only certain constituent particles as being the possible reason for the polymeric composite foaming behavior. This lined up with the images shown in Figure 44 and Figure 49 with some of the constituent particles having indications of thermal releases around them while others did not show such indications. In the case

of the AM MSC part in Figure 49, it was assumed that the constituent particles suspected as being responsible for the large voids either remained loose in the interior of the void or became slightly imbedded on a side of the void from gravity during part cooling. These particles where then assumed to have been unable to be seen at the used depth of polishing or fallen out during the part fracture/cutting, or polishing process. Again, the AM MSC parts, once laid on the printing bed, did not have rapid material movement or pressure to offer any potential prevention or mitigation of the foaming behavior as was present for parts during MSC IM processing. Thus, the presence of more, larger sized voids seemed to suggest that thermal releases from the present MRS constituent particles likely caused the foaming behavior of the MSC material, and that such foaming behavior was more influential during the AM process as compared to the IM process due to the differences in material movement velocity and part pressure between the manufacturing processes. This provided support for the recommendation of future research into finding a method to remove the foaming behavior seen in the MSC materials at high constituent wt. % loadings to investigate the impact on MSC test part strength characteristics.

Certain regions of the AM MSC part shown in Figure 49 appeared to be similar in shape to the present large voids in the material yet consisting of a constituent that had not been previously seen in the IM MSC part material. Shifting the view of the microscope to the edge of the AM part provided a potential explanation for this unknown constituent. Figure 50 showed both the MSC material and epoxy used in mounting the sample as it was focused near the edge of the AM MSC part. The polished epoxy material shared similar shading and surface texture to the unknown constituent regions seen in the part in both Figure 49 and Figure 50. This suggested that these regions of unknown constituents were epoxy that seeped into the MSC part during mounting and curing of the sample. This was theorized to be a reasonable explanation as the presence and

prevalence of voids in the AM MSC part could have allowed for such epoxy seepage during mounting, especially during the use of the vacuum pump.

This conclusion aided in investigating other regions with previously unobserved elements of the AM MSC part with the further magnified views in Figure 51 through Figure 53. These figures observed higher magnifications of the material in the vicinity of the edge of one of the large voids in the AM MSC part. This area of the part contained regions of material that were different in shape and shading to the other constituents previously observed in the MSC material. From view acquired at 20X, as seen in Figure 51, these regions of unknown material had what can be described as a speckled appearance near the large void's edges. The observed regions' shapes, shadings, and close vicinity to the edges of large voids suggested that these were former sites of voids that had been filled with epoxy during the part mounting process. This was again thought to be a reasonable suggestion given the vacuum pressure which was applied to the epoxy and sample during the mounting process. Figure 44 through Figure 47 of the IM part made from the same MSC material showed no instances of such speckled regions which further indicated that such parts did not contain the same prevalence of voids as the AM MSC parts. Thus, the presence of the speckled regions near void edges in the AM MSC part provided additional evidence of the porous nature of the test parts due to the foaming material behavior seen when created using the AM process. This provided further support for future research to investigate ways of preventing the foaming material behavior during MSC part creation, potentially through the elimination/suppression of the thermal releases of the MRS constituents.

5.4.6. Simulant Thermal Release Investigation Closing Remarks

Investigating a way/method to remove this suggested thermal release by the MRSs before material processing would be the recommended step for future research projects related to this

topic. While the MRS constituent material's physical breakdown in response to heat may not be significant enough to influence a created part's material properties, the suggested gas release was significant in potentially explaining the observed material foaming behavior seen during material processing. Implementing a way to remove this gas release may lead to the material properties of MSC parts made from the raw materials used in this study to have closer values seen between the two manufacturing processes and improve the overall material properties of MSC parts made in this study.

CHAPTER 6. CONCLUSIONS

The completed research attempted to create MSC material parts using a neat polymer with potential for in situ creation on the surface of Mars, a variety of MRS source locations, multiple MRS wt. % loadings, IM material processing, and AM material processing. The intent was to learn material characteristic data from these parts as each of the parameters used to create them was varied.

MSC parts of varying wt. % loadings and source locations of MRSs were created using injection molding. The collected material data suggested that wt. % loading impacted all of the IM part material characteristics tested except for T_g. IM MSC tensile strength, after initially increasing from neat PP, was found to decrease as wt. % loading of MRS increased in value to a relatively high statistical degree. IM MSC tensile modulus, after initially decreasing from neat PP, increased to a relatively high statistical degree as wt. % loading of MRS increased in value. Test part flexural strength, flexural modulus, density, and HDT values for IM MSC materials increased in value from those found in neat PP as MRS increased in wt. % loading with statistical evidence suggesting the influence of this varied parameter was to a relative high degree. The impact toughness and CLTE of IM MSC test parts saw decreases in value to a relatively high statistical degree as MRS wt. % loading increased in value. The MSC materials' MFI values had evidence to suggest that they were influenced by the changes in wt. % loading of MRS used in the material though statistical evidence implied this influence was to a low degree, and the collected values did not show consistent data trends between the different used types of MRS to imply which had more or less favorable material behavior.

The data also suggested that MRS source location had influence over tensile modulus, flexural strength, T_g, MFI, and density values for IM parts. The amount of increase in tensile

modulus values as wt. % MRS increased from neat PP saw slight variance between the IM MSC test parts based on the used MRS type. Statistical evidence supported the idea that MRS type influenced MSC tensile modulus values while also suggesting that the degree of influence was relatively low. The flexural strength values of IM MSC test parts that utilized MGS-1C saw higher increases in value as compared to the other IM MSC test parts made with other MRSs as wt. % loading of MRS went up. The statistical analysis provided evidence to suggest that while the influence by MRS type on flexural strength values of IM MSC test parts was present, it was to a low degree. The T_g values of IM MSC parts showed slightly varied data trends as there was variation in the used type of MRS. The overall amount of variation seen was observed to be small. In addition, there were no clear, consistent trends in the T_g value data that were able to suggest which MSC material, as varied by used MRS type, had more or less desirable material characteristics as compared to the other MSC materials when looking at all of the used MRS wt. % loadings. This was supported by statistical data which suggested that the influence by the variation of MRS type in IM MSC test parts on T_g values was present, though low in degree. The MSC materials showed different MFI data trends from neat PP to 40 wt. % loadings of MRS depending on what type of MRS was used in the MSC material. While this indicated influence by the varied parameter, the data did not provide consistent enough trends to definitively suggest which general type of MRS used in an MSC material had more or less favorable MFI characteristics when considering all of the used wt. % loadings of MRS. In addition, statistical analysis suggested that the degree of influence by MRS type variance on MFI value was low. The density values of IM MSC test parts which utilized MGS-1S saw slightly smaller density values as compared to the other MSC materials, especially at higher wt. % loadings of MRS. Statistical

evidence supported this observation though indicated that the degree of influence from varying the type of MRS in IM MSC test parts on density values was relatively low.

The data collected for IM parts was able to be utilized in selecting candidate materials for the additive manufacturing of MSC parts. Select candidate MSCs made with 40 wt. % MGS-1 and 40 wt. % MGS-1C were used to create AM test parts. Varying the MRS source location used in the MSCs was found to result in variation of the tensile modulus, flexural strength, flexural modulus, impact toughness, and density values of the AM parts. AM MSC test parts saw an increase in tensile modulus from AM neat PP test parts with AM MSC using MGS-1C having higher tensile modulus values than those made using MGS-1. AM MSC test parts had decreases in flexural strength compared to those made with neat PP with the MGS-1C based MSC test parts having the least amount of decrease seen of the AM MSC test parts. The flexural modulus values of AM MSC test parts increased from neat PP test parts with MSC using MGS-1C having a higher value of flexural modulus as compared to MSC using MGS-1. The values of impact toughness for AM MSC test parts decreased from neat PP test parts with MGS-1 based AM MSC test parts having smaller decreases in impact toughness values compared to MGS-1C based AM MSC test parts. Density values of AM MSC parts saw general increases in their average values from neat PP test parts with MGS-1 based AM MSC test parts having slightly higher densities than those which utilized MGS-1C.

The AM test parts' collected material data was found to be generally different in value than that seen with IM parts made from the same materials, specifically with tensile and flexural data. The AM test parts were also found to have a different and unique surface finish from the IM parts made with the same MSC material. This variation from the IM MSC parts provided reason to

perform additional research on the raw constituents used to create the MSC materials for thermal releases.

Additional research on the MSC used MRSs was done in response to the noted differences seen in MSC test part surface finish and material properties when comparing the used manufacturing technique. The focus of this investigation was to offer an explanation for the observed foaming behavior of the MSC material during part manufacturing that occurred in some capacity for all MSC materials, and to a high degree for MSCs utilizing the MRS MGS-1S. This consisted of a brief moisture test on the MSC pellets used during additive manufacturing, additional TGA tests run on all of the MRS source locations, and a theoretical literature review of the potential thermal releases of the constituents present in the MRSs. The results from this investigation pointed to certain MRS constituents releasing small amounts of water and oxygen being the likely candidates for the general material foaming behavior seen for all MSCs during thermal processing, and the releases of the constituent gypsum being the reason for the extreme foaming behavior seen in the MSCs utilizing MGS-1S as a response to thermal processing. The investigation also suggested that the explanation for the difference in surface finish between the IM and AM parts made of the same MSC materials was that the IM process had rapid movement of the MSC material into a ridged mold which prevented the thermal releases of the MRS particles from causing significant influence on the resulting parts as the pressure on the material from this process both compacted the material and expelled any trapped releases in a polymeric composite part.

CHAPTER 7. FUTURE WORK AND RECOMMENDATIONS

The completed work provided material data for MSCs that was seen as a good starting point for looking at the differences between varying the type of MRS and manufacturing technique used in MSC part creation. The research and collected data also raised new questions related to the topic of additive manufacturing MRS based polymeric composites that would be worth looking into in the future. Looking forward, additional steps could be taken to answer some of the questions raised by the research, investigate this topic further, and possibly improve MSC material characteristics.

As mentioned previously, the ability to create raw polymer in-situ on an extraterrestrial body from the available material would be vital to furthering the ability to feasible create parts completely in-situ on an extraterrestrial body. This would aid in decreasing project dependence on Earth based materials sent to an extraterrestrial body as well as decrease the time required for suitable mission critical replacement parts to be available to any astronauts on said extraterrestrial body. Further investigating and experimenting with the feasibility to create polymer out of the theoretical resources available on the surface of Mars would be recommended as a key step in further improving the potential of MSC use on surface missions. The hope with such research would be able to create samples of polymer as made using only materials and processes theoretically available on the surface of Mars and get material characteristic data from such in-situ polymer either as neat material or mixed with MRS to create an MSC.

It is also recommended that additional polymers, or at least a different grade of PP, with Martian in-situ potential be used to create more MSC materials for the gathering of material characteristic data. An investigation into this topic could present options other than the PP used in

this research for MSC part creation which in turn could present more theoretical options for Martian regolith composites.

An investigation of wt. % loading values of MRS other than those used in this research should be done to see if larger values can be used to reduce the amount of polymer required in a created part. Finding the point at which usable test parts are no longer able to be created from the constituents would be useful in demonstrating the material saving potential that MSCs indicate for Martian regolith composites.

Future research could be done into the impact of other additives, in addition to MRSs and polymers, on the material properties of MSC test parts. Such studies could potentially find ways to improve the material properties of MSC materials while still minimizing the overall amount of polymer required to make a usable test part.

Unusual patterns near the border of some of the MRS constituent particulates were seen in some of the microscopy images such as in Figure 44, Figure 46, and Figure 50. The pattern in question appeared to be a second border line inside of the particulate that ran approximately parallel to the border line of the particulate. Future research is recommended to investigate what could be causing this pattern. Additional microscopy with the individual constituents used in the MRSs paired with further MSC material part production with other types of polymers could be completed to identify what constituents had this pattern, and if the type of polymer used impacted the presence of this observed pattern in an MSC part. This would be a starting point to understanding what caused this unusual pattern to occur in the MSC part.

Another question raised from the completed research was if the measured densities of the created MSC test parts would match up with theoretical density values of the same material calculated using the density values of the raw constituents. A follow up question to this would be

if they do not, could this difference in masses be the mass of thermal releases proposed to occur during polymeric composite material thermal processing. A future study could look into this idea by calculating the densities of MSC materials based on the densities of the raw constituents used and compare them to those collected in this research. Investigating this could provide additional insight into if thermal releases from the MRS constituent particles are the reason for the foaming behavior of the MSC material. At the time of writing this paper, the required density values of the MRSs from Exolith labs are not available. Once said MRS density values are available from the company, this topic could be investigated by a future study to start to address these questions.

It is recommended that further investigations be conducted on the specific reasons for the observed foaming behavior seen in the created MSC material during thermal processing. The thermal release study provided evidence backed suggestions as to the theorized candidate constituents for causing thermal release during polymeric composite material thermal processing which resulted in the foaming behavior of the MSC material. That being said, it is worth acknowledging that this research raised the question of if the foaming behavior was only caused by thermal releases of these MRS candidate constituents and not some additional factor such as the polymeric composite materials' rheological characteristics as they moved through the thermal processing equipment. Thus, studying the rheology, specific thermal releases by the MRSs with an evolved gas analysis machine, and the expected mass losses from thermal releases once more detailed density values are available for the MRSs could provide further insight as to the reason for the foaming behavior of the MSC materials. Looking into these items, along with performing appropriate material characteristic tests of new MSC materials, could also address if thermal releases from MRS constituents are the only item that caused the observed foaming behavior. Finding out the specific mechanisms that caused this phenomenon would be important to possibly

stabilize MSC material behavior during thermal processing and improve MSC test part strength characteristics. This would have particularly impactful potential for MSC parts created using additive manufacturing.

Finally, the potential use of regolith in polymeric composite materials on other extraterrestrial bodies being looked at for future astronaut crewed surface missions should be researched more in future studies. Astronaut crewed surface missions to the Moon in particular should be looked at for their potential in lunar regolith composite material creation and use during lunar surface missions. This recommendation is made as at the time of writing this research paper crewed missions to the Moon's surface are already planned and nearing completion. Thus, following a similar procedure to that used in this research to create Lunar regolith simulant composite materials could provide further insight into Lunar regolith's potential for use in polymeric composites, and attempt to address if variation of the type of Lunar regolith simulant would have an impact on the mechanical properties of test parts made from Lunar regolith simulant polymeric composite materials, particularly those created utilizing FGF additive manufacturing. Investigating the potential for in-situ part creation utilizing regolith on the surface of the Moon could provide potential avenues for future lunar surface missions to create usable mission parts while also minimizing the shipping mass of materials from the Earth's surface.

REFERENCES

[1] O. of the C. F. O. NASA Headquarters, “NASA’s FY 2021 Volume of Integrated Performance,” 2020. [Online]. Available: https://www.nasa.gov/sites/default/files/atoms/files/fy2021_volume_of_integrated_performance.pdf.

[2] National Space Grant Foundation, “Moon to Mars eXploration Systems and Habitation (M2M X-Hab) Academic Innovation Challenge-FY21 Solicitation on behalf of NASA Headquarters Human Exploration & Operations Mission Directorate The Advanced Exploration Systems (AES) Division,” Albany, Oregon, 2020. [Online]. Available: https://spacegrant.org/programs/xhab/.

[3] A. Goulas, J. G. P. Binner, R. A. Harris, and R. J. Friel, “Assessing extraterrestrial regolith material simulants for in-situ resource utilisation based 3D printing,” *Appl. Mater. Today*, vol. 6, pp. 54–61, Mar. 2017, doi: 10.1016/j.apmt.2016.11.004.

[4] Merriam-Webster.com, “Regolith | Definition of Regolith by Merriam-Webster,” *Merriam-Webster Dictionary*, 2021. https://www.merriam-webster.com/dictionary/regolith (accessed May 23, 2021).

[5] J. P. Rafferty, “Regolith | geology | Britannica,” *Encyclopedia Britannica*. 2018, Accessed: May 23, 2021. [Online]. Available: https://www.britannica.com/science/regolith.

[6] L. C. Simonsen and J. E. Nealy, “Radiation Protection for Human Missions to the Moon and Mars, NASA Technical Report 3079, pp. 1-30,” 1991. [Online]. Available: https://ntrs.nasa.gov/search.jsp?R=19910008686.

[7] J. Kozicki and J. Kozicka, “Human friendly architectural design for a small Martian base,” *Adv. Sp. Res.*, vol. 48, no. 12, pp. 1997–2004, Dec. 2011, doi: 10.1016/j.asr.2011.08.032.

[8] S. L. Taylor *et al.*, “Sintering of micro-trusses created by extrusion-3D-printing of lunar regolith inks,” *Acta Astronaut.*, vol. 143, pp. 1–8, Feb. 2018, doi: 10.1016/j.actaastro.2017.11.005.

[9] SpaceX, “Capabilities & Services: SpaceX Falcon 9 and Falcon Heavy Launch Services,” 2020. https://www.spacex.com/media/Capabilities&Services.pdf (accessed Aug. 04, 2020).

[10] J. M. Salotti, “Robust, affordable, semi-direct Mars mission,” *Acta Astronaut.*, vol. 127, pp. 235–248, Oct. 2016, doi: 10.1016/j.actaastro.2016.06.004.

[11] N. T. Redd, “How Long Does It Take to Get to Mars? | Space,” *Space.com*, 2017. https://www.space.com/24701-how-long-does-it-take-to-get-to-mars.html (accessed Aug. 11, 2020).

[12] H. B. Franz *et al.*, “Initial SAM calibration gas experiments on Mars: Quadrupole mass spectrometer results and implications,” *Planet. Space Sci.*, vol. 138, pp. 44–54, Apr. 2017, doi: 10.1016/j.pss.2017.01.014.

[13] R. M. Haberle, “Solar System/Sun, Atmospheres, Evolution of Atmospheres: Planetary Atmospheres: Mars,” in *Encyclopedia of Atmospheric Sciences: Second Edition*, Elsevier Inc., 2015, pp. 168–177.

[14] P. R. Mahaffy *et al.*, “Abundance and isotopic composition of gases in the martian atmosphere from the Curiosity rover,” *Science (80-.).*, vol. 341, no. 6143, pp. 263–266, Jul. 2013, doi: 10.1126/science.1237966.

[15] D. R. Williams, “Mars Fact Sheet,” 2020. https://nssdc.gsfc.nasa.gov/planetary/factsheet/marsfact.html (accessed Aug. 19, 2020).

[16] E. Umaras and M. S. G. Tsuzuki, “Additive Manufacturing - Considerations on Geometric Accuracy and Factors of Influence,” *IFAC-PapersOnLine*, vol. 50, no. 1, pp. 14940–14945, Jul. 2017, doi: 10.1016/j.ifacol.2017.08.2545.

[17] N. Leach, “3D Printing in Space,” *Archit. Des.*, vol. 84, no. 6, pp. 108–113, Nov. 2014, doi: 10.1002/ad.1840.

[18] I. Cheibas *et al.*, “Additive Manufacturing of Functionally Graded Materials With In-Situ Resources,” in *Aerospace Europe Conference (AEC 2020)*, 2020, no. June, pp. 0–12, [Online]. Available: https://www.researchgate.net/profile/Ina-Cheibas/publication/341990794_Additive_Manufacturing_of_Functionally_Graded_Materials_With_In-Situ_Resources/links/5edcf9e445851529453fd79d/Additive-Manufacturing-of-Functionally-Graded-Materials-With-In-Situ-Resou.

[19] K. M. Cannon, D. T. Britt, T. M. Smith, R. F. Fritsche, and D. Batcheldor, “Mars global simulant MGS-1: A Rocknest-based open standard for basaltic martian regolith simulants,” 2018, doi: 10.1016/j.icarus.2018.08.019.

[20] A. Alexiadis, F. Alberini, and M. E. Meyer, “Geopolymers from lunar and Martian soil simulants,” *Adv. Sp. Res.*, vol. 59, no. 1, pp. 490–495, Jan. 2017, doi: 10.1016/j.asr.2016.10.003.

[21] B. J. Chow, “Forming Infrastructural Materials by Mechanical Compaction of Lunar and Martian Regolith Simulants,” University of California, San Diego, San Diego, California, 2016.

[22] A. E. Jakus, K. D. Koube, N. R. Geisendorfer, and R. N. Shah, “Robust and Elastic Lunar and Martian Structures from 3D-Printed Regolith Inks,” *Sci. Rep.*, vol. 7, no. 1, pp. 1–8, Mar. 2017, doi: 10.1038/srep44931.

[23] M.-H. Y. Kim *et al.*, “Development and testing of in situ materials for human exploration of Mars,” 2000.

[24] S. Sargent, “W&M ScholarWorks W&M ScholarWorks Radiation Shielding Bricks for Mars Using Martian Regolith Radiation Shielding Bricks for Mars Using Martian Regolith Simulant and Hydrogen-Rich Polymers Simulant and Hydrogen-Rich Polymers,” *Diss. Theses, Masters Proj.*, Jan. 2018, doi: 10.21220/s2-acwh-k853.

[25] M. Arnhof, “Design of a Human Settlement on Mars Using In-Situ Resources,” in *46th International Conference on Environmental Systems*, 2016, no. July, pp. 1–15, Accessed: Jan. 19, 2021. [Online]. Available: https://ttu-ir.tdl.org/handle/2346/67561.

[26] L. Meza *et al.*, “Concept for a Fully In-Situ Resource-Derived Habitat for Martian Environment,” 2017.

[27] S. Sen, S. Carranza, and S. Pillay, “Multifunctional Martian habitat composite material synthesized from in situ resources,” *Adv. Sp. Res.*, vol. 46, no. 5, pp. 582–592, Sep. 2010, doi: 10.1016/j.asr.2010.04.009.

[28] N. Shiwei, S. Dritsas, and J. G. Fernandez, “Martian biolith: A bioinspired regolith composite for closed-loop extraterrestrial manufacturing,” *PLoS One*, vol. 15, no. 9, p. e0238606, Sep. 2020, doi: 10.1371/journal.pone.0238606.

[29] D. Karl *et al.*, “Clay in situ resource utilization with Mars global simulant slurries for additive manufacturing and traditional shaping of unfired green bodies,” *Acta Astronaut.*, vol. 174, pp. 241–253, Sep. 2020, doi: 10.1016/j.actaastro.2020.04.064.

[30] H. Li *et al.*, “3D printing and solvent dissolution recycling of polylactide-lunar regolith composites by material extrusion approach,” *Polymers (Basel).*, vol. 12, no. 8, p. 1724, Aug. 2020, doi: 10.3390/POLYM12081724.

[31] F. Zaccardi, E. Toto, M. G. Santonicola, and S. Laurenzi, “3D printing of radiation shielding polyethylene composites filled with Martian regolith simulant using fused filament fabrication,” *Acta Astronaut.*, vol. 190, pp. 1–13, Jan. 2022, doi: 10.1016/J.ACTAASTRO.2021.09.040.

[32] K. Grossman, “Regolith-Based Construction Materials for Lunar and Martian Colonies,” 2004. Accessed: Apr. 02, 2021. [Online]. Available: https://stars.library.ucf.edu/etd/6165.

[33] C. C. Allen, K. M. Jager, R. V. Morris, D. J. Lindstrom, M. M. Lindstrom, and J. P. Lockwood, “JSC MARS-1: A Martian Soil Simulant,” in *Space 98*, Apr. 1998, pp. 469–476, doi: 10.1061/40339(206)54.

[34] S. Do, A. Owens, K. Ho, S. Schreiner, and O. De Weck, “An independent assessment of the technical feasibility of the Mars One mission plan - Updated analysis,” *Acta Astronaut.*, vol. 120, pp. 192–228, Mar. 2016, doi: 10.1016/j.actaastro.2015.11.025.

[35] K. W. Leucht, “How NASA will use robots to create rocket fuel on Mars: The year is 2038,” *IEEE Spectr.*, vol. 55, no. 11, pp. 34–39, Nov. 2018, doi: 10.1109/MSPEC.2018.8513782.

[36] K. M. Cannon, D. T. Britt, T. M. Smith, R. F. Fritsche, and D. Batcheldor, “Mars global simulant MGS-1: A Rocknest-based open standard for basaltic martian regolith simulants,” *Icarus*, vol. 317, pp. 470–478, 2018, doi: 10.1016/j.icarus.2018.08.019.

[37] Exolith Lab, “Regolith Simulants – Exolith Lab,” 2021. https://exolithsimulants.com/collections/regolith-simulants (accessed Jan. 09, 2021).

[38] A. Abbud-Madrid *et al.*, “Mars Water In-Situ Resource Utilization (ISRU) Planning (M-WIP) Study,” 2016. Accessed: May 03, 2021. [Online]. Available: http://mepag.nasa.gov/reports/Mars_Water_ISRU_Study.pptx.

[39] M. N. Scheidema and P. Taskinen, “Decomposition Thermodynamics of Magnesium Sulfate,” *Ind. Eng. Chem. Res.*, vol. 50, no. 16, pp. 9550–9556, Aug. 2011, doi: 10.1021/IE102554F.

[40] M. R. Smith, J. L. Bandfield, E. A. Cloutis, and M. S. Rice, “Hydrated silica on Mars: Combined analysis with near-infrared and thermal-infrared spectroscopy,” *Icarus*, vol. 223, no. 2, pp. 633–648, Apr. 2013, doi: 10.1016/J.ICARUS.2013.01.024.

[41] J. Zhao, J.-J. Zheng, G.-F. Peng, and K. van Breugel, “Prediction of Thermal Decomposition of Hardened Cement Paste,” *J. Mater. Civ. Eng.*, vol. 24, no. 5, pp. 592–598, May 2012, doi: 10.1061/(ASCE)MT.1943-5533.0000423.

[42] A. Fairén and G. A. Marzo, “Recent Liquid Water on Mars Inferred from Shock Decomposition Analysis of Phyllosilicates within Impact Craters,” 2009, doi: 10.1029/2006JE002831.

[43] G. M. Nolis *et al.*, “Structure, defects and thermal stability of delithiated olivine phosphates,” *J. Mater. Chem.*, vol. 22, no. 38, pp. 20482–20489, 2012, doi: 10.1039/C2JM33183G.

[44] M. H. Haselkorn, “Dunite: Its Minerology, Thermal Decomposition and Reactions with Magnesia at Elevated Temperatures.,” University of Illinois at Urbana-Champaign, Ann Arbor, 1974.

[45] G. Chen and T. J. Richardson, “Thermal instability of Olivine-type LiMnPO4 cathodes,” *J. Power Sources*, vol. 195, no. 4, pp. 1221–1224, Feb. 2010, doi: 10.1016/J.JPOWSOUR.2009.08.046.

[46] M. Ristić, E. De Grave, S. Musić, S. Popović, and Z. Orehovec, “Transformation of low crystalline ferrihydrite to α-Fe2O3 in the solid state,” *J. Mol. Struct.*, vol. 834–836, no. SPEC. ISS., pp. 454–460, May 2007, doi: 10.1016/J.MOLSTRUC.2006.10.016.

[47] U. Schwertmann, J. Friedl, and H. Stanjek, “From Fe(III) Ions to Ferrihydrite and then to Hematite,” *J. Colloid Interface Sci.*, vol. 209, no. 1, pp. 215–223, Jan. 1999, doi: 10.1006/JCIS.1998.5899.

[48] T. M. McCollom, “Formation of meteorite hydrocarbons from thermal decomposition of siderite (FeCO3),” *Geochim. Cosmochim. Acta*, vol. 67, no. 2, pp. 311–317, Jan. 2003, doi: 10.1016/S0016-7037(02)00945-6.

[49] D. C. Golden *et al.*, “A simple inorganic process for formation of carbonates, magnetite, and sulfides in Martian meteorite ALH84001,” *Am. Mineral.*, vol. 86, no. 3, pp. 370–375, Feb. 2001, doi: 10.2138/AM-2001-2-321/Machinereadablecitation/RIS.

[50] E. R. D. Scott, “Origin of carbonate-magnetite-sulfide assemblages in Martian meteorite ALH84001,” *J. Geophys. Res. E Planets*, vol. 104, no. E2, pp. 3803–3813, Feb. 1999, doi: 10.1029/1998JE900034.

[51] D. Barthelmy, “Non Metallic Minerals by Hardness and Streak,” 2021. http://webmineral.com/determin/non-metallic_minerals_by_hardness.shtml (accessed Nov. 28, 2021).

[52] Hudson Institute of Mineralogy, “Mindat.org - Mines, Minerals and More,” 2021. https://www.mindat.org/ (accessed Nov. 28, 2021).

[53] RTP Company, “Minimizing Wear in Processing Equipment | RTP Company,” 2021. https://www.rtpcompany.com/technical-info/molding-guidelines/long-fiber-compounds/minimizing-wear-in-processing-equipment/ (accessed Dec. 05, 2021).

[54] M. Stopka, R. Kohar, P. Weis, and J. Šteininger, “Concept of modular 3D printer construction,” *IOP Conf. Ser. Mater. Sci. Eng.*, vol. 393, p. 12092, Aug. 2018, doi: 10.1088/1757-899X/393/1/012092.

[55] R. Sunga, “Density and Concentration Calculator for Mixtures of Isopropyl Alcohol and Water,” *handymath.com, Solutions for Technicians*. https://www.handymath.com/cgi-bin/isopropanolwghtvoltble5.cgi?submit=Entry (accessed Oct. 27, 2021).

[56] B. Rankouhi, S. Javadpour, F. Delfanian, and T. Letcher, “Failure Analysis and Mechanical Characterization of 3D Printed ABS With Respect to Layer Thickness and Orientation,” *J. Fail. Anal. Prev.*, vol. 16, no. 3, pp. 467–481, Jun. 2016, doi: 10.1007/S11668-016-0113-2/FIGURES/16.

[57] S. Wang, L. Capoen, D. R. D’hooge, and L. Cardon, “Can the melt flow index be used to predict the success of fused deposition modelling of commercial poly(lactic acid) filaments into 3D printed materials?,” *Plast. Rubber Compos.*, vol. 47, no. 1, pp. 9–16, Jan. 2018, doi: 10.1080/14658011.2017.1397308.

[58] C. Matetich and J. Vold, “Regolith Based Polymer Matrix Composites for In-Situ Material Creation for Long Term Extraterrestrial Missions,” *J. Aerosp. Eng.*, no. submitted for publication.

[59] D. H. Droste and A. T. Dibenedetto, “The glass transition temperature of filled polymers and its effect on their physical properties,” *J. Appl. Polym. Sci.*, vol. 13, no. 10, pp. 2149–2168, Oct. 1969, doi: https://doi.org/10.1002/app.1969.070131011.

[60] D. M. Brewis and D. Briggs, “Adhesion to polyethylene and polypropylene,” *Polymer (Guildf).*, vol. 22, no. 1, pp. 7–16, Jan. 1981, doi: 10.1016/0032-3861(81)90068-9.

[61] C. Mühlhan, S. Weidner, J. Friedrich, and H. Nowack, “Improvement of bonding properties of polypropylene by low-pressure plasma treatment,” *Surf. Coatings Technol.*, vol. 116–119, pp. 783–787, Sep. 1999, doi: 10.1016/S0257-8972(99)00203-0.

[62] E. Turianicová *et al.*, “A comparison of the reactivity of activated and non-activated olivine with CO2,” *Int. J. Miner. Process.*, vol. 123, pp. 73–77, Sep. 2013, doi: 10.1016/J.MINPRO.2013.05.006.

[63] G. Pieczara, M. Manecki, G. Rzepa, O. Borkiewicz, and A. Gaweł, “Thermal stability and decomposition products of p-doped ferrihydrite,” *Materials (Basel).*, vol. 13, no. 18, pp. 1–16, 2020, doi: 10.3390/ma13184113.

[64] S. Korichi, A. Elias, and A. Mefti, “Characterization of smectite after acid activation with microwave irradiation,” *Appl. Clay Sci.*, vol. 42, no. 3–4, pp. 432–438, Jan. 2009, doi: 10.1016/J.CLAY.2008.04.014.

[65] I. K. Tonle, E. Ngameni, D. Njopwouo, C. Carteret, and A. Walcarius, “Functionalization of natural smectite-type clays by grafting with organosilanes: physico-chemical characterization and application to mercury(ii) uptake,” *Phys. Chem. Chem. Phys.*, vol. 5, no. 21, pp. 4951–4961, 2003, doi: 10.1039/B308787E.

[66] van S. P. J. *et al.*, “Water Extraction from Rock Gypsum on Mars,” *Earth and Space 2021*. pp. 653–659, Apr. 05, 2022, doi: doi:10.1061/9780784483374.061.

[67] D. L. Hudson-Lamb, C. A. Strydom, and J. H. Potgieter, “The thermal dehydration of natural gypsum and pure calcium sulphate dihydrate (gypsum),” *Thermochim. Acta*, vol. 282–283, no. SPEC. ISS., pp. 483–492, Jul. 1996, doi: 10.1016/0040-6031(95)02819-6.

[68] S. Devasahayam and V. Strezov, “Thermal decomposition of magnesium carbonate with biomass and plastic wastes for simultaneous production of hydrogen and carbon avoidance,” *J. Clean. Prod.*, vol. 174, pp. 1089–1095, Feb. 2018, doi: 10.1016/J.JCLEPRO.2017.11.017.

[69] N. Khan, D. Dollimore, K. Alexander, and F. W. Wilburn, “The origin of the exothermic peak in the thermal decomposition of basic magnesium carbonate,” *Thermochim. Acta*, vol. 367–368, pp. 321–333, Mar. 2001, doi: 10.1016/S0040-6031(00)00669-9.

[70] L. Tian, A. Tahmasebi, and J. Yu, “An experimental study on thermal decomposition behavior of magnesite,” *J. Therm. Anal. Calorim.*, vol. 118, no. 3, pp. 1577–1584, 2014, doi: 10.1007/s10973-014-4068-9.

[71] K. M. Cannon, D. T. Britt, T. M. Smith, R. F. Fritsche, and D. Batcheldor, “Mars global simulant MGS-1: A Rocknest-based open standard for basaltic martian regolith simulants,” *Icarus*, vol. 317, pp. 470–478, Jan. 2019, doi: 10.1016/J.ICARUS.2018.08.019.

APPENDIX A. COMPILED ANOVA VALUE TABLES

Table A.1. Compiled IM MSC Part Two Factor ANOVA Test Values

Material Test Type	Df1	Df2	Critical F-Value (95% confidence)	MRS Source Location F-Value	MRS Loading Percent F-Value
Tensile Strength	3	9	3.86	0.12	78.36
Tensile Modulus	3	9	3.86	4.98	62.21
Flexural Strength	3	9	3.86	5.27	9.82
Flexural Modulus	3	9	3.86	1.41	83.51
Impact Toughness	3	9	3.86	2.70	26.23
Glass Transition Temperature	3	9	3.86	7.06	1.41
Heat Deflection Temperature	3	9	3.86	0.63	82.18
Melt Flow Index	3	9	3.86	4.98	4.94
Immersion Density	3	9	3.86	4.92	42.01
Coefficient of Linear Thermal Expansion	3	9	3.86	1.15	59.54

Table A.2. Compiled AM MSC Part One Factor ANOVA Test Values

Material Test Type	Df1	Df2	Critical F-Value (95% confidence)	MRS Source Location F-Value
Tensile Strength	1	10	4.96	2.70
Tensile Modulus	1	10	4.96	124.74
Flexural Strength	1	8	5.32	19.08
Flexural Modulus	1	8	5.32	17.12
Impact Toughness	1	18	4.41	7.04
Immersion Density	1	12	4.75	12.93

APPENDIX B. DMA RAW STORAGE MODULUS AND TANGENT DELTA DATA PLOTS

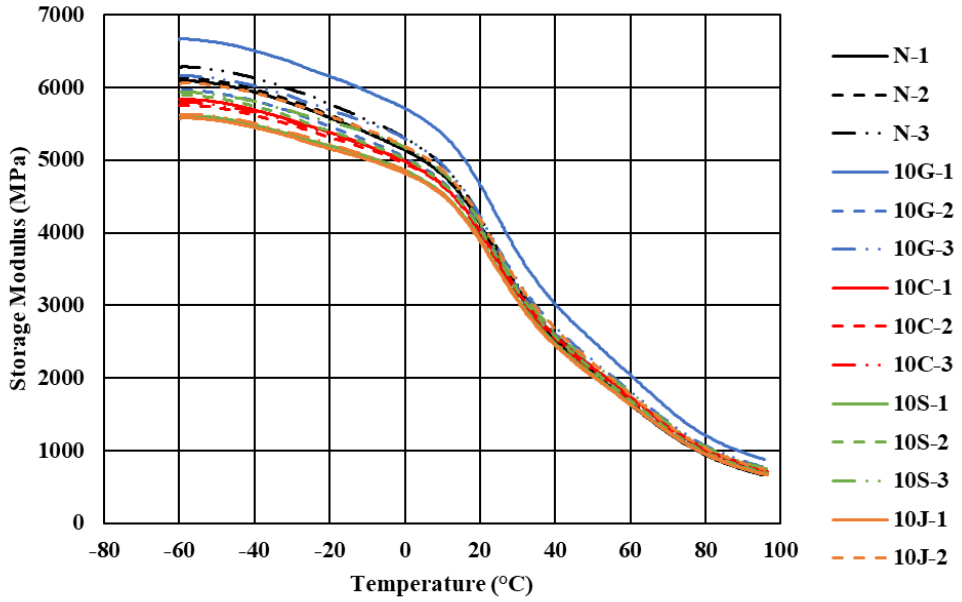

Figure B.1. Dual Cantilever DMA Storage Modulus of Injection Molded Neat PP and MSC Specimens Loaded with 10 wt. % MRS Varying by Source Location

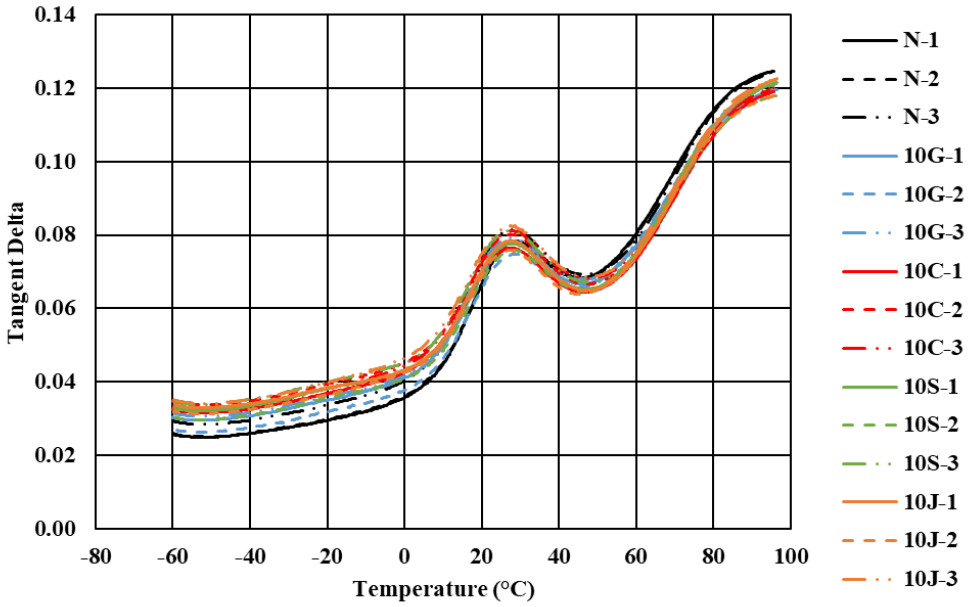

Figure B.2. Dual Cantilever DMA Tangent Delta of Injection Molded Neat PP and MSC Specimens Loaded with 10 wt. % MRS Varying by Source Location

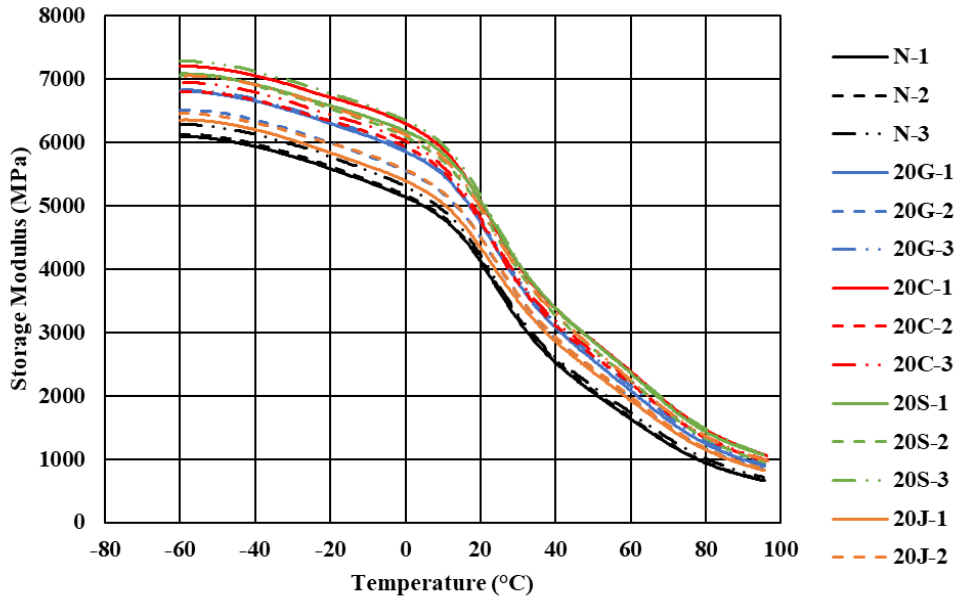

Figure B.3. Dual Cantilever DMA Storage Modulus of Injection Molded Neat PP and MSC Specimens Loaded with 20 wt. % MRS Varying by Source Location

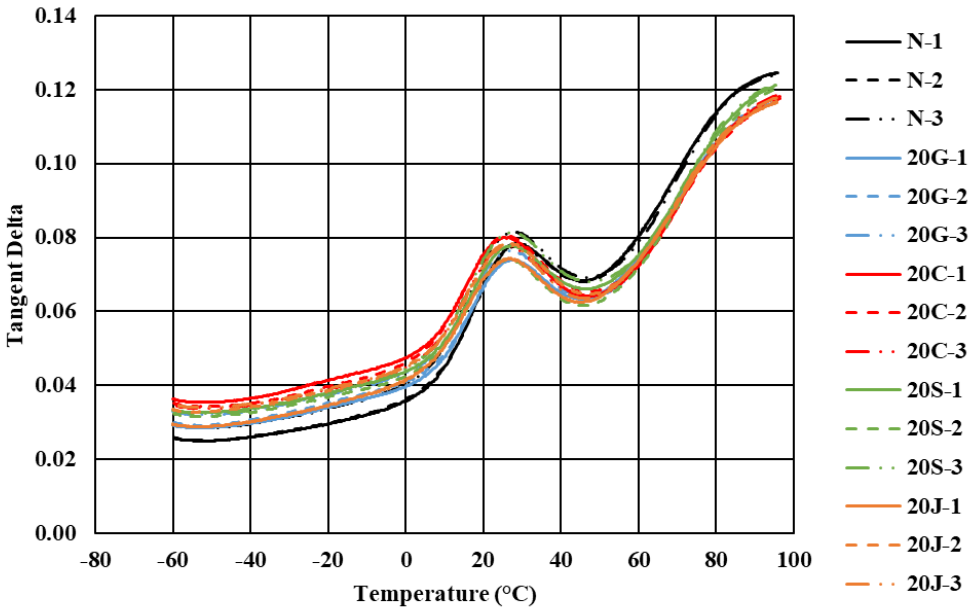

Figure B.4. Dual Cantilever DMA Tangent Delta of Injection Molded Neat PP and MSC Specimens Loaded with 20 wt. % MRS Varying by Source Location

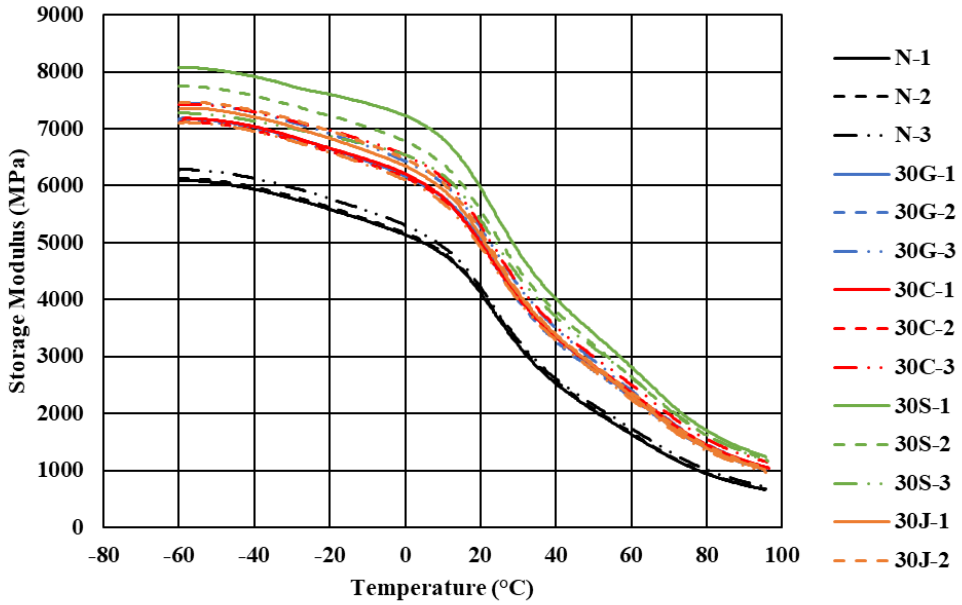

Figure B.5. Dual Cantilever DMA Storage Modulus of Injection Molded Neat PP and MSC Specimens Loaded with 30 wt. % MRS Varying by Source Location

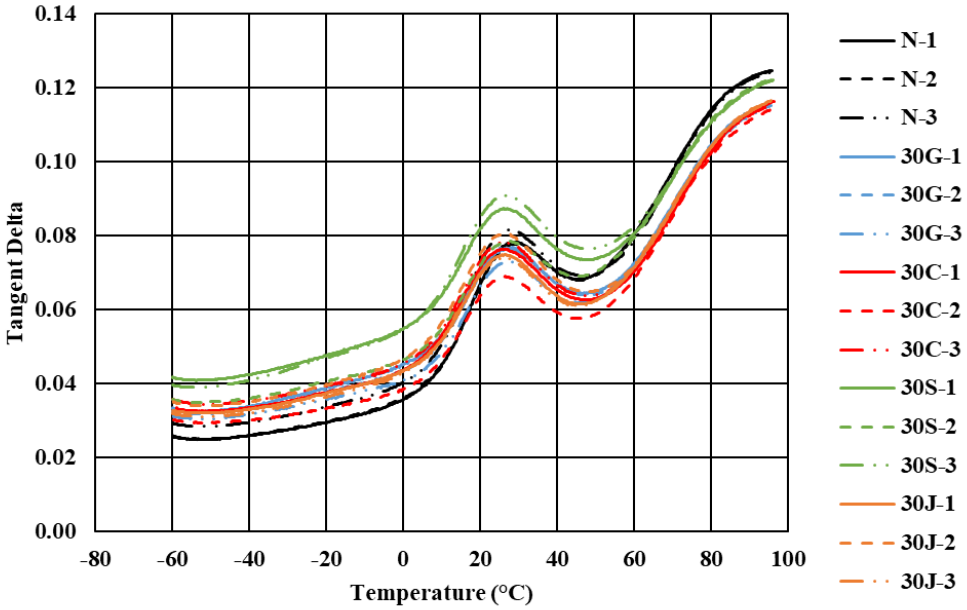

Figure B.6. Dual Cantilever DMA Tangent Delta of Injection Molded Neat PP and MSC Specimens Loaded with 30 wt. % MRS Varying by Source Location

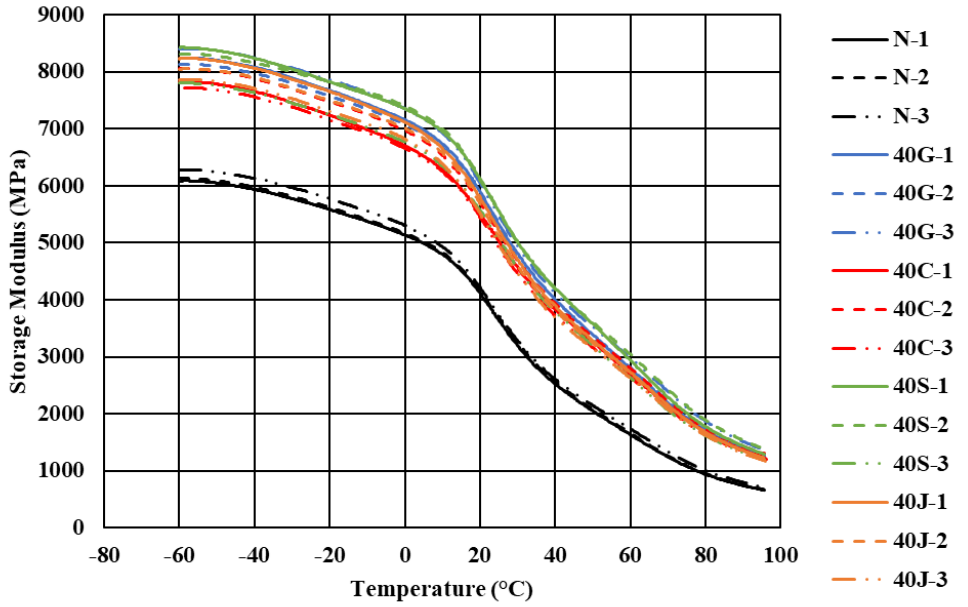

Figure B.7. Dual Cantilever DMA Storage Modulus of Injection Molded Neat PP and MSC Specimens Loaded with 40 wt. % MRS Varying by Source Location

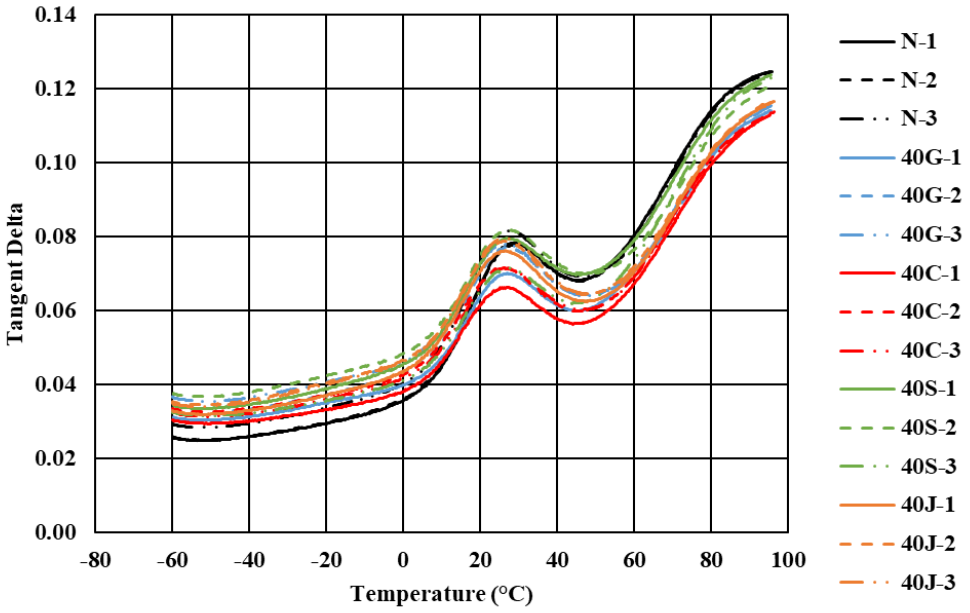

Figure B.8. Dual Cantilever DMA Tangent Delta of Injection Molded Neat PP and MSC Specimens Loaded with 40 wt. % MRS Varying by Source Location